Transfert thermique photo-induit par des nanoparticules d'or appliqué à la thérapie génique

Henryk Laszewski

université PARIS-SACLAY

NNT : 2019SACLN003

Thèse de doctorat

école normale supérieure paris-saclay

Light induced thermal energy conversion of gold nanorods applied to gene therapy

Thèse de doctorat de l'Université Paris-Saclay
préparée à Ecole normale supérieure de Cachan

École doctorale n°577 structure et dynamique des systèmes vivants (SDSV)
Spécialité de doctorat: biologie

Thèse présentée et soutenue à Cachan, 15/01/2019, par

Henryk Łaszewski

Composition du Jury :

Sebastien Bidault Chargé de Recherche, Institut Langevin (UMR 7587)	Rapporteur
Jean-Olivier Durand Directeur de Recherche, Université de Montpellier (UMR 5253)	Rapporteur
Marie Erard Professeure, Université Paris-Sud (UMR 8000)	Présidente
Zoher Gueroui Chargé de Recherche, École Normale Supérieure (UMR 8640)	Examinateur
Malcolm Buckle Directeur de Recherche, ENS Paris-Saclay (UMR 8113)	Directeur de thèse
Bruno Palpant Professeur, CentraleSupélec (UMR 8537)	Co-Directeur de thèse
Claude Nogues Chargé de Recherche, ENS Paris-Saclay (UMR 8113)	Invité
Cécile Sicard-Roselli Enseignant-chercheur, Université Paris-Sud (UMR 8000)	Invité

Table of Contents

1. Gold nanoparticles in technology and medicine

1.1. Gene therapy

1.1.1. The idea of gene therapy

Gene therapy is an extremely interesting approach for the treatment and/or prevention of genetic diseases. The basic idea is to avoid drugs and surgery by inserting a gene into cells and subsequently modify their biology in order to eliminate negative phenomena (e.g. the production of ineffective proteins). Several approaches have been used in applying this technique, such as the replacement of mutated genes by healthy copies, inactivation of improperly functioning genes and the introduction of genes increasing resistance towards specific diseases. From the very beginning this has been a dynamic field focused on targeted delivery because this therapy is extremely dependent on the need to efficiently introduce genes into the nucleus. However, because the method aims directly at inducing changes in human genetic material, it remains controversial (germline gene therapy; genome modifications of germ cells which pass on to next generations) and raises a set of questions concerning safety. Although, it seems a promising treatment for a number of diseases, the main focus is on those disorders for which no other cure currently exists.

The main issues that need to be addressed in the field of gene therapy pertain to the immune response and gene stability. The immune system evolved very efficient mechanisms to enable detection, recognition and, if possible, elimination of foreign bodies. Therefore, every therapy involving macromolecules, e.g. oligonucleotides, has to take into account these processes. The second important problem is gene stability; since modified genes are delivered in the form of DNA, or ideally RNA (biological functions are actively regulated by RNA) any change in their structure could result in therapy failure. Additionally, oligonucleotides are not generally very chemically stable in the environment of the human body; therefore, they need to be protected. In order to protect and efficiently deliver genes, viral vector have been used; cells are infected by their own genetic material reintroduced through viruses and thus viruses would appear to be well suited for gene delivery. Some viruses are even able to integrate genes directly into chromosomes, although very often the last step of viral vector activity involves simply transferring oligonucleotides into the nucleus. The extensive variety of viruses ensures a large

selection of different delivery processes, capsid size and number of oligonucleotides that can be injected into the cell. A review by C. W. Pouton listed 7 families of viruses with characteristic mechanisms for nuclear delivery[1]. Among them Parvoviruses, due to their small size, are even able to pass through the nuclear pore and enter the nucleus intact. There are two ways of exposing cells on vectors; injecting capsids into tissues, or removing patient's cells and exposing them to viruses under laboratory conditions (then subsequently transplanting the cells into the body). Both have advantages and disadvantages; however, a common concern involves targeting the correct set of cells e.g. cancer cells. This problem is significant in the case of vector injection directly to the tissue, because the lack of specific targeting renders the effects of this therapy relatively random. Another possibility is using genome-editing technologies that can mediate gene addition, gene ablation, "gene correction" and other genome modifications in cells[2]. This can be carried out inside the organism, by introducing the necessary machinery, or *ex-vivo,* associated with subsequent transplantation. Genome editing approaches are extremely interesting, because they can compete in various ways with viral delivery, due to decreasing tumour occurrence, better regulated gene expression, no oligonucleotide stability problems and, perhaps most importantly, regulation by more than one gene. The last one is especially attractive due to the growing number of diseases (many of them involving the failure of more than one gene) that can potentially be dealt with by gene therapy.

From the point of view of this thesis, it is interesting to examine those areas in which gene delivery has been implemented *in vivo*. Tests have been carried out using haemophilia B[3], however expression in human tissues was found to be much lower in comparison to *in vivo* studies in dogs[4]. Further research improved the results using longer activity and effective bleeding reduction[5]. An interesting example of gene therapy involved the use of viral vector injection into subretinal zones carrying genes responsible for the expression of retinal pigment (protein RPE65) to patients with inherited blindness (caused by RPE65 gene mutation)[6]. Also promising were early tests of treatment against neuromuscular diseases, such as Parkinson's; it was reported that following treatment, synthesis of the neurotransmitters dopamine and serotonin increased and the patient's motor performance improved[7]. Childhood-onset spinal muscular atrophy is another degenerative disease with a genetic background and for which successful trials using nucleoside-based gene therapy have been carried out[8]. A deeper understanding of the molecular genetic basis of the illness enabled sufficient curative engineering to be able to significantly slow down degeneration. However, there is still a great challenge to introduce this treatment as a generally applicable procedure.

Gene therapy is one of the most daring attempts in the history of medicine to cure diseases that are not treatable in any other way. It brings together a very deep understanding of the biology behind the disease, the huge effort of research laboratories, the invention of new targeting strategies and, critically, the injection of a huge amount of funding. Nowadays, laboratory trials are rapidly leading to clinical tests and undergoing commercial development. The main problem of gene therapy is that it remains expensive[9], and indeed, products that have already been approved for hospital use have had to be withdrawn because of their relative high cost[10].

1.1.2. Nanocarriers

Therapy optimisation is possible using a number of approaches, e.g. creating new drugs, increasing therapeutic concentrations, or by delivery only to those zones where the disease is located. The latter possibility creates an interesting opportunity to use already developed drugs that have been approved by the administration and also drugs at higher concentrations acting only at the targeted tissue. Additionally, such an approach may bring back into use those therapeutics which, in the absence of targeting, were found to be toxic. Thus, there is a rapidly growing interest in targeting using nanomaterials[11] which because of their small size transit through tissues with relatively high efficiency and possess huge potential in therapy-based applications due to their extraordinary chemical and physical properties. Nevertheless, although nanostructures are being increasingly used in medicine, the effect of their presence on the human body remains unclear and poorly catalogued[12]; mitochondria for example seem to be adversely affected by some types of nanomaterials[13]. Nonetheless, procedures for the use of nanoparticles in medical examination exist and certain parameters have been studied, these main characteristics being particle size, shape, surface coverage, and degree of protein absorption, uptake and clearance[14]. The main focus in the field is on polymeric micelles, liposomal, protein, and inorganic and crystalline nanoparticles. The main advantages of already approved approaches are improved stability (often obtained by pegylation), increased delivery to tumour sites (liposomal nanoparticles) and higher drug loading. Other criteria include different forms of hydroxyapatite nanostructures allowing bone substitution. Also, nanoparticles may be used as contrasting agents, but this is not directly of interest to this thesis since such materials were designed to be removed from the bloodstream as soon as possible after measurement.

In the case of gene therapy, the goal is more challenging, because drugs (oligonucleotides) need to be delivered into the cell cytoplasm[15]. It is important to note that

"free" oligonucleotides cannot be efficiently internalized by cells, because genomic molecules are susceptible to serum nucleases, phagocyte uptake and may cause an immune response thus resulting in toxicity. The most widespread current method uses viral vectors in an attempt to avoid eliciting an immune system response[16]. Nevertheless, this approach raises safety issues[17,18], and there is a real need to define non-viral gene carriers[19].

In response to these latter criteria numerous solutions have been proposed[20], including nanoparticle-based[21,22,23] and metallic based ideas[24]. The main advantage of nanoparticles is their size compared to virus capsids (20-500 nm in diameter) and this factor in fact, is decisive (larger structures may cause blood clotting). Nanoparticles can have modified and controlled surface properties, like hydrophobicity, charge and patchiness[25]. Additionally, in contrast to virus capsids, nanoparticles can offer controlled release e.g. by thermal release (plasmonic, magnetic structures). Still, however, this remains a challenging field of research, mainly due to the issue of material reproducibility; this is one of the reasons why mainly polyethyleneimine, poly (lactic-*co*-glycolic acid) and lipid nanostructures are now used for this purpose[26].

1.2. Gold nanorods as nanocarriers

1.2.1. Synthesis

Gold nanorods (GNRs) are one of the most frequently used types of nanoparticles in research; due to their relative ease of production, that allows accessibility to structures with extraordinary physical properties including efficient, tuneable absorption which can be shifted to the near-infrared (NIR) range and therefore overlapping the first optical window[27]. The first attempts of synthesis of anisotropic gold nanostructures came at the end of the 1990's[28,29] (electrochemical method) and at the beginning of the 21st century[30,31,32] (wet chemical method). There are continual improvements leading to new developments e.g. one-step wet synthesis[33].

For this thesis, wet chemical synthesis was selected due to its large scale, rapid synthesis and the possibility of modulating parameters such as the reaction temperature, concentration of crystals on nanorods and the number of elongation-controlling silver ions. Also, efficient optical characterisation (extinction spectrum) provides good information concerning the collective morphology; finally, it is possible to rapidly upgrade protocols in order to eliminate or decrease any negative effects (high dispersity, dumbbell nanostructures[34]). Therefore, wet chemical synthesis provides modifiable volumes of colloidal solution whose basic characteristics may be checked immediately after the reaction. Although GNRs do not oxidize, there are major issues with aggregation and reshaping[35]; the first problem is mostly solved by the presence of

surfactants. The second problem is more challenging, because the addition of Na_2S (which stops the dynamic process on gold surfaces[36]) also makes further functionalisation difficult. Consequently, such an approach is mainly used for physics-focused experiments e.g. laser-induced melting. An alternative solution involves covering the gold with a thin layer of silica, although in such a case functionalisation has to be based on silane compounds[37] which is less preferable compared to thiol-based surface attachment. A third possibility is to use nanorods obtained from synthesis before morphological changes occur. Given the relative ease of synthesis it is possible to prepare nanoparticles immediately before each set of experiments. In the end although GNRs synthesis is challenging, it offers the advantage of high chemical stability compared with other nanomaterials. Furthermore, although some morphological evolution takes place over time this can be controlled by surface modification or by taking advantage of the rapid synthesis time, by preparing a new batch of nanoparticles. The downside of wet chemical synthesis is that it requires the use of the toxic and difficult to remove surfactant, CTAB[38]. An additional obstacle in subsequent oligonucleotide functionalisation is the presence of a CTAB[39] bi-layer (formed on the GNR surface), resulting in a decrease in accessibility. To overcome this a plethora of different solutions has been proposed in the literature, ranging from the introduction of a surfactant mixture[40], salt-aging[41] to round-phase transition[42]. In conclusion, GNRs constitute a very promising material from the synthesis point of view (possibility to prepare large-scale synthesis), and therefore it was felt that the effort focused on functionalisation was justified.

1.2.2. Functionalization

The use of GNRs as prospective oligonucleotide carriers has a strong background; to date the functionalisation process has been carried out using essentially two different attachment approaches; covalent[43] and electrostatic[44]. Whatever the choice of methodology, it has however to be adjusted according to the desired end function of the nanocarrier. In this thesis, quantitative, light-triggered oligonucleotide release and its time resolved evolution by optical methods was the goal. This requires knowledge of the specific characteristics of the attached DNA/RNA, as well as specific protocols for immobilisation. The "active" oligonucleotides should be labelled with fluorescent dyes, to enable observation using, for example, confocal microscopy (this is illustrated later in the GNRs-cell experiments). Although the presence of these ssDNA/RNA could not be observed on the nanoparticles (direct immobilisation on gold surfaces causes effective quenching of the dyes), there is a need to observe the oligonucleotides before and after release. Furthermore, the process of detachment

should be strictly separated during measurement; for these purposes two solutions were used: following changes of emission of one fluorophore[45] (in this case the fluorophore could be deposited on GNR surfaces), or using Forster Resonance Energy Transfer (FRET)[46] (emission has to be registered before dehybridisation). The fluorescent dye in the presence of gold nanoparticles can be quenched (again by close proximity to the surface), exalted, or unchanged depending on the size and shape and the distance at which e.g. exaltation occurs[47]. These three cases provide an interesting opportunity to detect release, however, scattering and nanostructure absorption will impact on experimental noise and the emission intensity. Nevertheless, this approach has been successfully implemented to good effect in numerous studies[48,49]. For this method dyes can initially be in either a quenched or exalted zone (preferably quenched, because release can be clearly detected by the appearance of fluorescence), so electrostatic (layer-by-layer) deposition and thiol-bonds are suitable. The second approach that involves following changes in FRET requires that the pair of fluorophores are in the exaltation or neutral zone since emission has to be detected from the onset of the experiment. Additionally, the emitters need to be maintained at a constant distance from the surface, this eliminates the use of a layer-by-layer approach because electrostatically deposited layers intrinsically have various thicknesses. Moreover, as release will be associated with the disappearance of FRET then the method of choice will have to be dehybridisation which is better suited for the case of a pair of thiolated oligonucleotides with the non-thiolated strand separating from the immobilised thiolated ssDNA/RNA. Therefore, using FRET at any step of this thesis required the use of thiol-based functionalisation of GNRs surface.

FRET was therefore used in order to measure the number of complementary strands immobilised on GNRs; therefore, thiolated oligonucleotides were used and functionalisation carried out through the formation of thiol-gold bonds. The experimental approach therefore was to attach SH-DNA to the surface and subsequently hybridise it with complementary strands. Additional modification of both, for example by labelling with fluorophore, could then be carried out under specific conditions.

1.2.3. Retention and uptake

Gene therapy is dependent on how the nanocarrier operates, i.e. where it is located, inside tissues; clearly, nanoparticles have to be in the cytoplasm before cargo release. Nanorods possess the advantage of being small; rods with 10 nm diameters and 40 nm lengths have efficient absorption in the NIR range. However, the delivery of nanomaterials to specific cells is difficult and, additionally, the uptake pathway is often unpredictable.

GNRs, as nanoparticles, face the problems of opsonization and phagocytosis. The first phenomenon concerns the attachment of different proteins and serum components, onto nano-object surfaces. This effect can be reduced by surface engineering and more specifically by reducing the charge of the particle. For this purpose, the most efficient and widely used molecule is polyethylene glycol (PEG). Long strands of this polymer mimic to some extent some of the properties of water, so biological molecules interact with this polymer as they would with water molecules. Furthermore, experiments have indicated that pegylation reduces opsonization and consequently reduces the efficiency of recognition by the immune system[50]. Apart from the chemical composition of the particle's surface, size plays an important role; the immune system had to evolve a fast and effective reaction to objects on a nanoscale because these are optimal sizes for penetration of tissues from the bloodstream[51]. GNRs have to be functionalised by oligonucleotides; it has already been shown that the immune system is extremely aggressive towards NP-DNA hybrids (surface charge)[52,53]. Such objects are clearly dangerous for organisms and therefore their elimination was clearly a priority during development of the immune system. The creation of mixed layers on the surface i.e. DNA with PEG, could reduce the area of direct interaction between GNR attached oligonucleotides and external factors.

Another problem faced by all drug carriers is the mode of delivery – active, or passive. For the size of GNRs used in this thesis, there is no evidence to assume passive accumulation in cancer tissue over short times[54] (as in the case of gold nanoshells (GNShs)[55]), therefore some kind of active targeting is required. Amongst the many methods available, in all cases molecules have to be attached to a metal surface. Therefore, GNRs need to carry oligonucleotides and PEG to prolong the circulation time. Also, if active targeting is selected, then the interesting phenomena of protein corona creation around nanoparticles becomes less likely. Layers created in a targeting approach can screen the activity of molecules supposed to detect cancer cells. The most widely spread approach in this sense is to use antibodies[56,57]. Antibodies may be attached via electrostatic, thiol, or amine bonds; molecules with sulphur in their chemical composition can directly interact with the gold surface. However, this raises the problem of specificity and the amount needed for effective functionalization. Nonetheless, this approach has been carried out and it was even possible to obtain Janus ligands surface immobilisation of two different antibodies[58]. The other approach, via amine bonds, is more promising, because it may provide higher specificity; there is a drawback in the method however which introduces functionalisation of GNRs by thiolated compounds with -COOH groups. In this case EDC/NHS

may be used for activation of carboxylic groups and subsequent attachment of amines. This approach is popular for antibody attachment to nanoparticles. Another solution is to use other types of ligands with completely different types of chemistry. An attractive possibility is to use aptamers[59], because they are oligonucleotides, functionalisation can be still done in 3 steps (as per the basic plan): oligonucleotide attachment, pegylation and duplex DNA formation. The ratio between aptamers and oligonucleotides for hybridisation can be easily modified simply by varying the concentrations. Additionally, by increasing the number of ssDNA on the surface such nanostructures are more likely to be internalised by cells[60].

The next issue concerns uptake[61,62,63] ; in the case of *in vitro* experiments, although it is likely that at sufficient concentrations nanoparticles will be, in some part internalised, this may not be the case *in situ* in a therapeutic context. After injection into the bloodstream, the nanocarriers will be pushed through the blood vessels until removed by phagocytes (although as mentioned before, the retention time can be prolonged by pegylation). Thus, within this limited time frame, GNRs have to be internalised into the cancer tissue and spend sufficient time in contact with specific cells for cellular uptake to occur. Unfortunately, nanostructures do not deposit passively at the tumour site, because of their small size. Even uptake (most probably by endocytosis) is not the last step of delivery, because the final destiny will be, most likely, inside the lysosome. Also, the cell will try to destroy the perceived hazard by increasing the pH inside the lysosome (which may reach as low as pH 2). On the other hand, the defence mechanism of the cell may tricked into use for delivery as described in the literature by the "proton sponge"[24] mechanism which involves subsequent disruption of the lysosomes and release of the nanostructures into the cytoplasm. Nanomaterials have to accept protons and in consequence perturb the lysosome mechanism of providing more protons to the nanostructure. Polyethylenimine (PEI) is particularly efficient at this; the amine groups in the PEI strand can be additionally protonated. The issue then becomes the pH inside the lysosome before bursting, because it may cause denaturation of double stranded oligonucleotides, which will occur at low pH (pH=<2). This approach nevertheless, is a promising way of introducing nanocarriers into the cytoplasm.

In conclusion, SH-PEG (with a molecular mass high enough to provide longer retention times) has to be present with thiolated DNA on the surface and the material has to be able to absorb protons produced by the cell to decrease the pH inside the lysosome.

1.2.4. Light into thermal energy conversion

As indicated before, the operating part of functionalisation was supposed to be a DNA duplex with non-thiolated "active" oligonucleotide. This type of architecture determines the release mechanism; the environmental conditions have to be altered causing dsDNA denaturation. This can be achieved by low/high pH, increase of temperature or decrease of ionic strength. However, as the experiment is supposed to be controlled by outside triggering and carried out inside the cell, the biological environment is already pretty much established and controlled, therefore only local temperature increase is a realistic possibility.

Nanoparticles with gold components are widely known for their photothermal properties and in this context the most popular are nanoshells[64,65]. These nanostructures, with absorption in the NIR have the tendency, due to size, of accumulating into tumours. Therefore, they may follow the passive targeting, allowing efficient treatment; there are on-going clinical tests for therapies based on this scheme. As discussed above, passive targeting is rather unlikely in the case of GNRs, however the release mechanism should be based on thermal phenomena. This raises the exciting possibility of controlling the process by triggering using a laser beam at a chosen time and space and to follow changes in a highly controlled way.

The mechanism of release has to be strictly connected with uptake; following the fluorescence emitted by nanohybrids will precise the moment when they enter cells. This measurement may be performed in two ways: Fluorescence-activated cell sorting (FACS), or optical microscopy. Both methods are highly effective and can provide complementary data, e.g. FACS gives a histogram of cellular conditions; microscopy can indicate zones in which GNRs accumulation occurs. Therefore, the most promising approach would be first to carry out FACS measurement and collect data covering the minimum time needed for efficient uptake. Subsequently confocal, or total internal reflection fluorescence (TIRF) microscopy can be used to indicate in which zones of the cells the nanohybrids have accumulated. This information can be essential, if the lysosome burst mechanism were implemented then fluorescence emission would indicate lysosome breakage and GNRs diffusion into the cytoplasm. Additionally, microscopy can be conjugated with laser illumination and a systematic study of release may be possible.

Nevertheless, the preparation of release has to be founded on a sound experimental and theoretical background, allowing a swift transition to a biological environment. For this purpose, the nanohybrids have to be prepared in a way that provides the possibility for

temperature measurements. The need for such measurements comes from the as yet unclear influence of gold nanoparticles on dsDNA melting temperature for which the literature contains contradictory observations[66,67,68,69,70]. This is the reason for the strong motivation to create a temperature map covering zones around GNRs which would allow prediction of the laser power needed for total release of complementary DNA.

Measuring temperature on a nanoscale is a challenging task, however in the last few years numerous methods have been proposed[71,72,73,74]. However, in this thesis we decided that the most interesting approach was based on oligonucleotides. Thiolated, fluorophore-labelled hairpin DNA can act as an effective thermometer if the strand in the closed state has quenched emission. Such a system is already in use; however, the novelty here involves controlling the distance from the surface by modifying the spacer length (the multi-thymine part of the spacer sequence following the thiol modification). Using such an approach it is possible to change the position of dsDNA by one base. On the other hand, this method is valid only as long as the spacer remains rigid (therefore it can not be too long). Additionally, in order to have a molecular beacon, several have to form a duplex – so the melting will indicate the temperature of the zone. Differences in fluorescence between "closed" and "open" states should be clear enough so as to avoid any doubt that a transition has occurred. Moreover, the process of hairpin opening involves denaturation, so it should be possible to check the influence of different environment features (salt concentration, molecular crowding) on the release mechanism.

Another possibility is to use material that would measure temperature changes by varying physical properties, e.g. fluorescence lifetime, emission intensity. In this case there is also the possibility to label dsDNA with such material (to keep the exact information covering fluorophore-GNR surface distance). Such an approach would place the indicator further from the surface than dsDNA created with the molecular beacon. The distance could be controlled by modifying complementary (for thiolated oligonucleotides with longer sequence) labelled strand lengths.

1.2.5. Toxicity

The final issue which had to be addressed during planning of this thesis was nanomaterial toxicity[75]. This can have different origins; however, the main reason is surface chemistry[76], fortunately in the case of GNRs there have been numerous studies and a lot of data has been collected[77], covering size, shape and different coatings. The main conclusion is that complete removal of CTAB greatly improves nanorods biocompatibility.

Therefore, a discussion of the potential cytotoxicity of the planned nanohybrids is inevitable; as described before, GNRs were intended to be functionalised with: SH-DNA, complementary ssDNA, SH-PEG and possibly PEI. The first modification step deals with the attachment of thiolated oligonucleotides, it is clear that negatively charged phosphate groups on the DNA backbone can interact with CTAB. Additionally, replacement on the surface is incomplete. Therefore, the first step of functionalisation can only disturb the bi-layer of CTAB on the GNRs, without removing it, so this is hardly a "detoxification". The next step involves attachment of SH-PEG; the polymer is not charged, no interactions with surfactant are predicted. However, the creation of thiol-gold bonds in this case does not remove CTAB from the system. The crucial part of the process has to be between pegylation and DNA hybridisation; this step is necessary due to a possible excess of thiolated oligonucleotides in solution. If they remain, dsDNA could be formed independent of GNR surfaces and the number of deposited strands will decrease. The point is to use the washing steps to allow effective CTAB removal from the surfaces and nanohybrid systems. For this purpose, the concentrated GNRs could be diluted by water, this is probably effective in destroying the bi-layer, while it may not be very effective in detaching single molecules from phosphate groups and gold surfaces. Another approach proposed here concerns the replacement of CTAB by low toxic, uncharged surfactants like Tween20, Tween80, or Triton X-100 at high concentrations. The idea is to create micelles of "neutral" surfactant into which CTAB molecules can integrate; similar structures have in fact already been observed[78,79,80]. The same process is responsible for high cytotoxicity; CTAB accumulates in cell membranes changing their physical properties[81]. Additionally, Tween, or Triton may have the tendency to create micelles on gold surfaces and therefore compete with CTAB. 2-3 rounds of rinsing with charge-neutral high concentration amphiphilic compound should be able to remove most of the cytotoxic surfactant from the system and increase biocompatibility.

The other toxicity-associated issues are mostly not associated with the surface chemistry addressed in this thesis. The only possible changes from this point of view is modifying PEG/ssDNA/dsDNA ratio on GNRs. An increase of the number of PEG strands deposited on a surface will improve the properties of the nanomaterial with respect to any immune reaction, but it raises the issue of the number of oligonucleotides that may be delivered into the cell; the accessibility to thiolated DNA would be strongly decreased and release could also be impacted (blocking of leaving strands). The way to improve biocompatibility would be by encapsulating the GNRs into biofunctionalized vesicles, but this approach eliminates the simplicity of

nanorods-based delivery and would thus have little applicability to medical applications at this point; a GNRs-vesicle system would be difficult to envisage in terms of reproducibility. Another solution could involve opsonization, before use in biological systems, by previously selected compounds but whilst this approach is possible, it may eliminate pegylation and thus active targeting is impossible.

In conclusion, the most important issue in order to reduce GNRs cytotoxicity is removing CTAB from the system. Without this, any possibility of biological use is highly unlikely. The toxicity caused by size, or shape cannot be reduced in the nanomaterial which is supposed to release drugs in a controlled way and have a potential role in active targeting.

1.3. Approach

1.3.1. Optical-based characterization

Preparing nanomaterial for biological/medical use is a challenging task because at one point the laboratory experiments have to be scaled up; tests on cell cultures and animals, require a lot more material than characterising measurements. For this purpose, in parallel to nanohybrid development some work was planned to create a protocol which will allow to characterise, in as detailed and cheap and easy a way as possible.

The first part was characterisation of GNRs – using their dependence on size and shape that dictates how they interact with light. Shape anisotropy means that electrons can oscillate in two distinctive planes perpendicular to each other. The first, associated with the diameter is responsible for transverse plasmon resonance, the second, dependent on the length of GNRs, creates longitudinal plasmon resonance. Both can be easily recognized in an extinction spectrum, due to their high absorption cross-section. Careful analysis allows measurement of the aspect ratio between diameter and length, of some structural disorder and the general level of mono-dispersity. Nevertheless, more exact data about GNRs structure is provided by TEM images. Such measurements need only be performed once when synthesis is always carried out using the same protocol. In general, obtaining the concentration of nanorods based on extinction spectrum is challenging; there are approaches that use 400, 450 nm wavelengths, or follow the position and value of plasmon resonance absorption. In my opinion, the more accurate technique focuses on signals generated solely by GNRs, thus in a first instance by the longitudinal plasmon. This assumption is especially critical for this thesis because this is supposed to be in the range 750-800 nm, in the range of the optical window. Values obtained from longitudinal absorption band should be compared with transverse plasmon absorbance,

although this latter can be influenced by gold nanospheres that are usually present in post-synthesis solution. Additionally, there could be other nano-scale metal objects, without an exact geometry that, most likely, will interact with light of shorter wavelengths. The final important issue is accuracy which is a controversial matter, even in the case of nanospheres (simple geometry). There is no situation in which all of the nanostructures in a post-reaction mixture are rod-shaped with the same size. Therefore, every calculation based on extinction will cover a fraction of nanostructures; with higher mono-dispersity, the accuracy of concentration determination rises. On the other hand, focusing mostly on longitudinal plasmon absorption provides an estimation of the amount of the main fraction of GNRs; a comparison with TEM images and a resulting size histogram should provide a correction that shifts the result closer to a more precise value.

The second part of optical-based characterization concerns DNA functionalization; as mentioned before, for numerous reasons, the idea was to provide a fluorophore labelling on each oligonucleotide strand which was supposed to be deposited onto GNR surface (both by thiol-gold bond and hybridisation). Such an approach allows a more precise measurement of DNA concentration, because of the linear dependence between concentration and emission. There is also the possibility to follow the absorption peak at 260 nm, but ssDNA and dsDNA interact differently with this wavelength.

Introducing fluorescence to measure concentration dependence in solution without GNRs is not a difficult task. However, in the presence of nanostructures whose absorption overlaps with absorption/emission spectrum of the dye, the situation becomes more complicated. Moreover, fluorophores attached to surfaces via oligonucleotide strands can emit differently as a function of the GNR position in space; the phenomena of screening can occur. Therefore, the method of separating DNA from nanostructures should be introduced in order to facilitate data analysis. Such an approach should cover strands attached by thiol-gold bonds and hybridisation. One option is to dissolve GNRs using an HCl-HNO_3 mixture and measure the fluorescence in the presence of gold ions. Such an experiment could give exact data, however it requires highly concentrated acids and is precise only if oligonucleotides are specifically attached. The solution proposed in this thesis is to perform agarose gel analysis; if the percentage of agarose is low enough it is possible for GNRs to migrate into the gel. This is very important, because it may give some information about nanoparticle coverage by DNA. It is known that ssDNA and dsDNA migrate further than nanoparticles under the same conditions, due to much lower mass. Additionally, the electric potential is able to separate non-specifically

attached oligonucleotides from metal surfaces. However, in properly prepared experiments, with suitable running buffer, the oligonucleotides immobilised on GNRs via thiol-gold bonds and hybridisation remain attached. The issue was to change conditions in a controlled way, therefore two problems had to be solved; detachment of thiolated oligonucleotides and dsDNA denaturation. For the first one, the solution seemed obvious and involved the addition of low mass thiolated compound at high concentrations; since the thiol-gold bond is partially electrostatic, the result should be surface competition in favour of higher concentration molecules. For this purpose, the GNRs could even be aggregated, because the presence of free GNRs without DNA is not critical at this point. The second issue is more delicate; the optimal solution would be denaturation without disrupting the thiol-gold bonds. Among the possibilities of duplex denaturation are: increase of temperature over the melting point, decreasing ionic strength, and changing pH. In the case of temperature such an approach could not be applied, because following the temperature increase, the loading into a native gel (and running buffer) will inevitably be associated with some renaturation. Additionally, if the melting temperature is high, it may disrupt the thiol-gold bonds. The ionic strength is important for dsDNA structure, however decreasing the ionic strength may not lead to complete denaturation. Moreover, such low ionic strengths are incommensurate with the electrophoretic condition. Modifying the pH has similar problems to changing the ionic strength but by using a diffusion control i.e. by regulating the exchange surface this may be possible. If the DNA sample is introduced in a low pH azeotrope of running buffer plus 20-25% glycerol into the loading well of an agarose gel, then the DNA solution will occupy the lower part of the well, exchange with the running buffer will be slow and the denatured DNA will run into the gel before renaturation can occur. An added advantage is that there should be no effect on the gold-thiol bond. One source of inaccuracy especially for the fluorescent measurements would result from heterogeneity in loading samples into the wells but this could be factored into any quantitative analysis.

In summary, although a complete, optical-based characterisation of GNRs-based nanohybrids is theoretically effective it involves two procedures that require attention: First, measurement of GNRs concentration using extinction spectrum analysis and second, oligonucleotide characterisation based on fluorescence.

1.3.2. Electrostatic-based gold nanorods-cells interactions

Previous paragraphs have described the assumptions implicit for effective nanoparticle delivery *in vivo*; however, nanomaterials have to be used at both laboratory-scale research *in vitro* and *in situ* and at clinical diagnostic therapeutic levels *in vivo*. The transition from the first

to the second is not necessarily facile and the final application should be borne in mind when nanomaterial composition and synthesis protocols are being devised.

It is a self-evident fact that cell culture is a much less complicated environment than that encountered in living organisms. Of the many problems faced in transiting from the first to the latter the most important could be the menace of opsonization and the immune reaction; the goal is to limit removal of nanoparticles from the system and to increase their retention time by playing for example with positive/negative surface charge. It may not be necessary to screen DNA attached to the surface by PEG molecules but it is certainly necessary to maximise the uptake, this has been extensively studied and nanostructures covered by ssDNA turned out to be more efficiently internalized than those with dsDNA.

In this thesis, however, the focal point was to optimise the amount of oligonucleotides that can be delivered in the form of duplex DNA and released in a controlled way. For this purpose, additional experiments had to performed in order to determine the optimal range of dsDNA surface coverage for uptake. This strategy can be extended by testing different approaches for lysosome bursting; in addition to, or instead of, the "proton sponge approach", NIR laser heating may offer a credible alternative. Numerous sources indicate that nanoparticles have a tendency to accumulate after endocytosis; heating them could potentially destroy the lysosome membrane without causing additional harm to the recipient cell. This idea needs to be experimentally tested.

Of course, at the present moment, a medical approach which uses thermal bursting of lysosomes inside human tissues is not feasible because of the huge differences with controlled conditions in cell culture; dangers of necrosis leading to immune responses and so forth currently limit the *in vivo* clinical applicability.

However, the successful uptake and release of quantified doses of oligonucleotides into the cytoplasm at chosen times is a tangible possibility and we are at the beginning of a fascinating research era. Control of the number of GNRs in single cell and knowledge of the exact quantity of biologically active DNA/RNA associated with the GNRs opens up the way to follow biological activity in a way that has been hitherto impossible. Therefore, as well as being applicable for gene therapy, this approach opens up the possibility of finely tuned dose response therapy and the control of complex cellular processes.

A final issue concerns the use of pegylated nanoparticles in the presence of serum to determine the efficiency of specific targeting in association with techniques such as confocal/TIRF microscopy.

In conclusion, the study with cell cultures of the objects developed in this thesis is not only a prerequisite step before clinical experiments, but should become the object of a separate project with a high impact for understanding complex mechanisms in cell biology.

2. Materials and Methods

Introduction

The type of nanocarrier that is required depends upon the conditions under which the material will be prepared; in our case the goal is large-scale, highly reproducible synthesis and this requires rapid characterisation methods that allow control over the process at each step of surface modification. In order to fulfil these aims I decided to focus on optical methods for nanoparticle quality evaluation for thiol-based surface functionalisation and for strand hybridisation and thus to use absorption and fluorescence measurement; the final product being an effective characterisation protocol.

2.1. Chemical compounds

2.1.1. Non-organic products

Agarose, Phosphate Buffer Saline (PBS), Cetyl trimethylammonium bromide (CTAB), Chloroauric acid, Sodium borohydrate, Silver nitrate, L-ascorbic acid, SH-PEG_{6000}, were purchased from Sigma-Aldrich. Tris-borate-EDTA buffer (TBE) was prepared in the laboratory with components from Sigma-Aldrich.

2.1.2. Oligonucleotides

All nucleotides were purchased from Sigma-Aldrich. The number of bases of each sequence is indicated in the table below.

Table 1: oligonucleotides sequences and codes used during this thesis

DNA name	Sequence (5'-3')
SH-DNA40-Cy3	SH-C6-TTT TTC CAT CTG TCA CTC GGA TCC GCC ATC TTG CGA CTC G- **Cy3**
DNA23-Cy5	**Cy5**- TGG CGG ATC CGA GTG ACA GAT GG
DNA35-Cy3	CCA TCT GTC ACT CGG ATC CGC CAT CTT GCG ACT CG-**Cy3**
DNA35	CGA GTC GCA AGA TGG CGG ATC CGA GTG ACA GAT GG

DNA35-Cy5	**Cy5**-CGA GTC GCA AGA TGG CGG ATC CGA GTG ACA GAT GG
DNA35-Cy5-nC	**Cy5**- GCT CAG CGT TCT ACC GTA TAT TCT CAC TGT CTA CC
DNA50-Cy5	**Cy5**-TCG AAT ACT GCT AGA CGA GTC GCA AGA TGG CGG ATC CGA GTG ACA GAT GG
hDNA-Cy5	**Cy5**-CGC TCC CTA TTA TTA TTC GAG CGT TTT TTT TTT-C3-SH

Some of the oligonucleotides were end-labelled with fluorophores: Cyanine3 (Cy3), Cyanine5 (Cy5),.

Three groups of DNA were used in the experiments:

1) SH-DNA40-Cy3, DNA35-Cy3,
2) DNA23-Cy5, DNA35, DNA35-Cy5, DNA50-Cy5 - these oligonucleotides are complementary to group 1,
3) DNA35-Cy5-nC, oligonucleotide non-complementary to group 1 (nC is an acronym for "non-complementary") as controls.

Emission measurements (using a Varian Cary Eclipse Fluorescence Spectrophotometer) of samples containing more than one type of oligonucleotide were used for FRET measurements (therefore covering the range of emission for both dyes). In the case where only one type of DNA was used the spectrum range covered the single fluorophore emission. Labelling the thiolated oligonucleotides with fluorophore was used to obtain information about the coverage density. Pairing it with a dye able to trigger FRET was designed to provide proof of hybridisation on the surface. Thiolated strands without dye were used to check the influence of the fluorophore attached to the complementary strand by examining the influence of plasmon on the fluorophore. We also used different length oligonucleotides.

Table 2: excitation wavelengths for different fluorophores and the range of measurements

Fluorophore	Excitation [nm]	Aquisition range [nm]
Cy3	530	550 - 800
Cy5	630	650 - 800
Cy3 + Cy5 (FRET)	520	550 - 800

2.2. Technological processes

2.2.1. Gold nanorod synthesis in the presence of CTAB

The first step in the experimental part of this project was to produce gold nanorods (GNRs) with high monodispersity. The 2-step wet synthesis of gold nanorods consisted of first the preparation of a seed solution (small nanoparticles of 2 nm diameter) from which nanorods were grown in a second step[82]. The $NaBH_4$ solution was ice-cold (to avoid thermal decomposition) and all other solutions were kept at 28 °C in order to avoid CTAB crystallization.

The initial step involved seed formation in which small nanoparticles were formed. A solution of 900 µL of ice-cold $NaBH_4$ at 0.01M was injected into a mixture containing 9.8 mL of 0.1 M CTAB and 250 µL of 0.01M $HAuCl_4$. After 2 min of vigorous stirring this seed solution was directly added to a growth solution pre-prepared by diluting 0.1 M CTAB and 2.5 mL of 0.01 M $HAuCl_4$ into a final volume of 50 mL. After 10 min incubation, 375 µL of 0.1 M L-ascorbic was injected for gold (III) reduction to gold(I). Gentle mixing caused the pale-orange solution to become colourless indicating that the reaction had occurred. Next, 400 µL of 0.005 M $AgNO_3$ was added. The solution with growing nanoparticles was incubated for 2 hours. In order to remove the excess of chemicals from the growth solution and to decrease the concentration of CTAB from 93 mM to 5 mM, the growth solution was rinsed twice. The rinsing process consisted of centrifugation, removal of the supernatant and re-dispersion of the GNRs in pure water. To characterise the GNRs colloidal solution, the absorption spectrum was measured and the GNRs were visualised using transmission electron microscopy (TEM).

To improve the yield of synthesis, I decided to further optimise the synthesis protocol. The way to improve the yield without compromising the mono-dispersity of GNRs solution involved decreasing the scale of synthesis and to work under constant stirring (magnetic stirrer). In addition, I noticed that maintaining a constant temperature (28 °C) provided better quality but reduced the overall concentration of GNRs. As a final approach the reaction vessel was placed on a heating plate and stirred magnetically. However, this did not allow precise control of the temperature, although solution mixing turned out to be more important in obtaining monodisperse GNRs.

From a chemical point of view, the tests on seed solution concerned the amount of added $NaBH_4$ (0.01M) in the range 600 µl to 1200 µl. The optimal was 900 µl and this was then used for the comparison of solution colour (the darkest one was selected).

In the case of $AgNO_3$ two different concentrations were tested: 0.005 M and 0.010 M; 0.005 M turned out to be more preferable.

Major changes were made for seed addition: in the initial protocol this involved 600 µL (upscaling to a larger growth solution scale would then be equal to 50 mL), but I increased its volume to 10 mL. This increased the number of synthesized GNRs (as observed by changes in reaction solution colour) and did not influence their morphology (as seen by extinction spectrum measurements).

The purification method applied in the protocol is described in chapter 3.

2.2.2. Centrifugation

Centrifugation was a necessary step in every experiment because it allowed removal of an excess of chemicals from the colloidal solution after the incubation steps for bio functionalisation, adjusted the GNRs concentration and the composition of the solution without increasing the final volume. 50mL and 15 mL tubes samples were centrifuged at 7400 rcf for 60 and 30 min respectively. In the case of 1.5 mL tubes centrifugations were at 6500 rcf, 15 min for 200 µL and 8000 rcf, 30 min for 1000 µL. Adapting the centrifugation speed and time had a huge influence on the nature of the samples as it could cause irreversible nanoparticle aggregation (especially if they were functionalised with oligonucleotides). The result of centrifugation was usually GNRs pelleted at the bottom of the tube, however in situations where nanorods were previously destabilised by charge changes (e.g. attachment of oligonucleotides), this caused a pink-red precipitant to be deposited on the walls of the Eppendorf tubes.

2.2.3. Hybridisation

The functionalisation of gold surfaces requires the presence an amine/thiol group which is able to react with surfaces; in this thesis the SH- group was selected due to its stability. As the purchased oligonucleotides had oxidised SH- groups as S-S, chemical activation was needed. For this purpose aqueous 10 mM tris(2-carboxyethyl)phosphine (TCEP) with 50 µM oligonucleotides (from 100 µM stock) were incubated for 4 hours at room temperature. This was followed by centrifugation through a column (Micro Bio-Spin Columns) (4 min, 1000 rcf) to a final concentration of SH-DNA measured optically (NanoVue Plus Spectrophotometer). The final solution was aliquoted into 25 µL portions and stored at -20 °C. The process of functionalisation, a major part of this thesis is described in chapter 3.

Formation of double stranded DNA (dsDNA) on the surface of nanoparticles was a crucial point for bio functionalisation. As the main part of the work carried out here was with oligonucleotides forming 35 base pair duplexes (e.g. SH-DNA40-CY" and DNA35- Cy5), with high guanine-cytosine content, the melting temperature was 86.5 °C. The desired end point of the technological process requires hybridisation between strands; one of them being already attached to GNR by thiol-gold bonds. Therefore the conditions for hybridisation should not disrupt this bond; the thermal stability of the thiol-gold bond is about 80 °C[83]. The effect of gold nanoparticles proximity is described in the literature as being essentially to decrease the DNA melting temperature[84]. The hybridisation temperature was set to 70 °C for 5 min, but with a long (overnight) cooling process as a compromise for bringing the colloidal solution condition as close to the melting temperature as possible, with respect to thiol-gold bond stability. This high melting temperature was useful from the point of effective temperature measurements, as discussed in chapter 5.

2.3. Absorption

2.3.1. Theoretical introduction

Absorption spectroscopy of gold nanoparticles allows characterisation of their shape, their concentration and their colloidal stability. In this thesis it was crucial to measure the absorption spectra at each step of both synthesis and bio functionalisation in order to control that the absorption bands of GNRs do not vary upon treatment. Indeed, the NIR light conversion into thermal energy highly depends on the position of the NIR absorption band of GNRs. However, the measurements performed in the presence of GNRs are limited to extinction measurements, because the size of the nanorods is sufficient to cause scattering (extinction = absorption + scattering). This allowed estimation of nanoparticle concentrations at every step of the experiment as well as detection of the presence of oligonucleotides in the samples.

2.3.2. Measurements

Extinction measurements were carried out on a spectrometer (BioTek Instruments Uvikon XL UV-Visible) between 220-900 nm if the samples contained oligonucleotides as DNA absorbs light at 266 nm and between 400-900 for GNRs solution before functionalisation. The polymer cuvette of Eppendorf was used and 150 µL of sample and 300 µL for references were measured. Differences in volume were due to the use of a special holder allowing measurement of smaller amounts of material (especially when using precious functionalised

GNRs). References were composed of a solution of water, PBS or surfactants without the GNRs. The baseline was measured twice to reduce the noise caused by heating up by the lamp.

2.3.3. Data analysis

The absorption spectra of GNRs in solution are useful to define their shape, concentration and stability. For this purpose the range 400-900 nm was the most important, because the shape of the absorption transverse peak can provide information about nanorods deformations, and following the longitudinal peak gives information on the size, uniformity, and eventual presence of aggregates. Peak positions provide information about the size and aspect ratio of the most populated GNRs species[85]. The transverse peak is associated with plasmon properties coming from the diameter, whereas the longitudinal peak is associated with the length. An additional parameter is full width at half-maximum (FWHM) used for aspect ratio determination[86]. It is crucial to be able to calculate the concentration of GNRs using absorption spectra of colloidal solutions.

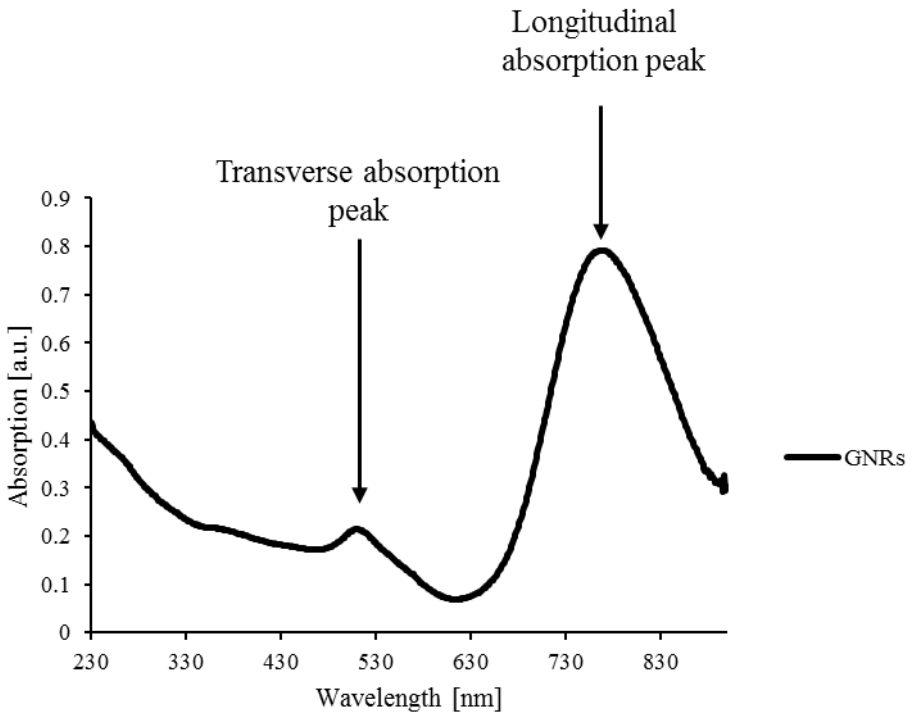

***Figure 1**:Typical absorption spectrum of GNRs. Arrows indicate the absorption maxima.*

According to the literature[88] it is possible to quantify GNRs concentration using the Lambert-Beer law:

$$A = l \cdot \varepsilon \cdot c$$

A = absorbance

l = optical pathway [cm]

ε = extinction coefficient [$M^{-1}cm^{-1}$]

c = concentration [M]

Expressing the concentration of nanoparticles in molarity is not completely correct, as their population is defined by different extinction coefficients, depending on individual shape and size (it would be more accurate to use gold concentration instead). Additionally, molarity refers to molecules, not objects with unknown (populations with different volume) mass. On the other hand, it is possible to calculate the extinction coefficient of single GNRs with a given size considering a monodisperse GNRs solution. It is important to determine the concentration of GNRs in solution so as to adjust the concentration of thiolated DNA in solution to control the surface density of DNA immobilised on the GNRs surface.

The literature[88] contains four calculated values for longitudinal peak positions, however in my experiments the peak was usually inbetween the indicated ones. A linear dependence was seen between the extinction coefficient and peak position (Figure 2) allowing calculation of the extinction coefficient for absorption maximum in the range 600-850 nm. Therefore, this allowed quantification of GNRs at every step of functionalisation (the peak was often shifting during the processing) using a simple formula for the extinction coefficient according to peak position.

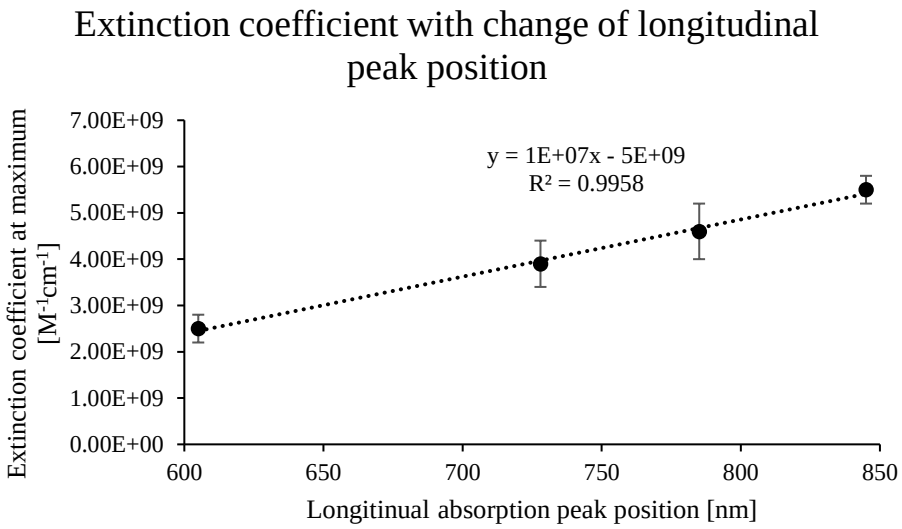

Figure 2: *The dependence between longitudinal peak position and the extinction coefficient of maximum. Values and deviation based on literature*[88].

The accuracy of optical-based quantification of gold nanoparticles is a subject of discussion[87]. However, a detailed study[88] provided values of transverse extinction coefficients according to different aspect ratios; this impacts on the accuracy of the calculations (different size nanoparticles were tested), because it can be compared with results obtained using longitudinal extinction coefficient. I followed changes of transverse peak position in the range 508-522 nm. Concentrations of GNRs with larger half-widths (e.g. caused by biofunctionalization) could be calculated. Calculating concentrations from this peak provided information on colloidal solutions with higher nanostructure dispersity.

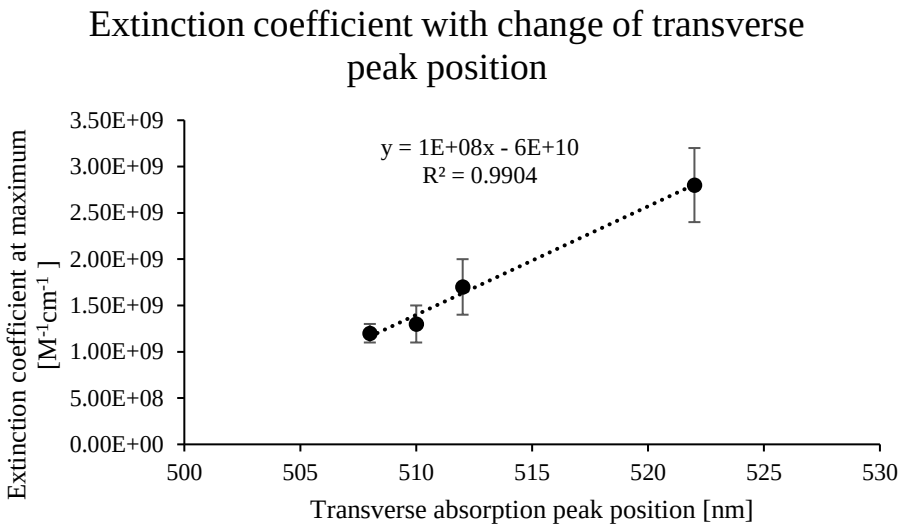

Figure 3: *The dependence based on data from the literature[88] of extinction coefficient at transverse absorption maximum to the position of that peak.*

By measuring GNRs absorption spectrum it is possible not only to calculate nanoparticle concentrations, but also to indicate the presence of oligonucleotides, which is rather relevant to this thesis. However, there is little information to be obtained from the DNA absorption peak at 266 nm of nucleotides immobilised on GNR surfaces (oligonucleotide absorption does not change when attached to gold surfaces). The few centrifugation steps remove all free DNA from the system, but may cause nanoparticle loss at the same time. There is a difference in absorption coefficient between ssDNA and dsDNA, but in a system containing GNRs and surfactants, I decided not to use it for hybridisation quantification. The reason being that the low values of both the peak and the change associated with duplex formation could be misinterpreted. An additional possible change of the extinction spectrum was a shift of the longitudinal absorption peak due to surrounding refractive index variations.

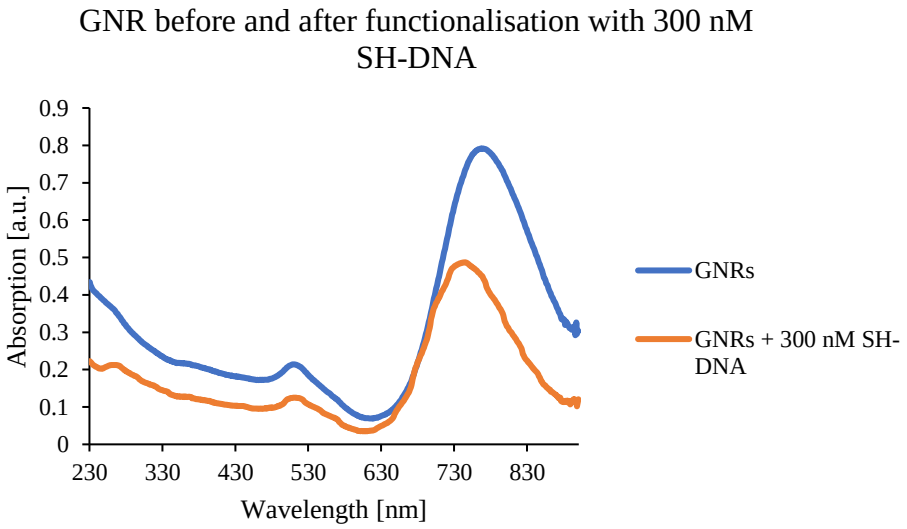

Figure 4: *Changes upon immobilisation of thiolated oligonucleotides and subsequent rinsing. The absorption spectrum was modified in terms of peak positions and intensity values. The calculated concentration of the stock solution was 0.179 nM, whereas after functionalisation it was 0.109 nM.*

There are clear changes in the absorption properties of GNRs before and after incubation with 300 nM thiolated ssDNA (Figure 4). First, during the process of functionalisation and rinsing, some nanoparticles are lost (strong decrease in the intensity of transverse and longitudinal peak values). Additionally, the longitudinal absorption peak is blue-shifted, therefore the local refractive index has changed certainly caused by the replacement of the CTAB layer by oligonucleotides on the surface of GNRs[89]. In addition, a peak at 266 nm cannot discriminate between oligonucleotides in solution and those attached to GNR surfaces via gold-thiol bonds.

2.4. Fluorescence

2.4.1. Theoretical introduction

Fluorescence emission arises from the relaxation of a photon from an excited single state to the ground state. The excitation state is obtained after the fluorophore absorbs light at a specific wavelength that depends on the fluorophore properties. The emission wavelength also depends on the fluorophore properties. The difference (in wavelength or frequency units) between positions of the band maxima of the absorption and emission spectra (fluorescence and Raman being two examples) of the same electronic transition is called the Stokes shift. The

quantum yield is a measure of the efficiency of photon emission and is defined by the ratio of the number of photons emitted to the number of photons absorbed.

Table 3: Fluorophore properties

Fluorophore	Quantum yield [%]	Absorption, emission maximum [nm]
Cyanine3	15 [90]	548. 561
Cyanine5	27 [91]	647. 665

Since the fluorescence emission depends on the electromagnetic field, the proximity of a plasmonic structure such as a GNR can lead to two competing phenomena depending on the distance between the fluorophore and the gold surface[92]: 1) at short distances, quenching caused by energy transfer to the plasmonic structure, 2) at larger distances, exaltation due to the creation of localised electromagnetic fields around the plasmonic structure.

2.4.2. Measurements

Samples were placed in polymer cuvettes to a final volume of 800 µL -1000 µL (800 µL is the minimum possible volume that can be measured with such cuvettes in this spectrofluorometer). Excitation was carried out with a slit of 5 nm, emission with 10 nm. The voltage in the lamp was set to 700 volts. Measurements were done over 2 ranges: 550-800 nm (Cy3), excitation 530 nm or 520 nm (only for experiments with FRET); 650-800 nm (Cy5), excitation 630 nm.

2.4.3. Data analysis

In most of the experiments the results of fluorescence emission intensity measurements are presented either as whole emission spectra (Figure 5), or as the intensity of emission maximum. In the case of emission spectra the measurement (and graphs) covered the emission maximum peak (if present) and the zone without noticeable fluorescence emission intensity (background) as shown in Figure 5, 750-800 nm.

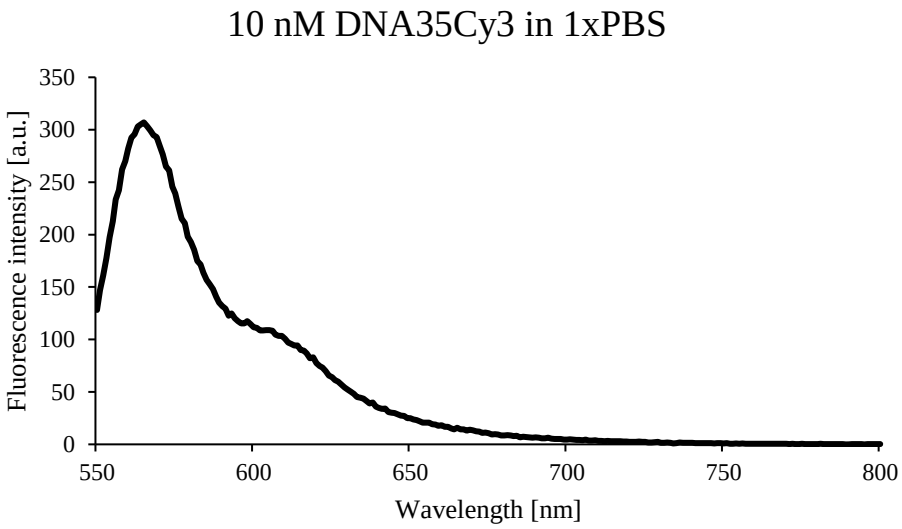

Figure 5: *Cy3 fluorescence emission spectrum. The maximum of emission intensity is 561 nm, the excitation was carried out at 530 nm.*

At this point the issue of fluorescence excitation and emission intensity in the presence of nanoparticles had to be taken into account. For this purpose I carried out two sets of experiments prepared in parallel: first with DNA35-Cy3 in 0.95x PBS and 0.1 % Tween20, second with GNRs functionalized with SH-DNA40 (without fluorescent labelling) and SH-PEG in the same medium. The ligands were supposed to prevent non-specific interactions between gold surfaces and non-thiolated oligonucleotides; deposition onto GNRs would cause Cy3 quenching.

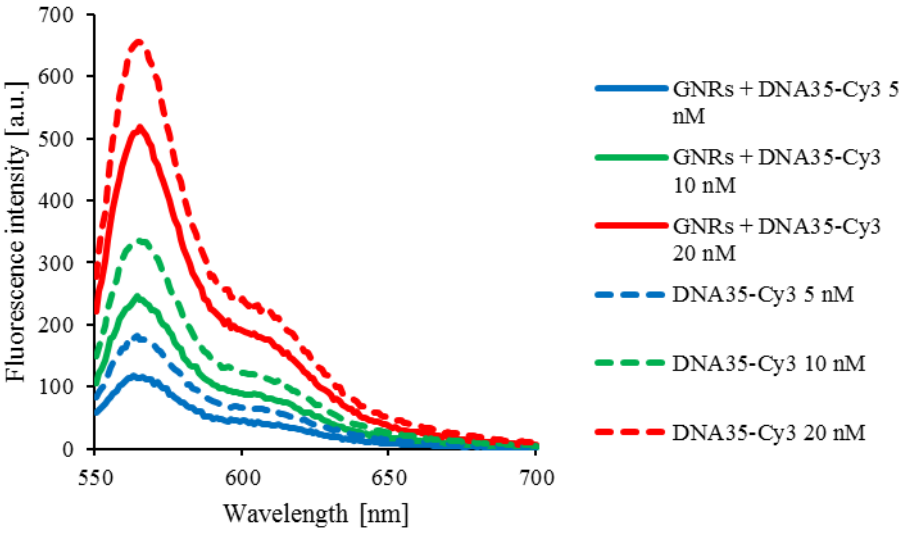

Figure 6: *Influence of GNRs absorption and scattering on Cy3 emission. Nanorods were functionalised with SH-DNA40 and SH-PEG in order to decrease non-specific interactions between gold surface and DNA35-Cy3. Excitation was done at 530 nm.*

In the presence of GNRs, Cy3 emission decreased (Figure 6); there are three main reasons for such behaviour: absorption, screening and scattering. The colloidal solution at the nanoparticle concentration used is pale-pink, therefore there is effective absorption. The absorption spectrum of Cy3 overlaps with the transverse plasmon peak, so screening occurs. Additionally, the presence of nanoparticles causes scattering, decreasing even more the registered signal.

2.5. Förster Resonance Energy Transfer (FRET)

2.5.1. Theoretical introduction

FRET is a non-radiative energy transfer phenomenon occurring between two fluorophores, a donor and an acceptor through dipole-dipole coupling. The necessary condition for its occurrence is a short distance between the two fluorophore and the overlapping of the donor emission spectrum and the acceptor absorption spectrum[93]. FRET results in the decreased emission of the donor fluorescence while excited and the increase of the acceptor emission. The efficiency of FRET can be described by (based on equation transformation[94]):

$$E = \frac{k_{ET}}{k_f + k_{ET} + \sum k_i}$$

E = FRET efficiency

k_{ET} = rate of energy transfer

k_f = radiative decay rate

k_i = rates of other de-excitation phenomena

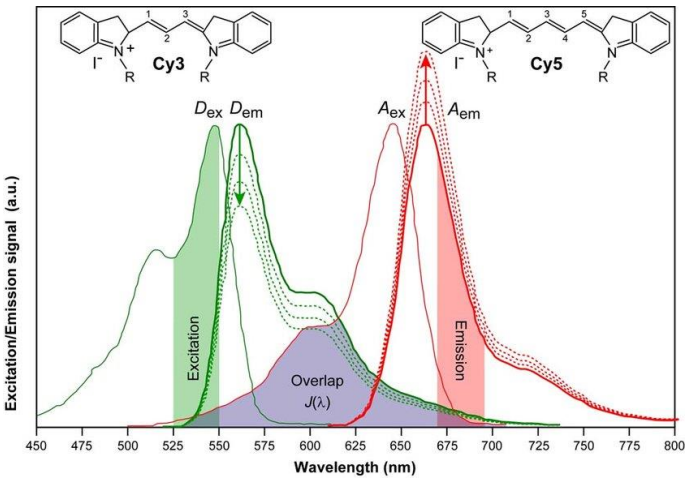

Figure 7: *FRET between Cy3 and Cy5. The donor (D) in this pair is Cy3and the acceptor (A) is Cy5. The graph presented is reproduced from the publication of H. C. Ishikawa-Ankerhold et al.*[95]

Additionally, there is a strong dependence of the distance between the donor and the acceptor for FRET to occur (based on equation transformation[94]):

$$E = \frac{1}{1 + \left(\frac{r}{R_0}\right)^6}$$

E = FRET efficiency

r = distance between fluorophores

R_0 = Förster distance (distance for pair of fluorophores at which FRET efficiency is equal to 50 %)

The Förster distance of the fluorophore pairs I used (Cy3-Cy5) is below 10 nM. The strong distance-dependence of FRET phenomena (distance factor is power of 6) has attracted a lot of attention in the field of nanotechnology, becoming a sort of nano-ruler, especially useful for the detection of reaction/conformation changes in biological samples[96,97,98].

Experimentally the FRET efficiency is best characterised by the decrease of donor emission, because of different de-excitation phenomena and the acceptor quantum yield (not all of the energy transferred from donor goes to the acceptor)[93,94].

$$E = 1 - \frac{F_{DA}}{F_D}$$

E = FRET efficiency

F_{DA} = fluorescence intensity of the donor in the presence of acceptor

F_D = fluorescence intensity of the donor in the absence of acceptor

2.5.2. FRET in this thesis

The experiments covering CTAB-DNA interactions were performed using FRET, because it follows variations of the spatial organisation of oligonucleotides in solution as a function of CTAB concentration. Two solutions were prepared: 1) CTAB solutions at concentrations ranging from 0 to10 mM in water, 2) CTAB solutions at concentrations ranging from 0 to10 mM in 1xPBS. Cy3- and Cy5-labelled DNA were added either one after the other with a 2 minutes incubation time between the two, or premixed in water or PBS at equal concentrations and then added to the CTAB solutions. The FRET of all samples was then measured and strong differences indicated that CTAB strongly influenced the distribution of DNA in solution: FRET only occurred when both DNAs were premixed even if the two strands were not complementary while no FRET could be detected with a step by step addition (Chapter 3).

2.5.3. Results analysis

The first step was to check the positions of the donor and acceptor peaks. As indicated in Figure 8 the emission peak of the donor could influence the measured value of acceptor (the donor slope probably overlapping the Cy5 maximum). In order to correct for this and extract only Cy5 emission values, a calculation of Cy3 emission values in the range of Cy5 emission was conducted. After defining the wavelength of the Cy5 maximum, this was adjusted using the theoretical value of Cy3 emission for the same wavelength.

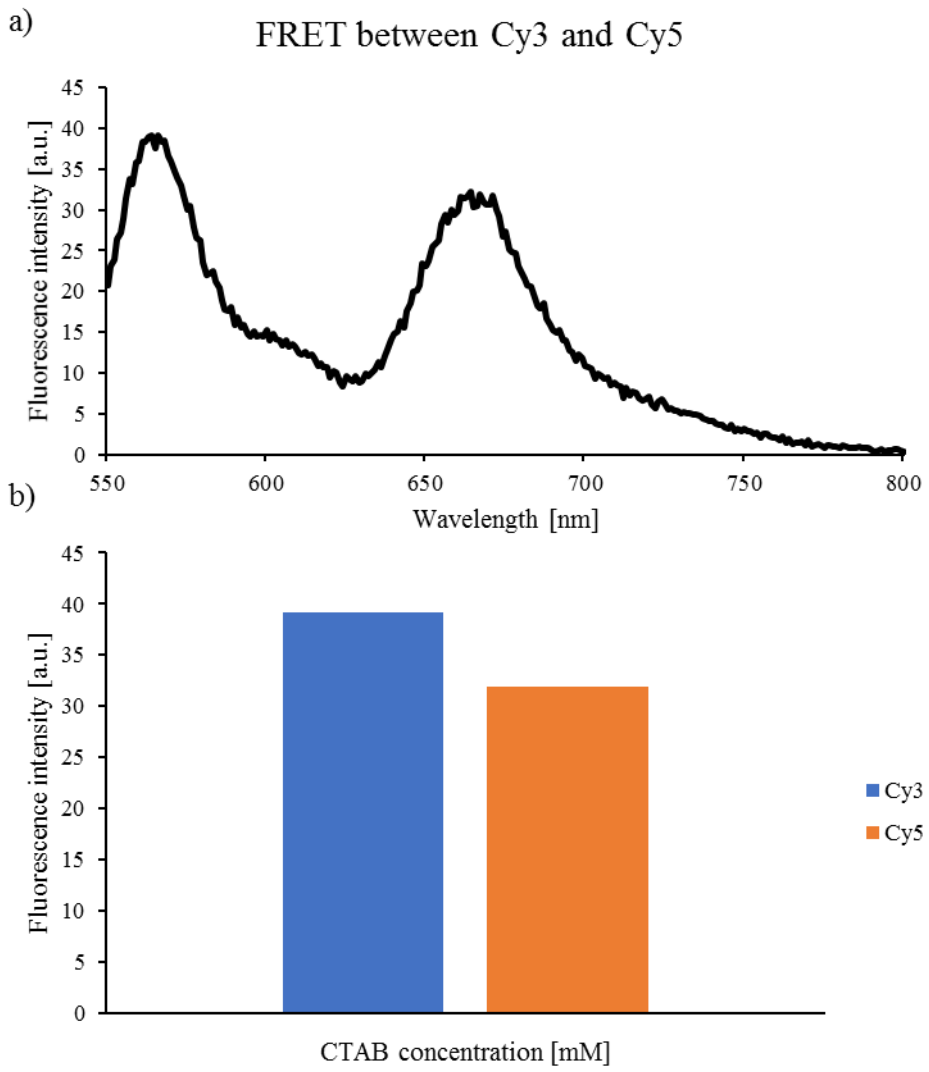

Figure 8: *a) FRET between 10 nM DNA35Cy3 and 10 nM DNA35Cy5 in 1xPBS solution incubated for 10 min at room temperature. The emission peak of Cy3 was recorded at 565 nm, and the emission peak of Cy5 at 667 nm. b) On the bottom graph is represented the intensity of the Cy3 and Cy5 at the maximum of the emission wavelength as a function of the sample conditions (here 1 mM CTAB).*

2.6. Agarose gel electrophoresis

2.6.1. Preparation

Agarose gels was prepared by heating a mixture of 0.4 g of agarose with 50 mL of 1xTBE buffer in a microwave oven until the agarose dissolved, however avoiding boiling to limit water evaporation. This was left for 5 min at room temperature to cool down before

pouring the gel. Gels were used just after solidification. The resulting 0.8 % agarose gels had a density permitting GNRs to enter and migrate within.

2.6.2. Electrophoresis and data analysis

After placing the gel in a large volume of 1xTBE, samples were loaded into the wells of the gel. Loading the samples was easier when the sample solutions were premixed with glycerol to increase the density. The potential was set to 50 V and left to run for 30, or 40 min, depending on the experiment. After running, the gel was placed under a Typhoon scanner and checked for fluorescence of Cy3-Cy5. When the concentration of GNRs is high enough it is also possible to perform measurements of total absorption to see the position of the GNRs in the gel (Figure 9).

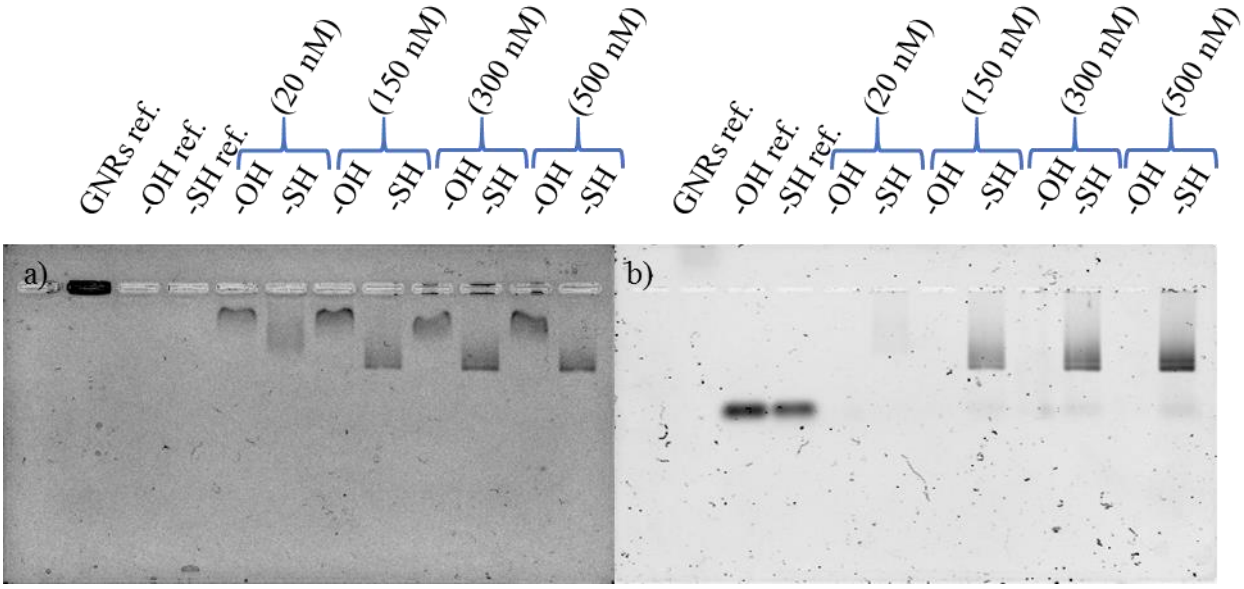

Figure 9: *Left, gel image scanned for absorption; right: Cy3 emission intensity measurements, excitation of Cy3 is fixed at 548 nm, non-thiolated DNA, DNA35-Cy3 was marked as -OH, thiolated DNA, SH-DNA40-Cy3, described as -SH. References DNA samples were set at 20 nM.*

The migration of DNA into the gel will depend on whether they are attached to the GNRs or free in solution. For DNA immobilised on the GNRs surface, the emission of fluorescence will therefore be detected at the same level than the migration bands of GNRs (measured in absorption, image on the left) while the free DNA will migrate with the DNA control or reference (Figure 9).

In the case of gels examined in absorption mode three main features were determined visually: aggregation, migration distance and shape of the band. Analysis in the case of

fluorescence measurement was performed by delineating the area of interest of the gel by a rectangular generated by the relevant software (an example is shown in Figure 10).

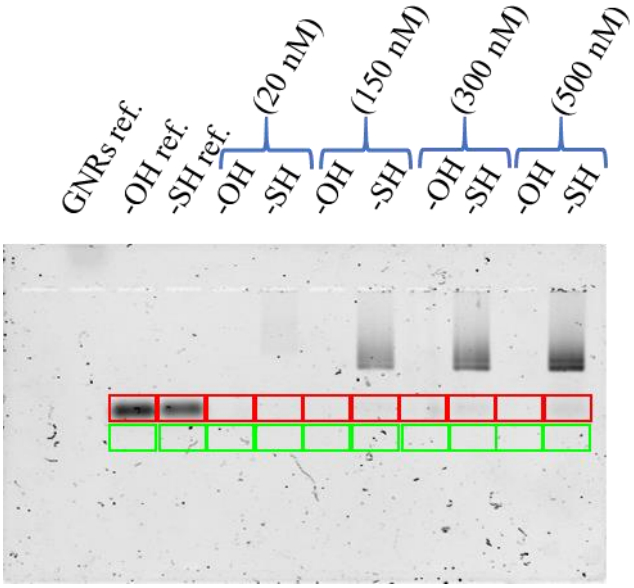

Figure 10: *The marking used in gel fluorescence analysis. Red rectangles were used to quantify the signal intensity in samples and green rectangles were used for background measurements.*

In some gels the background was visibly not uniform (smear, or non-uniform background fluorescence). The size of the rectangles depended on the gel but were of the same size on any one gel. The detected signal was averaged over the surface of the rectangles. A good example of the whole process is shown in the experiment performed to obtain the standard deviation (please see chapter 4, Table 1).

In order to calculate the standard deviation, the emission intensity in the bands was identified and marked by rectangles. Within the rectangle, the average fluorescence emission intensity was calculated and the results are shown in Table 4. The background emission values were also measured and the results of sample fluorescence could then be corrected. This allowed calculation of the average emission and standard deviation.

Table 4: emission intensity obtained from agarose gel

Samples emission intensity [a.u.]	782.38	781.41	777.47
Background [a.u.]	289.96	297.08	294.50
Samples correction	492.42	484.33	482.97
Average result	486.57±5.11 (1.05 %)		

In this example the whole analysis process can be followed; first by identifying rectangles associated with samples and obtaining the average emission. Secondly, doing the same to get background noise values. Next, the sample emission was corrected for the background. Analysis of three experiments gave a standard deviation for this approach.

The same steps were performed to determine the concentration of labelled DNA; in this case the corrected samples emission values were compared to references with known amounts of oligonucleotides.

2.7. Zeta potential measurements

2.7.1. Theoretical background

The zeta potential is a measurement of the charge of the layer surrounding nanostructures. It is widely used for analysis of structures made by layer-by-layer techniques where layers may have different charge (this type of deposition is often based on electrostatic principles). In the case of GNRs the charge of unmodified particles is positive, whereas oligonucleotides are negatively charged. As a result, successful functionalisation should cause switching of the detected charge from positive to negative. The importance of zeta potential measurements in this context is to predict colloidal solution behaviour, because values from -30 up to +30 suggest possible aggregation.

2.7.2. Samples preparation

Zeta potential in this thesis was used for GNRs functionalised only with oligonucleotides also used for fluorescence measurements and gel electrophoresis. After fluorescence measurements (during which GNRs were in 1xPBS, 1% Tween20) it was necessary to reduce the number of ions in the samples, therefore centrifugation was performed with subsequent rinsing by Milli-Q water. Such samples were placed in cuvettes and measured immediately on a Malvern instrument.

2.7.3. Analysis of the results

The zeta potential expressed in mV for single samples is not very discriminatory to characterise functionalised nucleotides since similar zeta potential value can be obtained for a wide range of immobilised DNA. Additionally, it is not possible to distinguish between oligonucleotides attached via thiol bonds or electrostatically. However, the zeta potential technique, because it is semi-quantitative, became popular for evaluating processing steps such as oligonucleotide attachment and layer deposition. It encounters drawbacks when it is used in

the context of a surface-liquid interface. Oligonucleotides immobilised via electrostatic interaction and thiol-gold bond may change the local charge by a similar amount indistinguishable by zeta potential measurements.

3. DNA-CTAB interactions

Introduction

In order to develop a nano cargo that would release a known amount of drugs upon light induced thermal release, the nanomaterial has to be stable in a colloidal solution: the size and shape of the GNRs has to remain constant upon bio functionalisation and cellular uptake. Nanomaterials need to have high absorption in NIR, in order to be efficiently heated up for dsDNA denaturation for release without degrading the nanoparticles and DNA, and without affecting the cells. Therefore, it is important to avoid aggregation as it modifies the overall extinction spectrum, shifting the longitudinal maximum toward the red. Moreover, larger nanostructures scatter light more efficiently, so the temperature increase will be less controlled. Further requirements are associated with the characterisation methods and stability of the hybrid system. We chose to use the fluorescence emission from DNA attached to GNRs and use the variation of emission to detect the light induced release of ssDNA. Additionally, as the time between nanomaterial synthesis, functionalisation and measurements in cells can vary and be up to a few days it is crucial that the overall monohybrid is stable in time. This is connected with the stability of dsDNA on the surface after hybridization; duplex degradation will impact fluorescence emission.

To summarise, all the following points have to be fulfilled in order to obtain efficient cargo nanoparticles for drug delivery:

1) Stable colloidal solution
2) High absorption in NIR (no aggregates)
3) The fluorescence signal emitted from labelled DNA attached to the surface has to be detectable
4) Similar optical properties between different functionalisation over long periods (absorption, fluorescence signal)
5) Controlled hybridisation between complementary strands in solution and the ssDNA bound to the GNRs surface at a specific density
6) Stability of GNRs covered by dsDNA.

In addition, biocompatibility and cell uptake need to be also optimised.

3.1. Gold nanorods synthesis and stability in water solution

3.1.1. Gold nanorods synthesis in the presence of CTAB

The first step in the experimental part of this thesis was to produce gold nanorods (GNRs) with high monodispersity. The 2-step wet synthesis of gold nanorods consisted of the preparation of a seed solution (small nanoparticles of 2 nm diameter) from which nanorods are grown in the second step[99].

As described in Chapter 2, Materials and Methods, the initial step involved seed formation in which small nanoparticles were formed. A solution of 900 µL of ice-cold $NaBH_4$ at 0.01M was injected into a mixture containing 9.8 mL of 0.1 M CTAB and 250 µL of 0.01M $HAuCl_4$. After 2 min of vigorous stirring this seed solution was directly added to a growth solution pre-prepared by diluting 0.1 M CTAB and 2.5 mL of 0.01M $HAuCl_4$ to a final volume of 50 mL. After 10 min of incubation time, 375 µL of 0.1M L-ascorbic acid was injected for gold (III) reduction to gold(I). Gentle mixing caused the pale-orange solution to become colourless indicating that the reaction had occurred. Then, 400 µL of 0.005 M $AgNO_3$ was added to allow the growth of nanorods. The solution with growing nanoparticles was incubated for 2 hours.

In order to remove the excess of chemicals from the growth solution and to decrease the concentration of CTAB from 93 mM to 5 mM, the growth solution was rinsed twice. The rinsing process consisted of centrifugation, removal of the supernatant and re-dispersion of the GNRs in pure water. Table 1 lists the composition and concentrations of each element in the seed and growth solutions. To characterise the GNRs colloidal solution, the absorption spectrum was measured and the GNRs were visualised using transmission electron microscopy (TEM).

Table 1: Composition and final concentration of the seeds and GNRs growth solution

Seed solution	
Component	Final concentration
CTAB	89.5 mM
$HAuCl_4$	0.2 mM
$NaBH_4$	0.8 mM
Growth solution	
CTAB	93.1 mM

$HAuCl_4$	0.39 mM
L-ascorbic acid	0.56 mM
$AgNO_3$	0.03 mM

3.1.2. TEM images of GNRs and size distribution

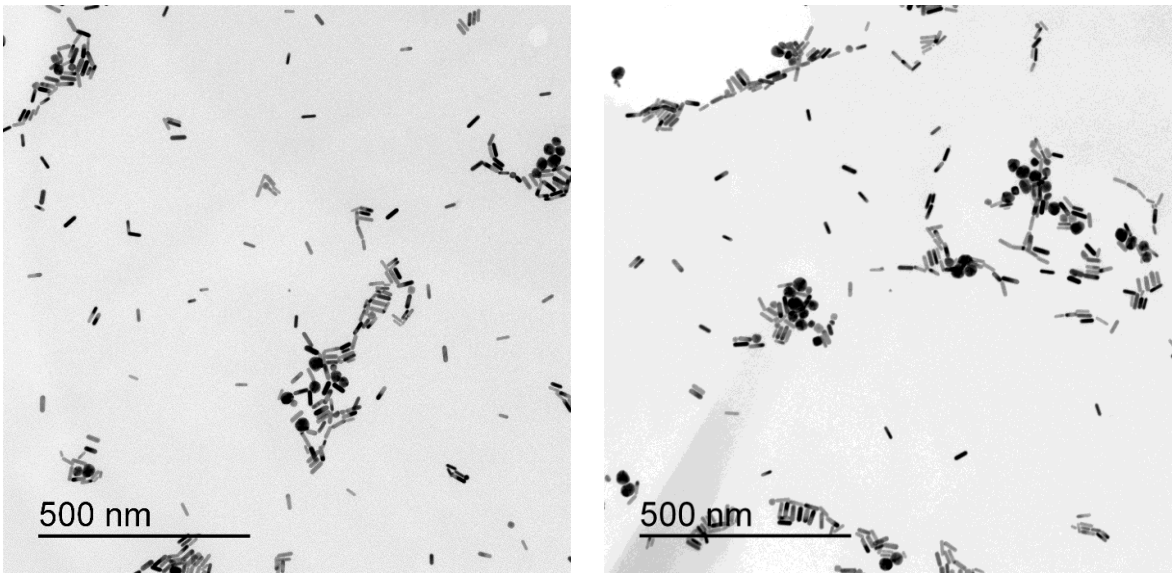

Figure 11: TEM images of GNRs produced following a 2-step wet synthesis.

The TEM images indicate the presence of a majority of nanorod shaped gold nanoparticles and the presence of large sphere-shape structures (Figure 1).

The TEM images were further analysed using ImageJ software, in order to calculate the average size of GNRs and extract the typical GNRs aspect ratio. Initially a threshold of intensity was applied to remove the background. This approach meant that many GNRs were not considered because they were too close to each other to characterise them individually. In addition, most of the spherical-shaped nanostructures were in agglomerates, therefore not counted. Additionally, a surface area threshold was used to eliminate structures that were too large.

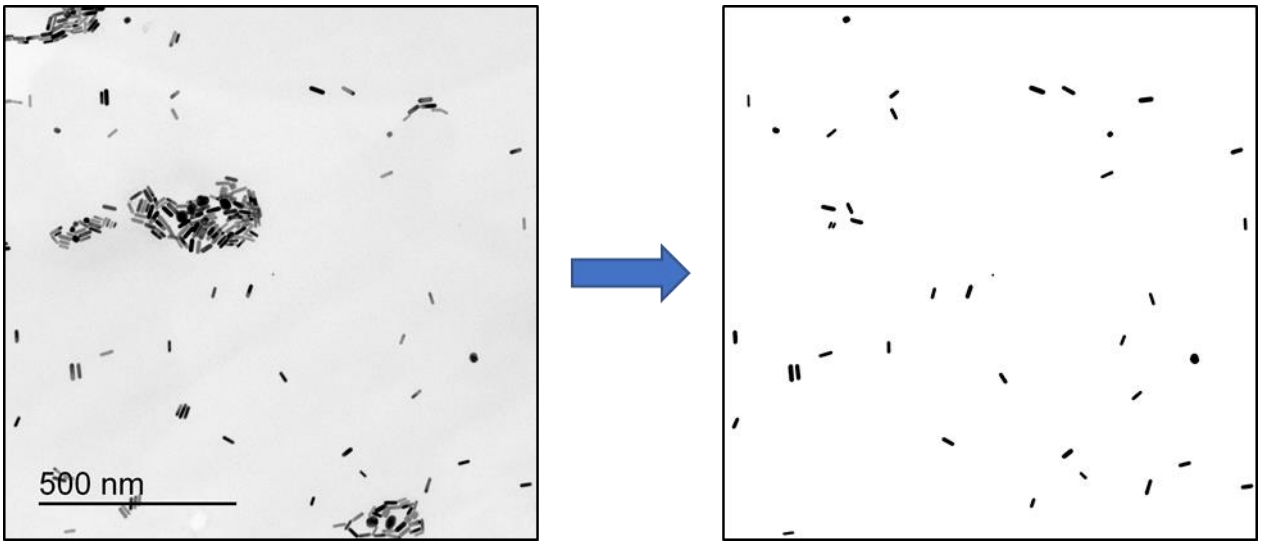

Figure 12: TEM image and masks used to calculate the average size of nanostructures.

The masks used in image analysis were intensity threshold (to eliminate background and set structures boundary) and large grouping of particles that prevented the characterisation of single nanoparticles (typically structures larger than 600 nm^2). Structures smaller than 25 nm^2 were also eliminated. Results in the form of histograms are shown in Figures 3 and 4 for the GNRs width and length, respectively.

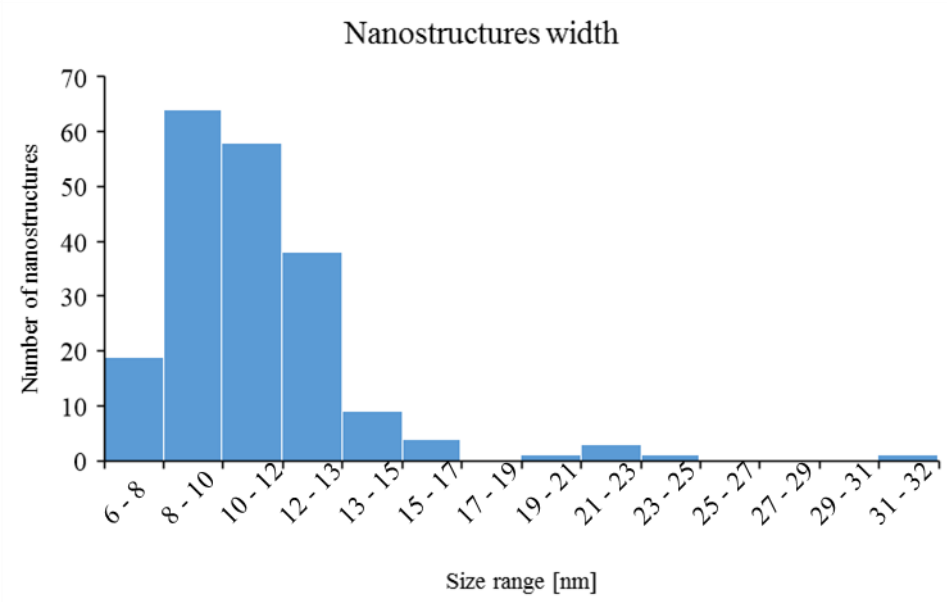

Figure 13: *Width of nanostructures based on 198 objects selected by applying the mask on the TEM images of freshly prepared GNRs.*

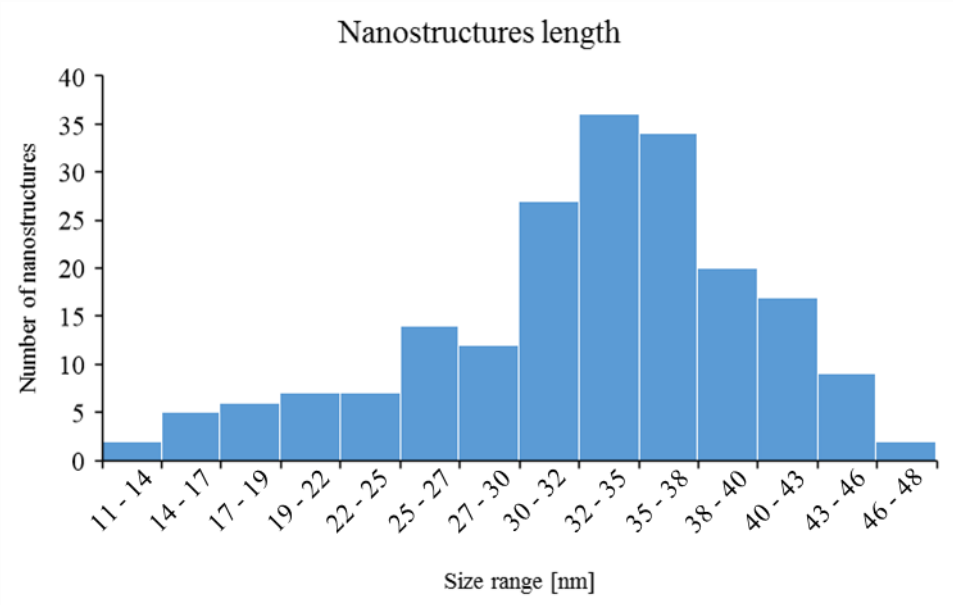

Figure 14: *Length of nanostructures based on 198 objects selected by applying the mask on the TEM images of freshly prepared GNRs.*

The majority of nanostructures had a width in the range of 8-13 nm (Figure 3). The observation of larger widths was mainly due to the presence of spheres that are larger than the average widths of GNRs. The length of the majority of selected nanostructures was in the range 30-38 nm (Figure 4). The wide range of estimated length is certainly due to the different size of GNRs but also to the orientation of GNRs on the TEM image.

Nevertheless, TEM results showed that the majority of freshly synthetized nanoparticles had a rod shape with a length of 32.7±7.4 nm and a diameter of 10.7±3.2 nm. The calculated average aspect ratio of GNRs freshly prepared was 3.2±0.8 (average of all measured nanostructures aspect ratios). As the optical response is proportional to the volume of the GNRs, therefore sample absorption spectra may indicate even higher aspect ratios. In order to check this possibility, absorption measurements were performed.

3.1.3. Visible-NIR absorption spectrum of gold nanorods.

The absorption spectrum of GNRs is composed of two peaks corresponding to the oscillation of free electrons along and perpendicular to the long axis of the GNRs, respectively. The higher energy transverse mode shows a resonance at about 520 nm. The lower energy longitudinal mode is red-shifted and its spectral position strongly depends on the nanorod aspect ratio *R*, which is defined as the length of the rod divided by the width of the rod. In Figure 5 the maximum of the longitudinal band was at 785 nm that should correspond to an aspect ratio of 3.5 nm, which agrees well with the data extracted from the TEM images.[100]

The absorption spectrum (black curve in Figure 5) of a freshly prepared GNRs solution did not show a high amplitude ratio between the two plasmon bands (the ratio of the two maxima of the absorption peaks was 2.2). A low amplitude ratio was due to the presence of nano spheres and aggregates as shown by TEM (see Figure 2).

In order to obtain a mono-disperse solution of GNRs, I developed a method of purification based on centrifugation which allows separation of nanoparticles by their size and their shape. Figure 5 shows the different spectra obtained before and after centrifugation of 1 min and 2 min. To confirm the efficiency of the separation according to the nanoparticles size and shape, the spectra of both the pellet (heavier nanoparticles) and the supernatant (smaller nanoparticles) are shown. The centrifugation speed and time are important parameters to optimise in order to obtain an efficient size and shape separation. Here, the centrifugation rate was optimised to 19090 rcf (relative centrifugal force) and times of 1 and 2 min and the solution was 1 ml in a 1.5 ml tube.

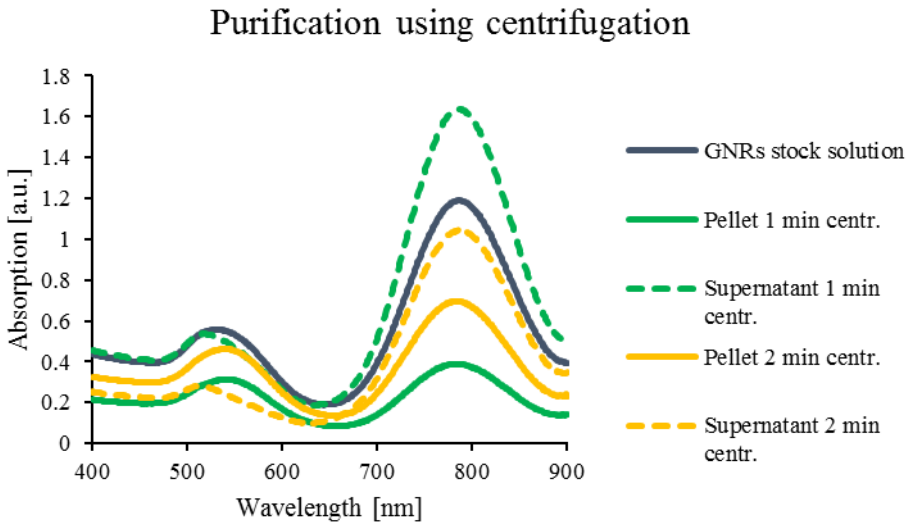

Figure 15: *Absorption spectra of GNRs during purification based on centrifugation.*

With absorption spectra it is possible to follow the effects of centrifugation on the composition of the colloidal solution. After centrifugation for 1 min and 2 min, the difference in the amplitude ratio of the two peaks intensity between the nanoparticles that pelleted at the bottom of the tube (pellet) and the supernatant is significant. Starting from an amplitude ratio of 2.2 for the freshly prepared nanoparticles in solution, it increased to 3.8 and 4 in the supernatant (after re-dispersion in water) after centrifugation for 1 min and 2 min respectively.

In the pellet, the aspect ratio decreased to 1.3 and 1.6 after centrifugation for 1 min and 2 min respectively.

Since the theoretical amplitude ratio for GNRs with a longitudinal absorption band placed between 750 and 800 nm is 3.6[100], this suggests that the larger nanospheres moved down the tube upon centrifugation while the GNRs remained in solution (supernatant). The difference between the two centrifugation times does not seem to have a great influence on the separation of the nanoparticles.

At the end of the synthesis and purification steps the GNRs were dispersed in water and diluted 20-times. To optimise the immobilisation protocol of DNA on the GNRs surface, it is important to also characterise the concentration of the GNRs stock solution.

3.1.4. Determination of gold nanorods concentration

As mentioned in chapter 2, one can calculate GNRs concentrations using their absorption spectrum. For this the positions and values of absorption maximum were recorded (Figure 6).

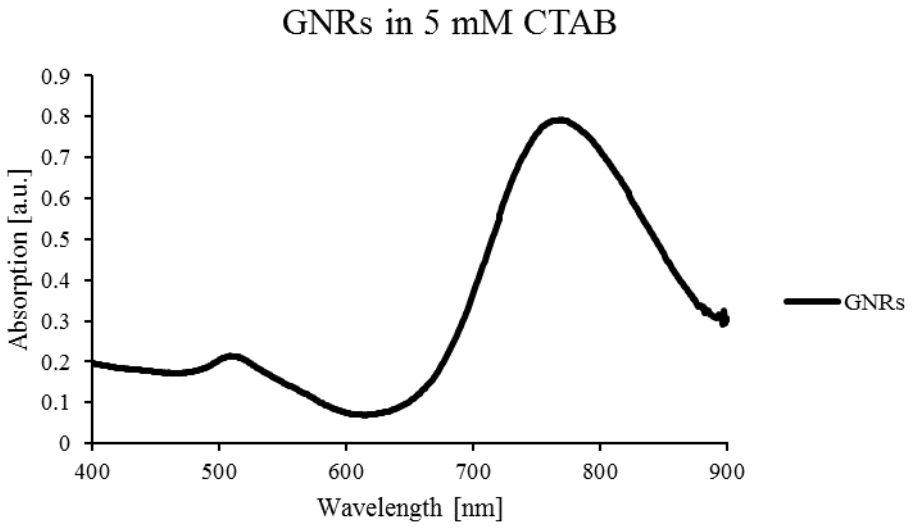

Figure 16: *Absorption spectrum of 6.6-times diluted GNRs batch used for functionalisation experiments.*

The concentration of GNRs obtained from absorption spectra was carried out using the methodology presented in detail in chapter 2.

This method is based on the Beer Lambert law:

$$c = \frac{A}{\varepsilon \cdot l}$$

where:

c = concentration [M]

A = absorption

ε = extinction coefficient [M^{-1} cm^{-1}]

l = length of optical pathway [cm].

The results of the calculations are presented in Table 2.

Table 2: Concentration calculations based on plasmon band absorption peaks

	Absorption peak position [nm]	Absorption peak value [a.u.]	Concentration [nM]
Transverse peak	510	0.1576	0.114
Longitudinal peak	768	0.7920	0.179

Depending on the absorption peak used for the calculation, the GNRs concentration of the stock solution was either 0.75 nM or 1.18 nM (Table 2, taking into consideration the dilution factor imposed to record the absorption spectra). The concentration calculated from the longitudinal absorption peak is more reliable because this absorption peak arises exclusively from the rod-shaped nanoparticles while transversal peaks arise from GNRs and nanospheres if still present in solution. The differences between transverse- and longitudinal-based concentration calculations reflect therefore the nanoparticles dispersity. For all experiments, only the concentrations resulting from calculations based on the longitudinal absorption peak were taken into account.

3.1.5. Conclusion

Optimisation of the GNRs synthesis protocol and development of a method to further purify the resulting GNRs produced well-characterised GNRs colloidal solutions. TEM allowed characterisation of the GNRs length and diameter (32.7±7.4 nm × 10.7±3.2 nm) placing the longitudinal plasmon band at 765 nm. The aspect ratio of the GNRs stock solution after purification (3.6) was close to the expected value calculated with the Gans theory as described in the literature[100], confirming the high quality of the developed protocol to obtain stable colloidal GNRs solution. The calculation of the concentration of the GNRs stock solution based

on the absorption spectra gave a value of 1.2 nM. The GNRs are diluted in water with 5 mM CTAB. In these conditions, the GNRs stock solution was stable as a colloidal pink solution for weeks.

3.1.6. Surfactant bi-layer

During and/or after their synthesis, gold nanoparticles have to be stabilised by a surfactant. In the particular case of gold nanorods, Cetyl trimethylammonium bromide (CTAB)[101], or a mixture of surfactants, CTAB and sodium oleate for example, was used during the synthesis of GNRs and was kept at 4.7 mM in the stock solution after synthesis[102]. As described in chapter 2, Materials and Methods, CTAB was used during the synthesis and also in the colloidal stock solution. The final concentration of CTAB of the freshly synthesized GNRs was 93 mM quickly diluted down to 4.7 mM by centrifugation and redispersion steps.

The interaction of CTAB with GNRs surfaces has been described in detail[103,104]; CTAB forms a double layer, micelle-like structure that surrounds nanorods (Figure 17). The positively charged, hydrophilic part (around the nitrogen atom) is facing toward the metal and on the other side, toward the aqueous solution. The hydrophobic hydrocarbon chains are therefore in between the hydrophilic part and the aqueous solution. A bi-layer thickness of 32±1 Å has been measured[103]. It was demonstrated that the CTAB double layer structure protects GNRs very efficiently against aggregation as long as the surfactant is in excess in solution[105]. The CTAB double layer is disturbed if the CTAB concentration in solution is below the critical micelle concentration (0.91 mM in water), or the presence of ions (e.g. NaCl)[106,107]. Decreasing the surfactant concentration in solution leads to a situation where there are insufficient molecules to keep the double layer structure stable and prevent the nanoparticles from aggregation. The presence of ions in solution decreases the critical micelle concentration by decreasing the Debye screening length[108]. For example, the presence of increasing concentrations of NaCl in solution leads to GNRs aggregation[109]. In addition, the presence of different amphiphilic compounds clearly influences the bi-layer structure as it is incorporated in the double CTAB layer[110]. Another feature of the double CTAB layer surrounding GNRs is that the molecular density and therefore the structure of the double layer is different at the tip of the GNRs and on the sides; this difference was used for zone-specific functionalisation[111].

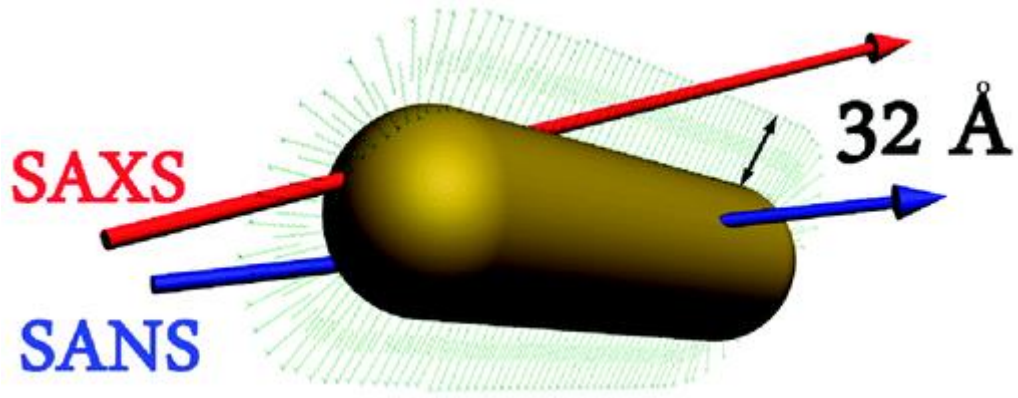

Figure 17: *Representation of the CTAB bi-layer proposed by S. Gomez-Grana et al [103]. SANS - small-angle neutron scattering, SAXS - small-angle X-ray scattering, methods used for evaluating the CTAB bi-layer thickness.*

3.1.7. Environment of GNRs functionalised with thiolated single strand DNA

Colloidal solutions of GNRs always contained a large excess of CTAB, a cationic surfactant known to interact electrostatically with anionic DNA[113,114]. The functionalisation of GNRs with thiolated single stranded DNA molecules is therefore affected by the presence of CTAB. For GNRs functionalisation with thiolated ssDNA, the presence of CTAB affects essentially the yield of immobilisation since not only does CTAB block the surface of GNRs preventing thiol binding but it is also known that cationic surfactant vesicles sequester long anionic DNA molecules in solution[112]. The interaction of short double stranded DNA with CTAB has already been described using FRET[113,114]. There is evidence that the duplex can decorate the outer surface of the cationic CTAB micelles. The dsDNA structure can also be stabilised by the surfactant under specific conditions.

To understand if these electrostatic interactions between CTAB and ssDNA have an impact on the functionalisation process an important part of the thesis was to characterise the nature of DNA-CTAB interactions. It has been shown that the micellar concentration of CTAB is 0.91 mM in water and 0.074 mM in PBS[106]. Therefore, we can consider two regimes where DNA would interact with free CTAB molecules in solution for CTAB concentrations below the critical micelle concentration (CMC), and where DNA will also interact with the cationic CTAB micelles surface.

3.2. ssDNA spatial organisation in solution in the presence of CTAB

3.2.1. The proposed approach

The primal goal of the experiments was to characterise in detail the interaction of CTAB and ssDNA in solution. In water, as soon as ssDNA is introduced to a solution containing CTAB, DNA is expected to interact electrostatically with CTAB molecules. In PBS, the electrostatic interactions between DNA and CTAB are expected to be influenced by the presence of ions.

In order to study how CTAB interacts with ssDNA and how it influences its solubility, accessibility and overall repartition in solution, two ssDNA were used; either complementary or not complementary labelled with two fluorophores, Cy3 and Cy5, able to undergo FRET when at a permissible distance for FRET. The two ssDNAs were introduced in the CTAB solution either step-by-step (one after the other) or pre-mixed together. For the two complementary strands, FRET should be detected only in PBS and not in water solutions. For the two non-complementary strands, no FRET should be detected either in water or in PBS.

All FRET experiments were carried out as follows: the excitation wavelength of Cy3 was fixed at 530 nm, and the emission intensities of Cy3 and Cy5 were registered at maxima (as described in chapter 2).

Table 3: ssDNA used for the experiment - pairs of oligonucleotides

Complementary DNA	DNA35-Cy3	DNA35-Cy5
Non-complementary DNA	DNA35-Cy3	DNA35-Cy5nC
Thiolated DNA	SH-DNA40-Cy3	SH-DNA40-Cy5

The difference in oligonucleotides length was due to the addition of a 5 thymine base spacer placed between the thiol group and the ssDNA. Thymine bases are regularly used as spacers and thymine has been shown to have the least non-specific interactions of nucleic acids with gold surfaces[115]. As a consequence, the DNA with just the thymine sequence next to the thiol group has the lowest probability to interact with the gold surface allowing the whole ssDNA strand to be oriented towards the solution.

3.2.2. Influence of CTAB on the emission of fluorescence of Cy3 and Cy5

First, a fundamental question was how CTAB concentration influences the emission of Cy3/5 alone. The range of CTAB concentrations was from 0.01 mM to 10 mM. The critical micelle concentration is 0.91 mM in water and 0.074 mM in PBS.

In all of the following, we characterised the maxima of the Cy3 and Cy5 emission intensities where the Cy3 is excited at 530 nm and Cy5 is excited at 630 nm (figure 8 and 9).

The addition of even small amounts of CTAB (0.01 mM) in water and in PBS caused a significant decrease (up to 50%) of the Cy3 emission intensity compared to the ssDNA-Cy3 in pure water (Figure 8). The emission intensity of Cy3 did not vary with increasing concentration of CTAB (from 0.01 to 10 mM).

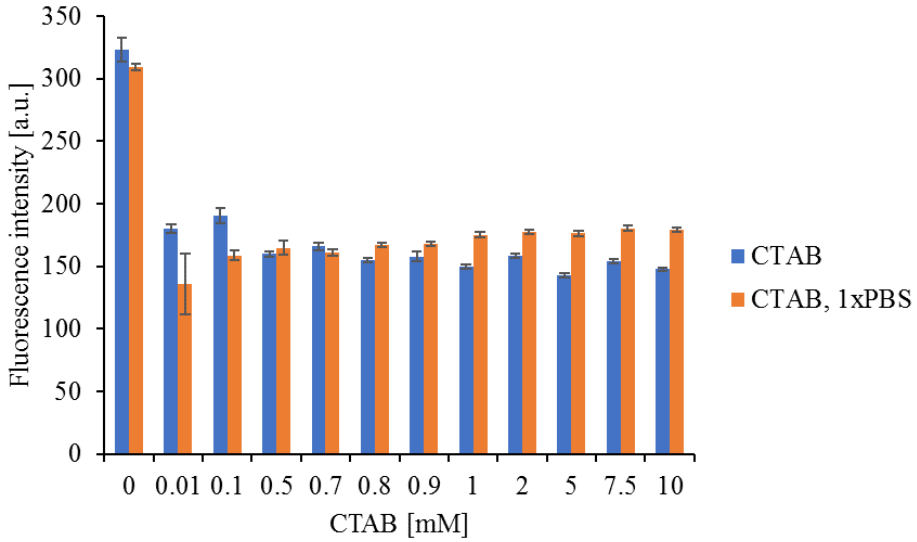

Figure 18: *DNA35-Cy3 fluorescence emission as a function of CTAB concentration in water and in PBS.*

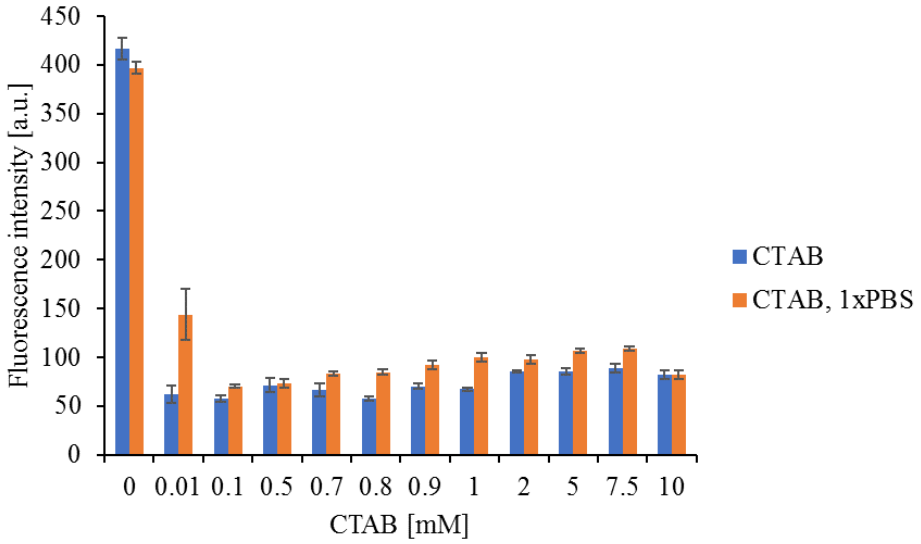

Figure 19: *DNA35-Cy5 fluorescence as a function of CTAB concentration in water and in PBS.*

In the case of Cy5-labelled strand, we observed a 75% decrease in the fluorescence emission intensity (figure 9). As observed with the emission intensity of Cy3, the Cy5 emission intensity did not vary with increasing concentrations of CTAB (up to 10 mM).

The decrease of the emission intensity both of Cy3/5 indicated that CTAB quenched the fluorescence emission. This quenching had an obvious impact on the FRET analysis. Indeed, in FRET experiments, the emission intensity of Cy3 should decrease while the emission intensity of Cy5 should increase. Consequently, no quantification of FRET is possible. A correction that includes the CTAB effect on the fluorescence emission for the FRET measurement has to be applied to follow the variations of both the Cy3 and Cy5 emission as described in Chapter 2, Materials and Methods.

3.2.3. Interactions between two complementary ssDNA

The first experiment concerned interactions between two complementary strands at different CTAB concentrations in water and in PBS. The importance of this step is essential: in water hybridisation does not occur, therefore if duplex formation takes place it means that the surfactant is able to keep the strands together. In phosphate buffer dsDNA forms, so it may be used as a reference sample. Since the two complementary stands are tagged with Cy3 and Cy5, FRET will indicate the proximity of the two strands in solution. The concentration of both oligonucleotides was 10 nM. They were premixed in water or in PBS CTAB solutions with subsequent incubation at ambient temperature for 15 min before FRET measurements.

The graphs showing the results of FRET phenomena (Figure 10 - 12) are corrected from the CTAB quenching effect on the emission of fluorescence. For the donor, the correction was associated only with CTAB quenching (the value of the emission maximum was increased according to Figure 18 with respect to the surfactant concentration). For the acceptor, the correction was done in two steps; first, the Cy3 emission had to be removed in the range 660-680 nm (providing values close to 0, when FRET was not observed). With data covering Cy3 emission alone it was possible to calculate those values that will occur in the range where Cy5 maximum was supposed to appear (660-680 nm). This step was very important, because previously, the spectra could imply that there was no emission coming from the acceptor (no peak appeared), but values in the range of Cy5 maximum were much higher than the background ones. This was due to the Cy3 wide emission spectrum that extends to the range between 660-680 nm. Taking this into account it was possible to decrease these values down to a level closer to the background level (e.g. Figure 10a for samples without CTAB; the emission of Cy5 has a very low value). The second step involved a correction related to the influence of CTAB on the emission (Figure 9).

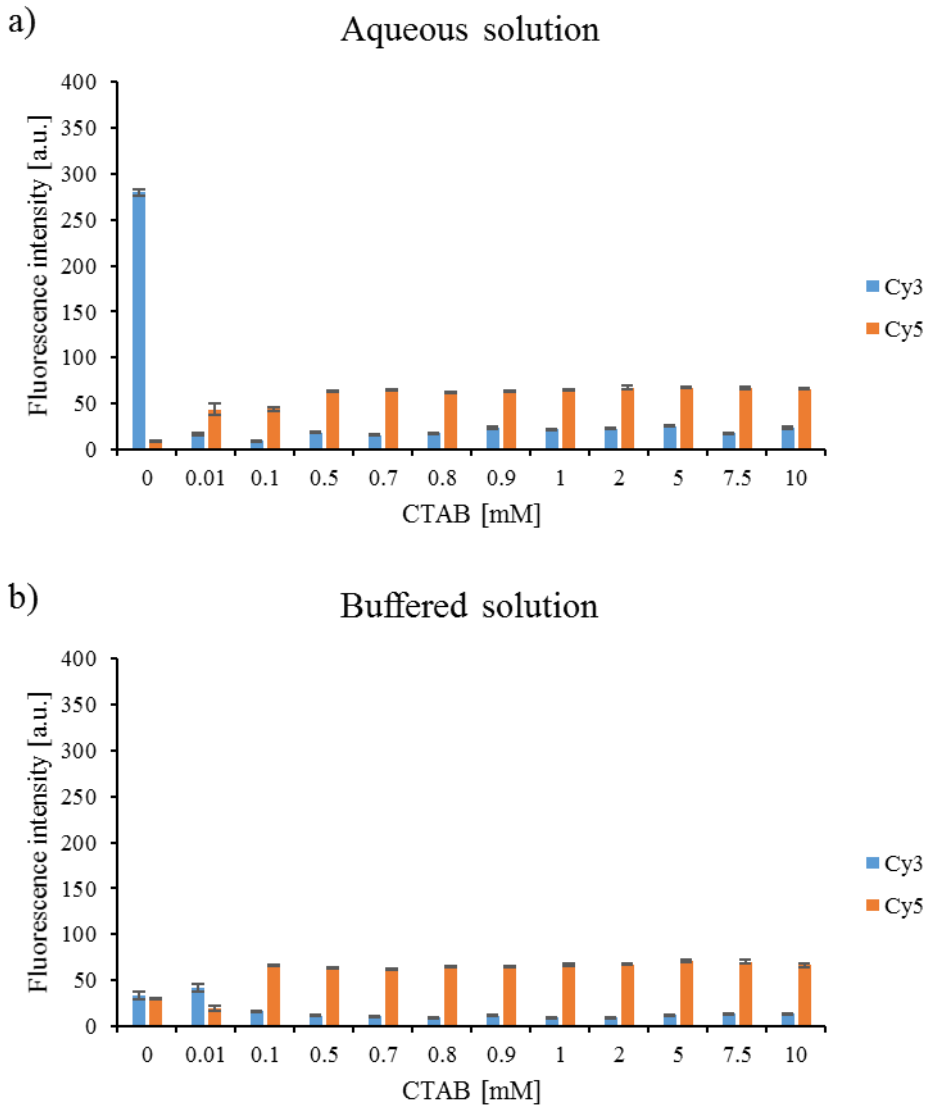

Figure 20: *Pre-mixed complementary oligonucleotides. Fluorescence emission intensity in samples containing various CTAB concentrations in a) water solution, b) 1x PBS.*

In water, at 0 mM CTAB the intensity of Cy3 was maximal while the emission intensity of Cy5 was negligible. Indeed, in water and at ambient temperature, the two complementary strands did not hybridise and therefore FRET could not occur. With 0.01 mM CTAB in water a large decrease of the emission intensity of Cy3 was observed while the emission of Cy5 increased suggesting that FRET occurred. Increasing further the concentration of CTAB did not change significantly the emission of Cy3 compared to Cy5. FRET occurred from 0.01 mM CTAB to 10 mM CTAB in water. There are two possible explanations for this behaviour: 1) CTAB in water provides suitable conditions for the two complementary stands to hybridise; 2) CTAB interacts with pre-mixed DNA such that they are kept together at distances compatible

with FRET. It is important to notice that the CMC for CTAB was 0.91 mM in water. Therefore, at concentrations lower than 0.91 mM no micelles should be present in solution when the pre-mixed DNA was added. As a consequence, CTAB must interact strongly with DNA immediately upon the addition of DNA in solution, preventing the DNA strands from being solubilized and diffusing homogeneously into solution.

In 1x PBS, where the two complementary strands can hybridise, we observed FRET even at 0 mM CTAB. Indeed, the emission of Cy3 was lowered and the emission of Cy5 was detected. The emission of Cy5 increased whereas Cy3 dropped for CTAB concentrations reaching 0.1 mM and remained constant for higher concentrations up to 10 mM. In PBS micelle formation is at 0.074 mM CTAB[106], indicating, as in water, that the presence of micelles did not influence FRET.

When DNA was sequentially added to the CTAB solution (step-by-step injections) FRET was only observed for concentrations of CTAB that did not exceed 0.1 mM (Figure 11). At such concentrations, the efficiency of FRET is much lower than for DNAs premixed in water and then introduced in the CTAB solution (see Figure 10). For CTAB concentrations higher than 0.1 mM no FRET was observed suggesting that the two DNA strands did not hybridize or were not at a distance that allowed FRET. At these CTAB concentrations the DNA molecules were probably surrounded by CTAB molecules that prevent them from being hybridised.

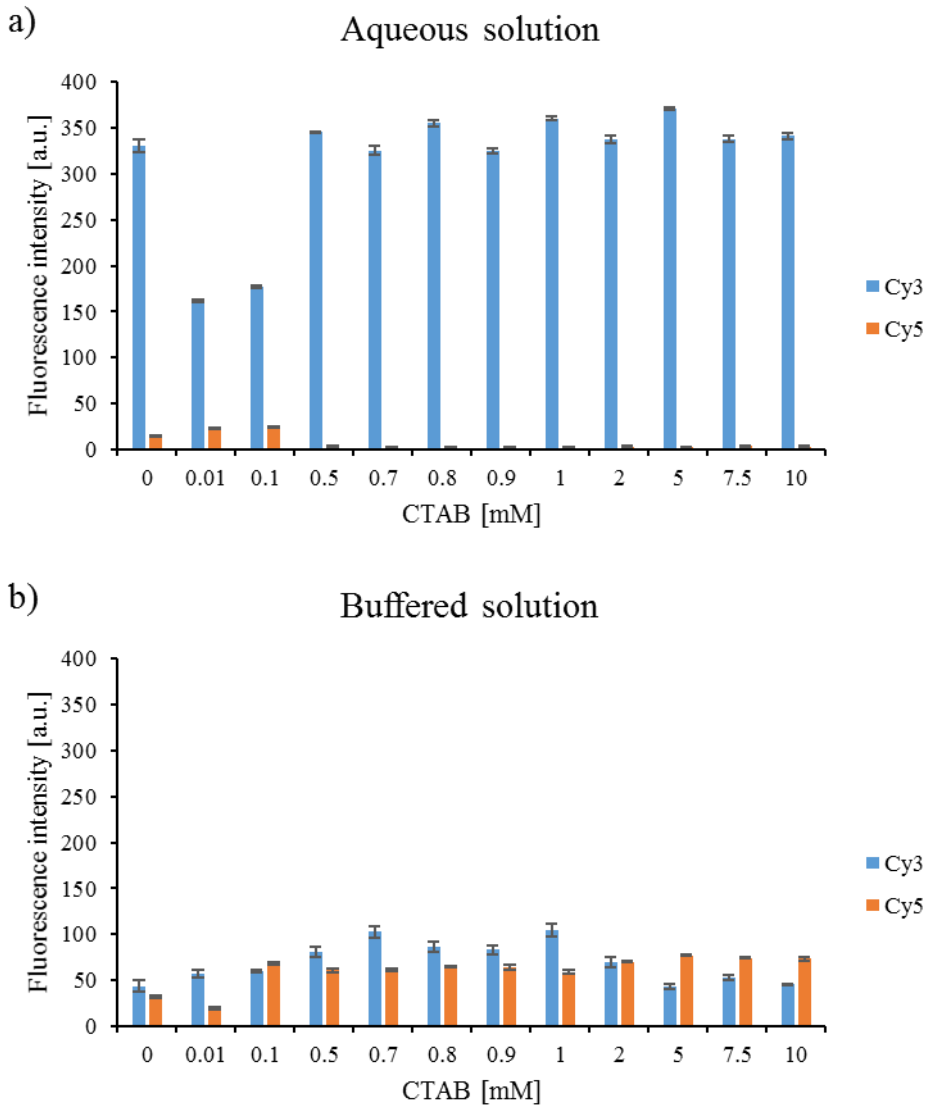

Figure 21: *Step-by-step injection of complementary oligonucleotides. Fluorescence emission intensity in samples containing various CTAB concentrations in a) water solution, b) 1x PBS.*

Lack of FRET in samples in water was a very interesting observation because it indicated a strong difference between samples injected step-by-step or pre-mixed. This difference raised the question of how CTAB impacts on GNRs functionalisation efficiency.

In buffered solution FRET was still observed after a step-by-step addition, so in 1x PBS, DNA can hybridise independent of the CTAB concentration in solution. One explanation may be that there is a competition between cations from PBS (e.g. Na^+) and CTAB to compensate the negative charges on DNA.

Experiments with complementary DNA indicated that in some ranges (0.1 – 10 mM) of CTAB concentration, the pre-mixed Cy3- and Cy5-labelled oligonucleotides are close to each other. The actual distance turned out to be so short, that effective FRET was recorded. The opposite situation occurred when differently labelled DNA was added step-by-step (aqueous solution without buffer) and FRET was not observed. This suggests very strong interactions taking place at the moment of diluting oligonucleotides into aqueous solutions of surfactant. Experiments were therefore conducted with non-complementary DNA.

3.2.4. Interactions between non-complementary DNA

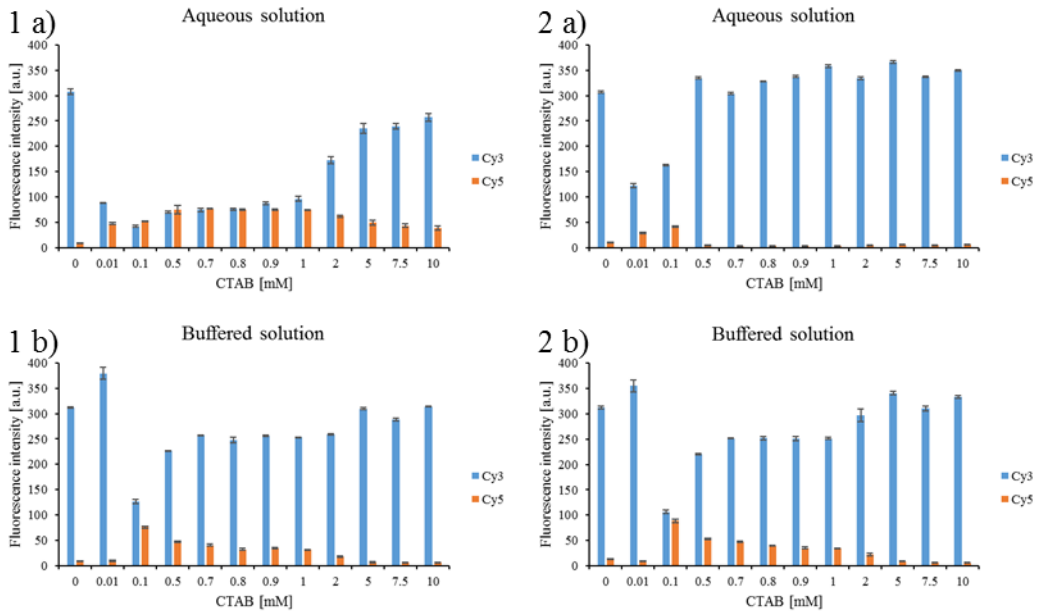

Figure 22: *1/ Pre-mixed non-complementary oligonucleotides. 2/ Step-by-step injections of non-complementary oligonucleotides. Fluorescence emission intensity of samples at increasing CTAB concentrations in a) water solution, b) 1x PBS.*

For the pre-mixed DNA sample and at 0 mM CTAB in water and in PBS, no FRET was observed. Indeed, the two strands were not complementary so we should not expect to have the two fluorophores close enough to exhibit FRET in the absence of CTAB.

Surprisingly, FRET was observed in water with pre-mixed oligonucleotides that were not complementary in 0.01 mM CTAB. This was strong evidence for the role of the surfactant in maintaining both ssDNAs close enough to detect FRET.

The emission intensity of Cy3 at 0.01 mM CTAB decreased 3-fold in comparison to pure water. From 0.01 mM CTAB to 1 mM CTAB the emission intensity of Cy3 did not vary significantly. Simultaneously, the intensity of the emission of Cy5 increased strongly from background level at 0.01 mM CTAB and reached a plateau in the range 0.5 mM to 1 mM CTAB,

indicating FRET. From 2 mM CTAB the emission intensity of Cy3 increased significantly, and was accompanied by a decrease of the intensity of the Cy5 emission, indicative of a lower FRET efficiency.

In 1xPBS FRET was only observed from 0.1 mM CTAB where the Cy3 emission intensity decreased more than 3-times and the emission intensity of Cy5 increased. Then, with increasing CTAB concentration, the FRET efficiency decreased as indicated by the increase in the Cy3 emission intensity concomitant with the decrease of the Cy5 emission intensity.

For the step-by-step addition of the two non-complementary DNA strands in water or in PBS, we observed identical behaviour of the FRET characteristics than for the pre-mixed DNA solution in buffer solution where the FRET efficiency was higher at low CTAB concentrations and lower with increasing CTAB concentrations. This behaviour demonstrated that the two DNA strands that are not complementary were not in close enough proximity to allow FRET. Nevertheless, the FRET efficiency was higher in buffer solution indicating that the interaction between the DNA strands and CTAB was influenced by the buffer solution.

In general, for all conditions, the FRET efficiency was significantly higher for complementary strands than for non-complementary strands when the DNA was pre-mixed prior to dilution in the CTAB solution. For step-by-step addition no FRET was observed for complementary or non-complementary strands when CTAB and DNA were in water, while FRET was only observed with complementary strands in buffered solution.

3.2.5. Influence of SH-group labelling

The final part was to test thiolated DNA. The experimental approach was kept the same with step-by-step additions. Results obtained for thiolated DNA (see Figure 13) were very similar to those obtained for strands without the thiol group (Figure 22): no FRET at 0 and 0.01 mM CTAB, high FRET at 0.1 mM that decreased until 1 mM and very low, or no FRET at all, from 5 to 10 mM CTAB. This suggests that the thiol group does not impact on the DNA-CTAB interaction.

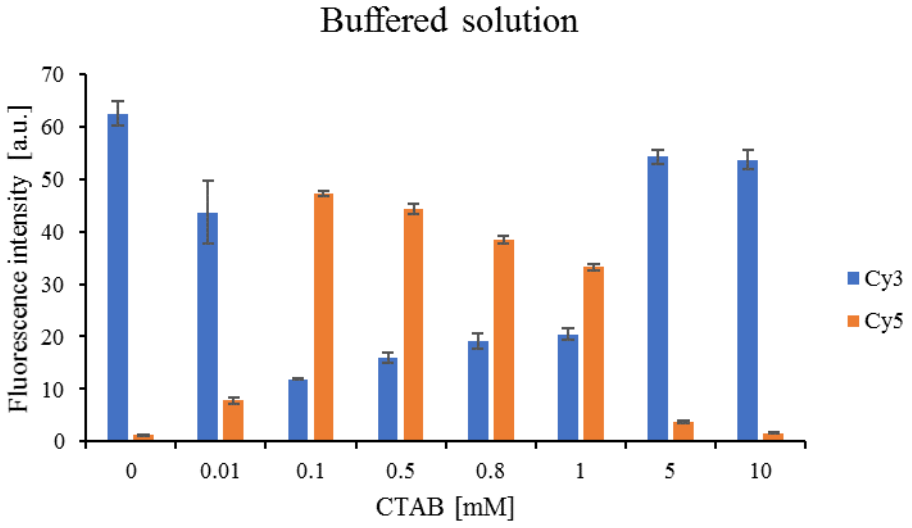

Figure 23: *Emission spectrum of thiolated DNA labelled with Cy3 (SH-DNA40-Cy3) and Cy5 (SH-DNA40-Cy5).*

Figure 13 indicates that FRET occurrence is rather similar to interactions recorded with non-complementary DNA on the boundaries of the CTAB concentration range. More efficient energy transfer in the transition could be associated with the possibility to create a duplex of 8 bp as 8 bp out of 40 bases were complementary.

3.2.6. Conclusion: impact on the functionalization approach of GNRs

These experiments demonstrated three main characteristics of the DNA-CTAB system: 1) oligonucleotide (ssDNA) addition caused an immediate interaction with the cationic surfactant in water; the CTAB encircled the ssDNA. This trapping could be overcome for non-complementary strands by increasing the CTAB concentration above the critical micelle concentration; this changes the system's stability and the DNA is more frequently found to be decorating micelles rather than being trapped. In the case of complementary strands, the emission characteristics did not change. It is therefore difficult to decide if there is a spatial reorganization. 2) Non-complementary strands in the presence of CTAB can give rise to FRET emission confirming the close proximity of the two strands in the presence of CTAB. Such behaviour constitutes an additional argument for the necessity to have complete removal of CTAB from systems where any DNA-DNA interactions are in play. 3) The impact of oligonucleotide trapping can be eliminated by increasing the ionic strength of solutions (1xPBS).

The outcome of experiments focused on DNA-CTAB interactions was that the presence of cationic surfactants could encircle and trap oligonucleotides, probably decreasing their

ability to attach to GNR surfaces. A promising approach to eliminate this involved increasing ionic strength thus allowing ssDNA to separate from each other. Thus, the aim was to find conditions in which oligonucleotides are fully solubilised in solution and GNRs are still stable in solution (non-aggregating). The optimum condition for DNA solubility was found to be 1xPBS and 5 mM CTAB as no FRET was observed for non-complementary strands and hybridisation was still possible. The question now is to study the stability of the GNRs colloidal solution in these conditions.

3.3. CTAB protected gold surface

3.3.1. Functionalization methods in the literature

The presence of a well-organised, low molecular weight protective bi-layer is an important factor for functionalisation. Most of the approaches in current use are based on aminated, or thiolated molecules that displace the CTAB molecules from the metal surface. The main issue is then to free some gold surface to allow the thiol or amine groups to bind to GNRs without disturbing too much the CTAB double layer and preventing the GNRs from aggregating. The thickness of the double layer has been estimated to be 3.2 nm[103], sufficient to prevent gold-ligand interactions. There is no major problem reported with functionalisation by mercapto-based hydrocarbon derivatives (e.g. 11-Mercaptoundecanoic acid), because they do not interact strongly with CTAB. Additionally, they can pass the double layer due to their similar chemical composition with the hydrophobic part of the surfactant. Moreover, they are usually added at very high concentrations[116,117] so that the reaction occurs rapidly and the GNRs surface is still protected. In the case of oligonucleotides, the situation is different: the phosphate groups forming the DNA backbone are negatively charged, so they can interact with the hydrophilic part of CTAB; oligonucleotides may then decorate the double CTAB layer, thus preventing thiol-gold bound formation. In this case adsorption would be due to electrostatic interactions and not via the stronger thiol-gold bond. In addition, the molecular mass of DNA is much larger than that of 11-Mercaptoundecanoic acid and the concentration of the stock solution of thiolated DNA is limited to the micro-molar range (100 µM) so the adsorption of thiolated DNA on GNRs is extremely slow compared to 11-Mercaptoundecanoic acid.

The most commonly used methods to functionalise GNRs with DNA are the following[118] (authors have checked different oligonucleotides concentration):

1) GNRs (OD=1) were incubated with thiolated oligonucleotides in water (molecular ratio of DNA-SH and gold nanorods was adjusted to be approximately 1.5:1) for 96 hours [119],

2) GNRs (OD=0.8) were mixed with thiolated oligonucleotides (1.96 μM) and incubated 30 min. Subsequently sodium hexametaphosphate (10 mM) and NaCl (0.3 M) were added and incubated for 48 h at 25 °C [120],

3) 1x TBE and 0.1% SDS were mixed together at pH=3 (adjusted with HCl). Subsequently SH-DNA was added to this mixture. In the next step, the freshly synthesized GNRs (OD=1.5) were added to the solution. After several minutes, the mixture was centrifuged (20 mins, 7000 rpm) three times and resuspended in 1xTBE[121].

4) SH-DNA was slowly injected to GNRs solution (OD=0.9) and SDS was added dropwise to achieve 0.01% concentration. Subsequently mixture was placed into an ultrasonic bath for 10 s at ambient temperature and incubated for 24 h. The solution was then centrifuged and re-dispersed in buffer (10 mM HEPES, 0.01 % SDS and 10 mM NaCl)[118].

Following these methods, it is possible to observe that (with the exception of the first one) the goal is to destabilise the CTAB bi-layer. This was done by adding different surfactants with different charge (SDS for example), or by increasing the ionic strength (NaCl). At the same time, there is a strong focus on keeping nanorods in a colloidal solution; this is additionally difficult, because attachment of negatively charged DNA reduces the electrostatic repulsion, therefore charge changes are introduced slowly. As a consequence, the described protocols are time-consuming, with the exception of the 3rd method in which low pH changes the equilibrium of charge interactions, but the stability of GNRs in solution is fragile.

A potentially interesting method was developed and fully described in the literature to create DNA-nanoparticle origami[122]. This required very high efficiency and controlled immobilisation of DNA on the nanoparticles. Indeed, in this case, any non-specific immobilisation of DNA on nanoparticles would not lead to the desired origami structures. Non-specific interactions involve adsorption of DNA on the nanoparticles surface by means other than the thiol-Au bound. For this purpose, routes enabling fast functionalisation were often selected; in fact by setting pH=3[122,123,124] but it was pointed out that this method is only possible with freshly prepared GNRs solution.

In parallel, a study described the possibility of electrostatic-based oligonucleotide attachment to GNRs surface and its use to develop a layer-by-layer deposition[125]. Such interactions are also used to detect complementary or non-complementary ssDNA in solution: the non-thiolated oligonucleotides are added to the nanoparticle solution containing the surfactant and the buffer. The design is such that as long as the complementary DNA analyte is not injected, the nanoparticle absorption spectrum will not change. When a complementary oligonucleotide is added, the GNRs aggregate upon hybridisation[126,127] (data attached to publications indicate a decrease of absorption throughout the spectrum). When non-complementary strands are added, the extinction spectrum does not undergo any changes. The mechanism of aggregation is explained by the fact that duplex formation between DNA previously deposited onto different GNRs can cause formation of aggregates (which are initially still in colloidal form) – this assumption was supported by DLS measurements.

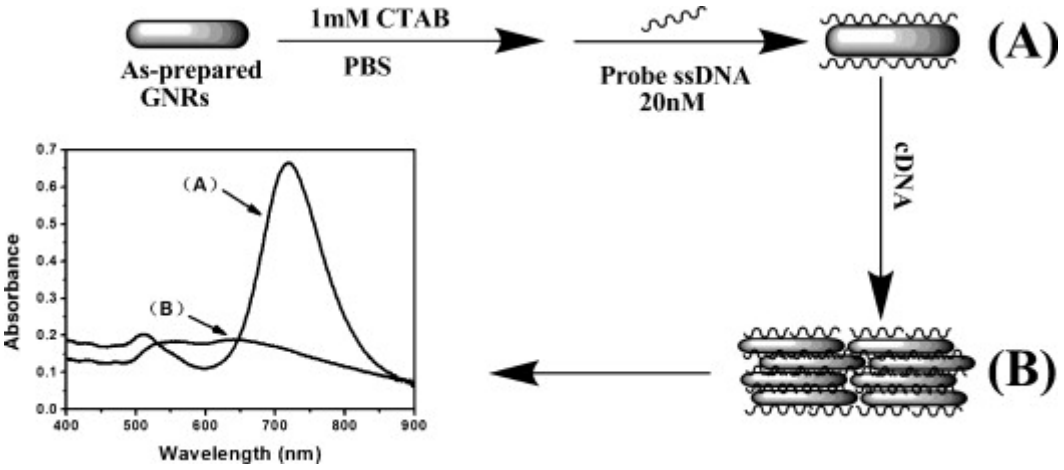

Figure 24: *Mechanism of GNRs aggregation in the presence of cDNA. A represents situation in presence of one type of ssDNA, B after addition of complementary strands. Reproduced from Z. Maa et al.*[126]

The approach to obtain well controlled DNA-GNRs hybrids was to associate the GNRs-based DNA complementarity detection method based on electrostatic interaction with thiol-gold bond functionalisation. The first step is oligonucleotide deposition on GNRs surfaces involving electrostatic interactions. Then, the close proximity between the gold and SH-DNA favours formation of gold-thiol bonds in conditions where the CTAB double layer would be weakened.

3.4. Methods of functionalisation developed in the thesis

3.4.1. Stability of GNRs in the presence of PBS and different concentrations of PBS

The CTAB/DNA interaction study demonstrated that solubility of DNA is possible in the presence of 1xPBS and 5 mM CTAB. Indeed, no FRET between two non-complementary strands was observed in these conditions, and hybridisation of the two complementary strands was possible. The next step was to study the stability of GNRs in solution under these conditions. For this purpose, two sets of samples were examined, with and without PBS.

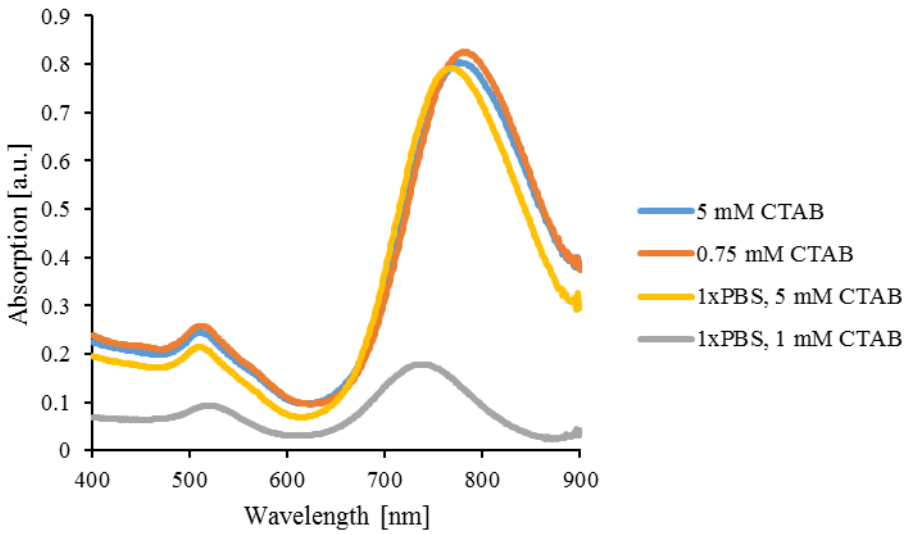

Figure 25: *Absorption spectrum of GNRs in solutions containing CTAB and PBS.*

For these experiments, 2 samples without PBS were measured: in 5 mM CTAB and in 0.75 mM CTAB. 5 mM CTAB was the standard concentration at which GNRs were stored and were stable in water, and 0.75 mM CTAB was below the surfactant CMC. In both cases the absorption spectrum was identical and typical of a GNRs stable colloidal solution. Therefore, decreasing the concentration below the CTAB CMC concentration does not lead to the aggregation of GNRs. Thus, both environments could be tested for the DNA immobilisation protocol.

In buffer solution (1xPBS), two CTAB concentrations were tested: 1 and 5 mM CTAB. It was clear that increased ionic strength caused large losses of GNRs in 1 mM of CTAB and 1x PBS as seen by the decrease of the intensity of the absorption spectra (Figure 25). Interestingly, the longitudinal absorption peak was shifted to a lower wavelength, but the

overall optical properties were preserved confirming that DNA could be detected in solution based on electrostatic interactions[126]. In addition, the lower absorption intensity could be caused by the sample preparation method where GNRs are centrifuged and re-dispersed in 1x PBS and 1 mM CTAB. In the case of re-dispersion in 1xPBS and 5 mM, the absorption spectrum was very similar to that obtained with GNRs in 5mM CTAB diluted in water (without PBS). This implies that the optical properties have been preserved and that the GNRs morphology did not vary. In conclusion, GNRs are stable in 1xPBS and 5 mM CTAB.

3.4.2. GNRs functionalisation with SH-ssDNA

The next step was the addition of thiolated-ssDNA to the GNRs colloidal solution in 1xPBS and 5 mM CTAB. The experiments were divided into two parts – with a "low" and a "high" DNA to GNRs ratio (the concentration of GNRs was 0.18 nM). The first range was set between 0 and 110 strands/GNRs (see Table 4). The second range was up to 2800 strands/GNRs (concentration from 20 nM to 500 nM of SH-DNA). The reason for this was based on literature values where high ssDNA surface coverage is obtained with a large excess of ssDNA (high DNA/GNRs ratio). On the other hand, from a theoretical point of view it was considered relevant to follow the ssDNA adsorption at lower DNA strand concentrations and to compare both conditions.

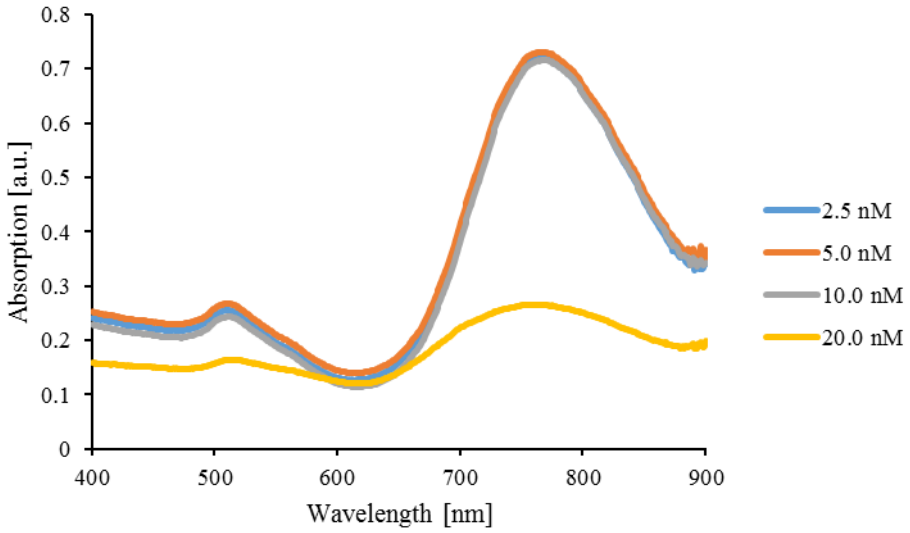

Figure 26: *Absorption spectrum of GNRs solution incubated overnight with increasing concentrations of SH-DNA in 5 mM CTAB and 1x PBS.*

Table 4: DNA/GNRs ratio

ssDNA concentration (nM)	2.5	5	10	20
DNA/GNRs	14	28	56	110

According to the literature[128] the density of oligonucleotide strands deposited onto gold spheres can reach $2.5 \cdot 10^{13}$ strands/cm^2 (corresponding to 0.25 strands/nm^2). Using the size histograms allowed an estimation of the statistical size of GNR to 10 nm diameter and 35 nm length. The surface area of these structures would be 1100 nm^2, so the expected number of strands, with maximum possible density, is 275 strands per GNR.

The absorption spectrum does not vary when 2.5, 5 and 10 nM of SH-DNA was incubated with 0.18 nM of GNRs diluted in 1x PBS and 5 mM CTAB. Nevertheless, it is clear that the whole spectra decreased in intensity when 20 nM of SH-DNA was added (Figure 26).

We therefore noticed that the effect of the SH-ssDNA concentration on the GNRs stability in solution is sudden. Indeed, no influence on the absorption spectrum could be detected for DNA concentrations lower than 10 nM, and a sudden drop in the intensity of the absorption spectrum is clearly noticed when 20 nM of DNA is added to the GNRs solution. The decrease of the absorption spectrum could suggest aggregation and subsequent precipitation, however no aggregate in the reaction tube could be detected. Instead, the colour of the solution changed from pink to colourless after overnight incubation with 20 nM SH-DNA, while the solution remained pink for SH-DNA concentrations lower than 10 nM.

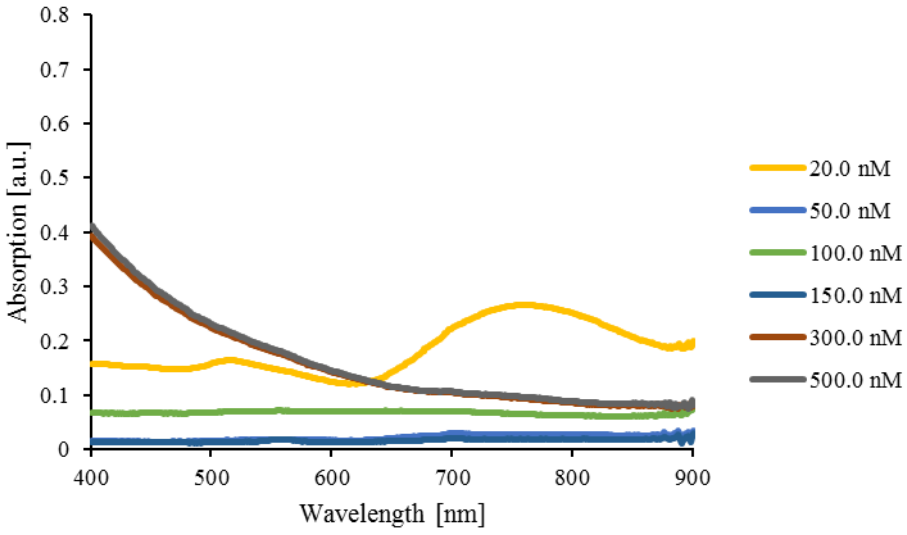

Figure 27: *Extinction measurements performed after overnight incubation of GNRs with increasing concentration of SH-DNA in presence of 1xPBS, 5 mM CTAB. No rinsing was performed.*

Table 5: DNA/GNRs ratio

ssDNA concentration (nM)	20	5	100	150	300	500
DNA/GNRs	110	278	555	833	1667	2778

For high concentrations of SH-DNA (from 20 nM to 500 nM) in solution we observed the extinction of the absorption spectrum of GNRs. At 20 nM, as shown in Figure 25, the two absorption bands of the GNRs were still detected confirming the presence of GNRs in solution at lower concentrations than for GNRs incubated with lower SH-DNA concentrations (lower than 10 nM, Figure 25). For increasing concentrations of SH-DNA, the absorption spectrum intensity decreased to a level reflecting the scattering of large structures in solution when SH-DNA is in large excess (from 300 nM to 500 nM).

Again, no aggregates could be detected in the Eppendorf tube and the solution became colourless after an overnight incubation.

We expected that for large excess of SH-DNA in solution (more than 20 nM) the adsorption of SH-DNA on the GNRs surface, either electrostatically or via the thiol-gold bonding, would impact strongly on the overall GNRs charge: the CTAB double layer around the GNRs is positively charged and electrostatic repulsion keeps the GNRs stable in solution

even in the presence of 1xPBS. The adsorption of DNA on the GNRs surface leads to a charge compensation or to negatively charged GNRs when DNA is in large excess in solution. According to the literature[129], when the zeta potential is close to neutral, the electrostatic repulsion should decrease to levels at which nanostructures could interact with each other, thus forming aggregates. However, the experimental data do not fully support such a mechanism since the absorption spectra decrease in intensity without any spectrum shape modification typical of aggregation. Therefore, we suspected that when GNRs covered with DNA became neutral they interacted with the walls of the Eppendorf tubes. GNRs deposition onto the reaction vessel surface, would thus explain the decrease in intensity of the absorption spectra. Nevertheless, any change of CTAB-protected particles charge had to be due to interactions with DNA. Therefore, the change of colour of the solution was a strong indication of GNRs interacting with oligonucleotides. In order to further characterise if the DNA was adsorbed to the GNRs via the S-Au bound or electrostatically, the GNRs had to be dispersed in solution.

3.4.3. Redispersion of nanohybrids

The decrease of the absorption spectra and the lack of clear signs of aggregation in the solution of GNRs incubated with excess of SH-DNA raised the question of the fate of the nanoparticles. The most apparent explanation was the deposition of GNRs-DNA structures onto Eppendorf walls; this would be caused by changes in the surface charge of GNRs (instead of the cationic CTAB bi-layer, neutral or negative charges appear). The assumption is that the change of the surface charge from positive (CTAB) to neutral or negative (ssDNA) causes deposition onto the walls of the Eppendorf tubes. In order to check this hypothesis, two different approaches for redispersion were tested:

1) Addition of SDS – as an anionic surfactant it can interact with CTAB and change CTAB-DNA interactions equilibrium. SDS has been used in the literature for functionalisation-assistance[130] but no reports on GNRs interacting with the tube walls were described.

2) Addition of Tween20 – without charge. In the literature[121] CTAB has been reported to be removed from GNRs surface by Tween20 and the GNRs subsequently functionalized. There is also a patent[131] covering nanorods functionalisation in the presence of this surfactant; in this case the surfactant is supposed to prevent aggregation. In this thesis the idea was to disrupt the CTAB-DNA system by intercalation of CTAB

structures by Tween20; based on hydrophobic interactions. Therefore, the use of Tween20 described in the literature is quite similar to SDS but is less toxic.

In addition, SDS in the presence of potassium that is present in PBS buffer solution precipitates. We therefore decided to use Tween20 for further experiments.

GNRs diluted in 5 mM CTAB and 1xPBS were incubated with 20, 150, 300 and 500 nM of DNA. To verify that the interaction of the GNRs/DNA hybrids with the Eppendorf walls was electrostatic, each sample was incubated with thiolated DNA and non-thiolated DNA. After 4 hours of incubation, Tween20 was added to all samples so that the final solution had 2 % Tween20. After 30 min of incubation and mild mixing the samples were characterised.

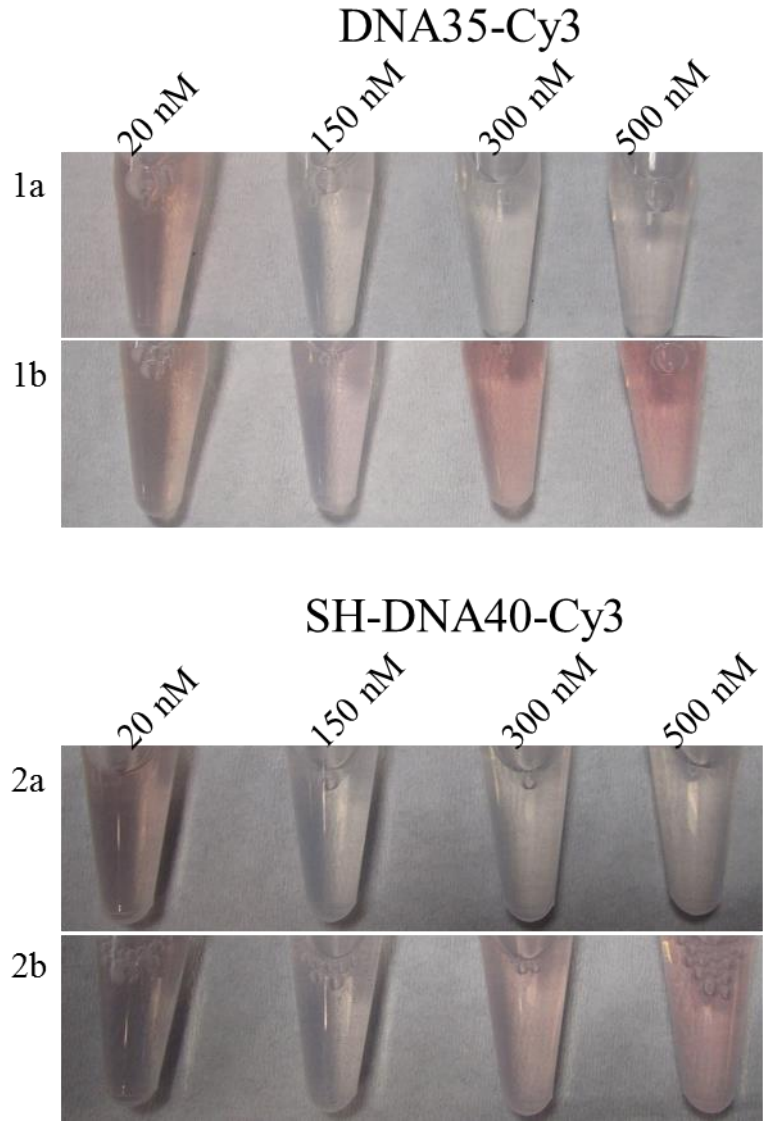

Figure 28: Redispersion of GNRs nanohybrids with Tween20 2%. 1- GNRs incubated with non-thiolated DNA a) before and b) after the incubation with Tween20. 2- GNRs incubated with thiolated DNA a) before and b) after the incubation with Tween20.

Figure 28 shows a photo of the samples of GNRs incubated with either non-thiolated (Figure 28-1) or thiolated DNA (Figure 28-2) in Eppendorf tubes before (a) and after (b) the addition of Tween20.

It is clear that after incubation of non-thiolated or thiolated DNA at concentrations higher than 20nM, the sample solution became colourless (as seen in the sample of GNRs and 20 nM of DNA, the solution was pink). It is important to note that the DNA used for these experiments was labelled with Cy3, which is pink at high concentrations. Therefore, the fact that the solution becomes colourless indicates that DNA and GNRs were interacting with the walls of the Eppendorf tubes even for large excess of DNA.

After the addition of Tween20, we noticed that the sample solution recovered the pink colour showing that GNRs and DNA were re-dispersed in solution. At 20 nM the variation of colour is not clear in the photographic analysis, because we showed that at this DNA concentration some GNRs remained in solution. Since the intensity of the colours is strongly dependent on the DNA concentration (Figure 28-1b and 18-2b), it is important to follow the redispersion in solution of GNRs by measuring the absorption spectra.

The protocol optimisation steps indicated that the redispersion of GNRs after incubation with high concentrations of DNA requires long incubation (2 hours) and vigorous mixing after the Tween20 injection (e.g. use of vortex for 25-30 s). A different approach would be to centrifuge the samples exposed to Tween20 for 30 min and further rinsing in 2 % aqueous Tween20 solution. These protocols allowed very efficient re-dispersion of GNRs.

Samples were centrifuged twice and rinsed with 2% aqueous Tween20 solution of 2 % and finally after a third centrifugation step the samples were re-dispersed in pure 1x PBS before being characterised (Figure 29). The final concentration of Tween20 is 0.1%.

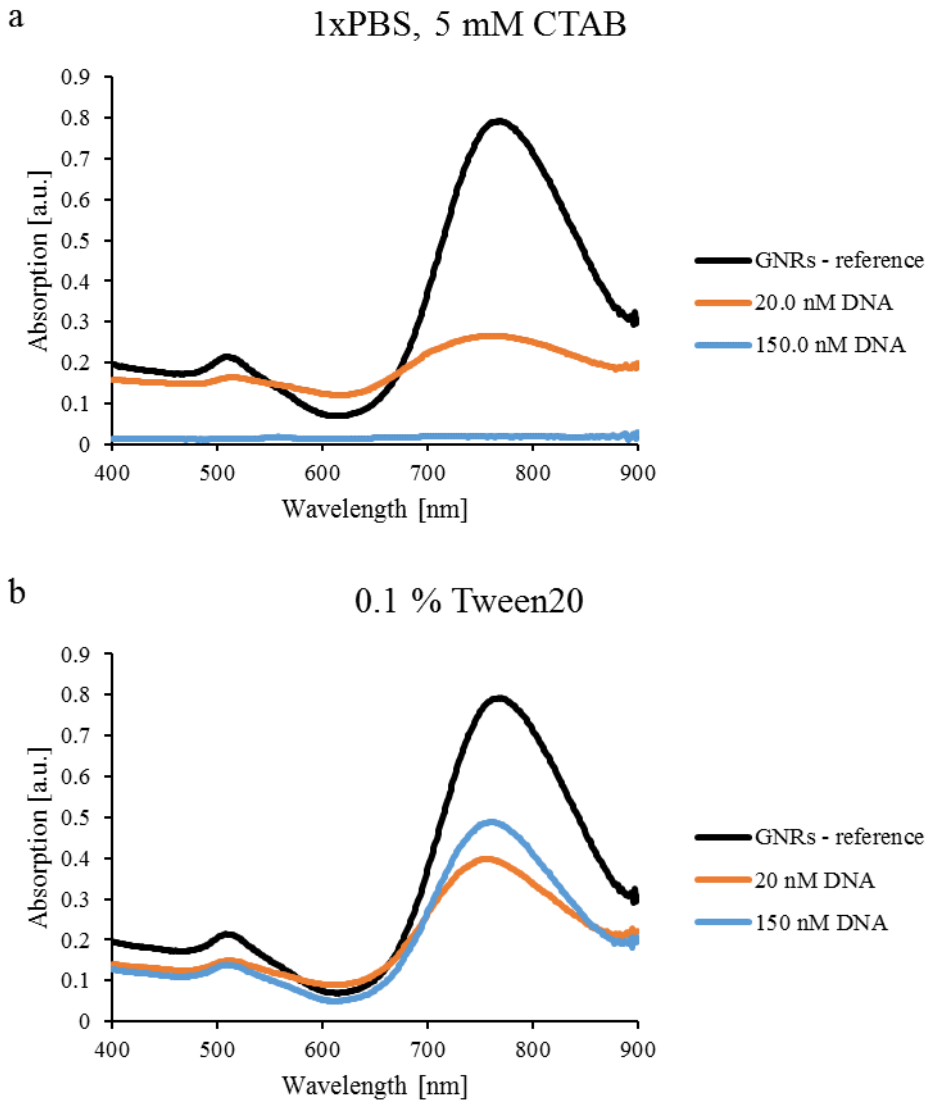

Figure 29: *Comparison of samples of GNRs incubated with 20nM or 150 nM thiolated DNA a) before and b) after the rinsing steps with Tween20 and final redispersion in 1x PBS..*

As described earlier, before rinsing, the overall absorbance spectra intensity decreased from the reference sample of colloidal GNRs solution in 1xPBS and 5 mM CTAB compared to the samples incubated with 20 nM and 150 nM of thiolated DNA (Figure 29). In addition, it is clear that a complete removal of nanoparticles from the solution is observed with GNRs sample incubated with 150 nM SH-DNA (DNA to GNRs ratio equals 833). The 3 rinsing steps (2 first with 2 % aqueous Tween20 solution, the last one with 1xPBS) resulted in re-dispersion of nanoparticles. The concentration of GNRs after re-dispersion compared to the reference samples indicated that there was a loss of GNRs during the process. Interestingly, it appears that the redispersion was more efficient for GNRs incubated with 150 nM of thiolated DNA than for 20 nM. Additionally, it is of note that losses of nanoparticles are not followed by

changes in the optical properties (the peak aspect ratio remains similar to the reference sample), so the aggregation of GNRs can be excluded.

The optimised method allows re-dispersion of GNRs from the walls of the Eppendorf tubes. The final GNRs were functionalised with DNA and the nanohybrids were stable in a colloidal solution in 1xPBS and 0.1% Tween20. The stability of the GNRs-DNA system in solution enabled further investigations to characterise the nature of the DNA to GNRs interaction (either electrostatic or via the thiol-gold bond) and to quantify the surface density of DNA on the GNRs surface. It is important to note that the samples incubated with non-thiolated DNA did not aggregate after the rinsing steps. A study to address this is presented in the following paragraphs.

3.4.4. Results confirmation

In order to discriminate between the presence of thiol-gold bond or pure electrostatic interactions between DNA and GNRs, gel electrophoresis was performed. Indeed, upon migration in the agarose gel, all electrostatically bound DNA must separate from the GNRs surface and migrate like free DNA while the DNA bound via the thiol-gold bond should migrate with the GNRs.

For comparison, samples prepared in 0.75 mM CTAB in water (below the critical micelle concentration the bi-layer on GNRs was expected to be disturbed) were also loaded on a gel. As discussed earlier, the GNRs are stable in a colloidal solution (Figure 27). In addition, in these conditions we observed FRET when two non-complementary strands were added to 0.75 mM CTAB in water (Figure 22 and Figure 23) suggesting poor accessibility of DNA for GNRs binding. On the other hand, below the CMC concentration in solution the CTAB double layer is weakened so that DNA adsorption could be favoured. The gel scanned in absorption (Figure 30) revealed those GNRs that migrated in the gel. To facilitate a good signal to noise ratio, all samples were concentrated with a centrifugation step before being loaded on the gel.

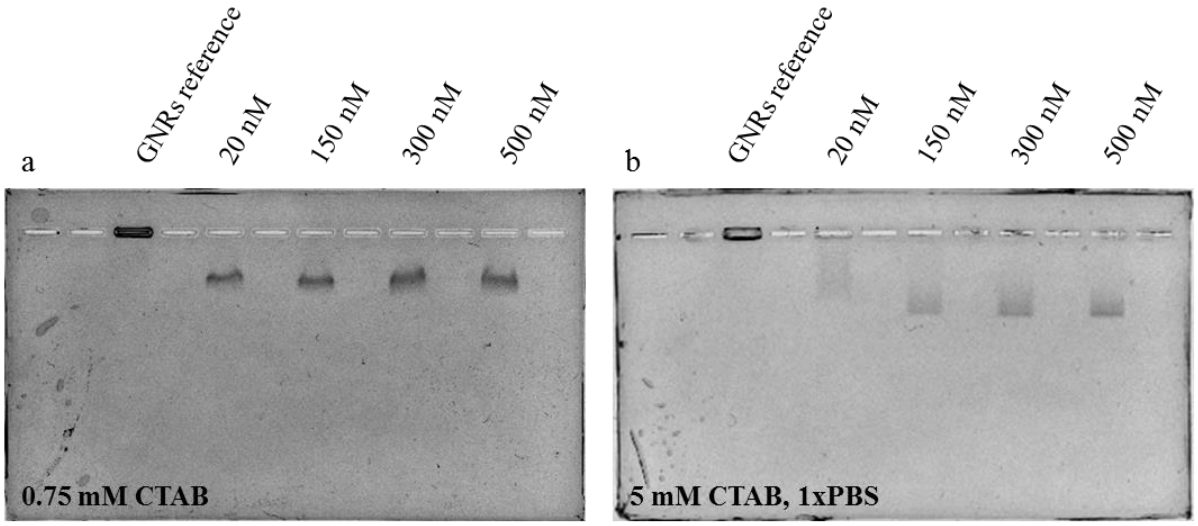

***Figure 30**:* Gel scan photo – a) samples prepared in 0.75 mM CTAB and b) samples prepared in 5 mM CTAB, 1xPBS. All GNRS samples were rinsed after incubation with different concentrations of SH-DNA-Cy3, by the 3 centrifugation steps as described in the text.

Figure 30 shows a photo of two agarose gels. Figure 30a shows the migration of loaded samples that were prepared in 0.75 mM CTAB diluted in water and Figure 30b shows the migration of loaded samples prepared in 1xPBS and 5 mM CTAB. On both gels, the first lane on the left corresponds to the reference of GNRs in the corresponding solution but without having been incubated with DNA. Then, from left to right, each lane corresponds to GNRs solutions incubated with increasing concentrations of DNA, as indicated in Figure 30.

For samples prepared in 0.75 mM CTAB or in 1xPBS and 5mM CTAB, the GNRs in the reference sample did not migrate in the gel despite the applied electrical potential. The direction of the electrical potential is from negative at the wells towards the positive potential down the gel. Non-functionalized GNRs are positively charged due to the CTAB double layer and, if stable, will therefore not migrate towards the positive end of the gel. In addition, the running buffer is a standard TAE buffer composed of Tris Base, Acetic acid and EDTA at concentrations that would lead to GNRs precipitation in solution and therefore in the wells of the agarose gels.

The incubation of GNRs diluted in 0.75 mM CTAB with 20 mM DNA and rinsed from the DNA excess, allows the loaded sample to migrate in the gel toward the positive electrode. The migration in the gel of GNRs was not influenced by their incubation with higher concentrations of DNA (Figure 30a). The incubation with DNA therefore changed the surface

potential of GNRs from positive to negative and protected the GNRs from aggregating in the wells of the gel when in contact with the migration buffer.

The migration in the gel of samples of GNRs incubated with SH-DNA in 1PBS and 5 mM CTAB was strongly influenced by the DNA concentration (Figure 30b). For GNRs incubated with 20 nM SH-DNA, the sample smeared upon migration (no clear band was detected). As the concentration of DNA increased, the migration was faster and a clear band appeared at the migration front. The migration front speed (or distance from the wells) is identical for 300 mM and 500 mM of DNA incubated with the GNRs in PBS and 5 mM CTAB. The incubation of GNRs in PBS and 5 mM CTAB and SH-DNA changed the GNRs surface charge from positive to negative and stabilized the GNRs in solution so that they did not aggregate in the gel and a clear migration front could be detected.

The next step involved measuring the fluorescence emission of SH-DNA-Cy3 in the gel to correlate the migration of DNA with the migration of GNRs. It is important to note that the gels presented in Figure 30 and Figure 21 are the same, just that the scan detection method is different: Figure 30 shows a photo of the gel, thus reporting the optical density, so only the GNRs are detected, in Figure 21 the gels are scanned with a laser at the excitation wavelength for Cy3 and recorded at the emission wavelength of Cy3 so only labelled DNA is detected.

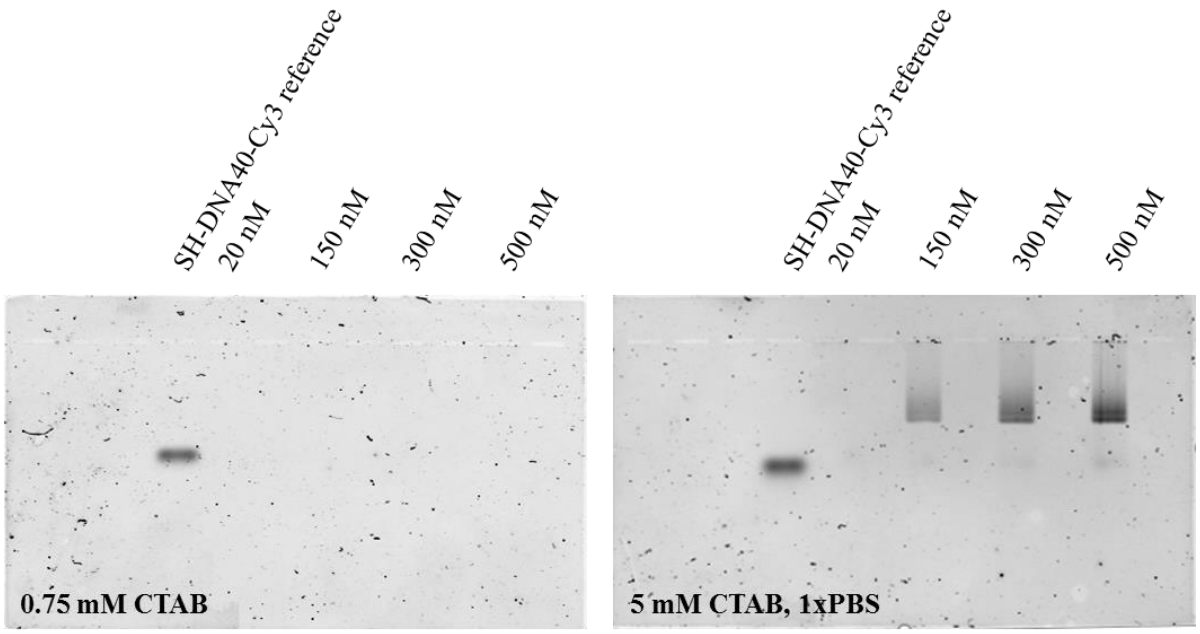

Figure 31: *Fluorescence emission of DNA labelled with Cy3 from GNRs samples incubated with different concentration of SH-DNA.*

The lane corresponding to the SH-DNA-Cy3 reference on both gels corresponds to free DNA loaded in the wells; the bands detected in the gel correspond therefore to the migration front of free DNA (Figure 21). No signal of SH-DNA-Cy3 was detected in the gel for samples of GNRs incubated with increasing concentrations of DNA in 0.75 mM CTAB in water (Figure 21a). It is clear that the GNRs were covered with DNA since the GNRs migrated in the gel as described in (Figure 30a) but the density of labelled DNA was too low to be detected. In samples prepared in PBS and 5 mM CTAB (Figure 21), the emission of Cy3 is clear and the migration of DNA-Cy3 corresponded to the position of GNRs (Figure 30). The intensity of the emission of fluorescence increased with the concentration of DNA incubated with GNRs. Although it is difficult to quantify the amount of DNA at this point because the samples were concentrated, it is clear that the SH-DNA-Cy3 was attached to the GNRs and their surface density strongly depends on the concentration of DNA used for sample preparation. There was a very weak signal below the main signal running at the same level as the migration of free DNA. This signal could be an indication that some DNA was electrostatically bound to the GNRs.

To further characterise the electrostatic interaction, the samples were loaded in the gel without any concentration step. In this case the GNRs concentration was too low to be detected by a scan of the optical density of the gels, but a clear signal from the labelled DNA was detected (Figure 22). In samples containing GNRs incubated with SH-DNA-Cy3 it is possible to observe two bands: first the DNA bound to GNRs, and second, free DNA in samples that migrated like the DNA references. This experiment clearly proved the usefulness of this technique in interaction-specific nanomaterial analysis.

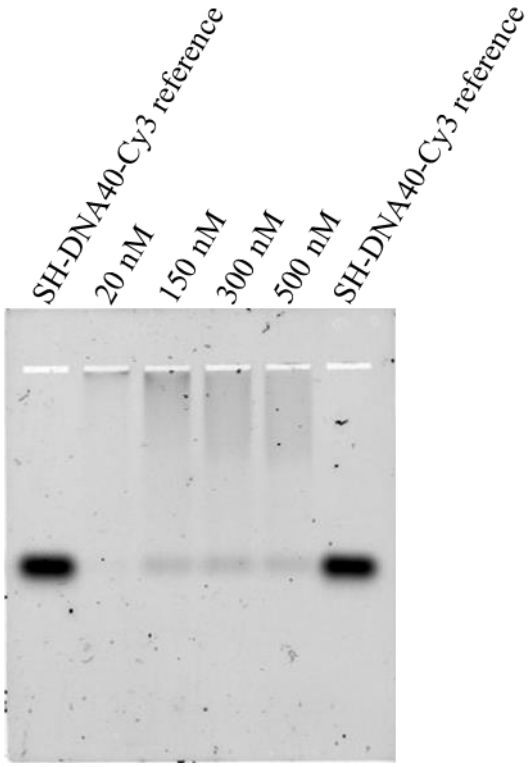

Figure 32: *Electrophoresis of GNRs functionalized by SH-DNA40-Cy3. The measurement was for Cy3 emission.*

The main result from these studies is a clear indication of SH-DNA40-Cy3 attachment to GNRs surface via thiol-gold bond for samples prepared in the presence of 1xPBS, 5 mM CTAB. The fluorescence analysis leaves little doubt, since the reference, free DNA of the same sequence, migrated in a completely different way than GNRs. Additionally; in wells with GNRs-DNA the signal from unbound DNA migrated exactly as free DNA[132]. In the case of samples prepared in 0.75 mM CTAB there is no fluorescence signal which supports the idea of functionalisation in these conditions. A probable explanation is that the number of strands per nanoparticle is too low to be registered during scanning. Additionally, in these samples GNRs accumulated in a narrow band, so scattering and absorption have an influence on the registered fluorescence.

In addition, the zeta potential of all samples could be measured after centrifugation and redispersion in water. Zeta potential measurements are often used for nanoparticle characterisation, however in this case, values did not correlate well with the electrophoresis results. It is possible that oligonucleotide strands were attached to GNR surfaces in 0.75 mM CTAB and therefore the overall charge of the nanoparticle was changed. GNRs did not aggregate when exposed to running buffer, as happens in the case of unmodified particles in 5

mM CTAB. Consequently, the use of zeta potentials is not an optimal technique for final characterisation in this instance. Some alternative approach is required.

Table 6: Zeta potential

Sample	Zeta potential	Standard deviation
Reference: GNRs in 0.5 mM CTAB	+27.7	±1.5
GNRs + SH-DNA40-Cy3 (20 nM) in 0.75 mM CTAB	-43.2	±3.1
GNRs + SH-DNA40-Cy3 (300 nM) in 0.75 mM CTAB	-38.0	±1.0
GNRs + SH-DNA40-Cy3 (20 nM) in 5 mM CTAB, 1xPBS	-27.8	±1.7
GNRs + SH-DNA40-Cy3 (300 nM) in 5 mM CTAB, 1xPBS	-29.9	4.6

The zeta potential measurements indicated however that a major change occurred in the system, a change of surface charge from positive (0.5 mM CTAB) to negative in samples exposed to oligonucleotides. The idea of decreasing the surfactant concentration down to 0.5 mM resulted from the need to reduce the ionic strength (CTAB is a cationic compound), so its concentration had to be as low as possible. In the case of SH-DNA containing samples they were clearly negatively charged, even more in the case of GNRs functionalised in 0.75 mM CTAB. This is in contradiction with the agarose gel analysis, where it was not possible to clearly show the presence of DNA on the nanoparticles surface. One possible explanation is that sufficient strands were bound to the surface to produce a change in the charge of the nanostructure but insufficient for fluorescent detection in the agarose gels.

3.4.5. Summary

Using electrostatic deposition for the immobilisation of DNA onto GNRs surfaces turned out to be an efficient process; – differences in migration rates during electrophoresis and

strong fluorescence testified to the success of binding. Samples prepared in 0.75 mM CTAB showed different behaviour during electrophoresis (independent of oligonucleotide concentration) and no fluorescent emission. Therefore, nanomaterials prepared in this way could no longer be considered as promising for the rest of this thesis. Thus, the focus now will be on functionalisation in buffered solutions.

4. Gold nanorods functionalisation

Introduction

In the previous chapter I determined the conditions in which thiolated oligonucleotides are able to reach GNRs surfaces despite the presence of CTAB in solution and bind via the thiol-gold bond to the GNRs. The SH-DNA/GNRs hybrids need to be further characterised in order to quantify the DNA surface density per GNRs and the number of double strands on GNRs surfaces after hybridisation with the complementary strand. In addition, GNRs surface modification was further optimised in order to improve the colloidal stability of the nano-hybrid system in buffer solution and also to control their cytotoxicity for eventual *in vivo* applications.

This chapter will describe the quantitative analysis method of functionalising GNRs. The detailed studies of the surface density of both ssDNA and dsDNA immobilised on the GNRs is also described. The method that was developed is based on agarose gel electrophoresis.

In parallel, the optical properties of the nanomaterials were examined using the fluorescence emission intensity of labelled DNA. Since the final goal is an *in vivo* application the idea was to develop a functionalisation method that is reproducible and very well controlled.

The results presented in this chapter cover the most salient features of nanomaterials, with repercussions for further biological and physical studies.

4.1. Thiolated DNA immobilisation, characterization

4.1.1. Samples rinsing

A method of functionalisation that allowed specific immobilisation of DNA on the GNRs via a thiol-gold bond is described. The next steps focus on protocol optimisation. The first issue was the removal of excess CTAB from the sample solution and the dispersion of functionalised GNRs in pure 1x PBS; necessary conditions for subsequent hybridisation.

An important aspect of GNRs surface functionalisation is the optimisation of the rinsing steps. Indeed, it is crucial that no free SH-DNA in solution is present during hybridisation.

In the previous chapter, we concluded that a large excess of SH-DNA compared to GNRs is best for efficient immobilisation (see table 5, chapter 3). The result of the rinsing optimisation is shown in Figure 33. After overnight incubation of the GNRs solution with

different SH-DNA concentrations in 1x PBS and 5 mM CTAB, each sample was rinsed 3 times which means 3 cycles of centrifugation, removal of the supernatant and dispersion in 2% aqueous Tween20 (first two cycles) and 1x PBS (last cycle).

Figure 1 shows an agarose gel scanned for the detection of the emission intensity of the fluorescence of the labelled DNA. The nature of the loaded samples is indicated in the figure: First, the reference sample is the free SH-DNA-Cy3 at 20 nM; then the GNRs/SH-DNA samples after the 3 rinsing cycles and concentrated before loading in the wells of the gel. Alternatively, the last supernatant of all samples was loaded as a control for the presence of free SH-DNA-Cy3 in the samples.

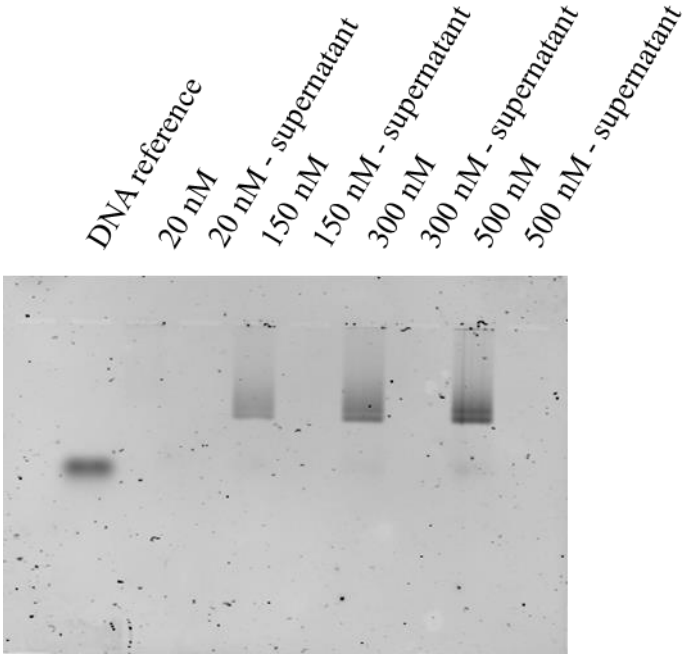

Figure 33: *Agarose gel electrophoresis of the samples containing GNRs incubated with SH-DNA-Cy3 and the corresponding supernatants after rinsing. The gel was scanned so the Cy3 emission intensity could be detected. The fluorescence excitation wavelength was 548 nm.*

After 3 cycles of rinsing, there was no fluorescence emission detected in the lanes corresponding to the loaded supernatants. Therefore, we can conclude that there is no detectable free DNA in solutions in the samples after the 3 rinsing cycles. The intensity of the signal detected in the lanes corresponding to the functionalised GNRs samples increased with the concentration of SH-DNA-Cy3 initially used to functionalise the GNRs. In addition, the detected signal of DNA-Cy3 migrated slower than the free DNA (DNA reference well) we therefore conclude that the density of DNA on GNRs strongly depends on the concentration of DNA used to functionalise GNRs. Furthermore, we detected a weak signal of DNA at the same

migration line than the reference DNA, which indicated that in the solution of GNRs samples some DNA was not bound strongly to the GNRs. Knowing that no DNA was detected in the supernatant we can assume that the detected unbound DNA was adsorbed on the GNRs surface via weaker interactions than the thiol-gold bound so the unbound DNA was desorbed from the GNRs surface upon migration in the gel to finally migrate like the reference free DNA.

We can therefore conclude that the rinsing protocol is optimal and removes all free DNA from the sample solution, that an extremely small amount is adsorbed non-specifically on the GNRs surface (most probably via electrostatic interactions) and that the density of DNA immobilised on the GNRs via the strong thiol-gold bound depends strongly on the DNA concentration used to functionalise GNRs.

4.1.2. Quantification of the DNA surface density on the GNRs

The method selected to characterise the density of immobilised SH-DNA is based on the emission intensity of the labelled DNA immobilised on the GNRs surface. However, the fluorescence emission from the DNA attached to the GNRs is difficult to interpret in terms of density since the close proximity of the dyes to the plasmonic structures can strongly influence the emission intensity. Indeed, it was shown that gold nanoparticles could quench or enhance fluorescence emission[133]. In addition, the presence of GNRs causes scattering, which also influences the fluorescence emission intensity. For these reasons, DNA has to be desorbed from the GNRs surface and then quantified as free DNA. 2-Mercaptoethanol was used at high concentration to displace the DNA molecules from the surface, as it reacts with the metal surfaces[134] and has already been tested in similar experiments[135]. The assumption was to use high concentrations of 2-Mercaptoethanol, to allow fast and efficient SH-DNA replacement on GNRs. The samples are then directly loaded on the gel (Figure 34).

In order to control the concentration in the loaded samples on the gel so that the amount of desorbed DNA could be quantified, the GNRs solutions were not concentrated.

The volume of GNRs functionalised with DNA samples was 1 mL so both the gel and the absorption spectra could be performed on the same sample solution in order to control the concentration of GNRs in all samples.

9 µL of DNA-GNRs solution were added to 4.5 µL of 50 % aqueous solution of glycerol and 4.5 µL of 95 % (14.3 M) 2-Mercaptoethanol. This was incubated (protected from daylight to avoid bleaching of the dyes) for 10 min to allow DNA desorption and directly loaded

in the gel wells: it was very important to transfer all the samples for quantification. Gel electrophoresis was carried out for 40 min at 50 V.

Fluorescence measurements were made using a Typhoon scanner whose software enables quantification of the signal intensity (Figure 34). For each gel two wells were filled with SH-DNA40-Cy3 reference solution at 20 nM diluted in 50 % glycerol in water.

The GNRs were functionalised with SH-DNA40-Cy3 at 20, 150, 300 and 500 nM SH-DNA40-Cy3 (Figure 34).

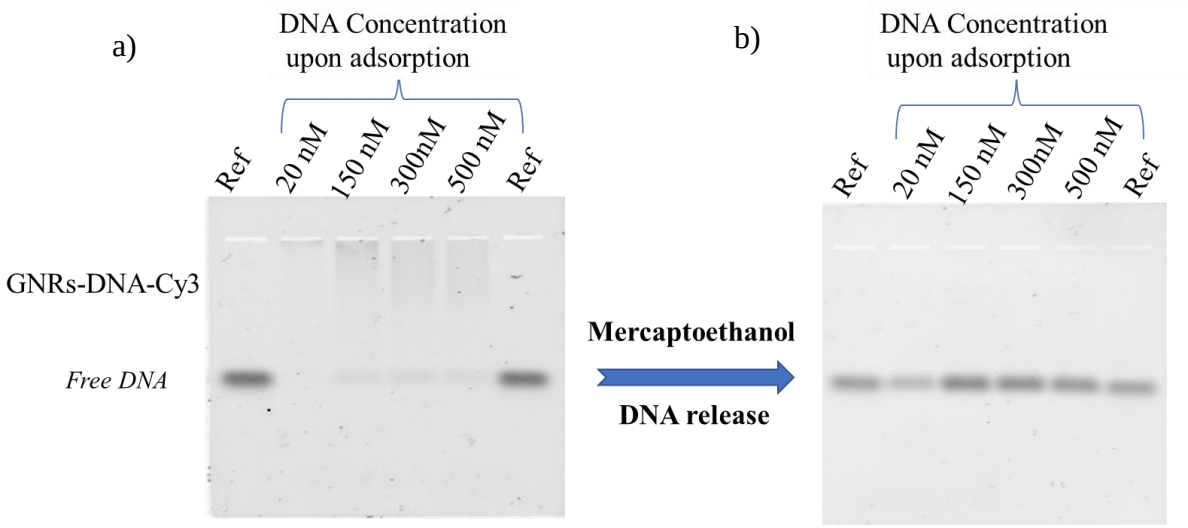

Figure 34: Gel electrophoresis scanned to measure the fluorescence of Cy3. Samples were GNRs incubated with 20, 150, 300, and 500 nM of SH-DNA-Cy3, incubated for functionalisation, rinsed and loaded in the gel a) before and b) after incubation with 2-Mercaptoethanol. Ref corresponds to the lane of the reference that consisted of 20 nM of free SH-DNA40Cy3. The fluorescence excitation wavelength was 548 nm.

In Figure 34a, we observed a single band for the two refs corresponding to the migration of the free SH-DNA-Cy3. For the GNRs functionalised with 20 nM of SH-DNA-Cy3 we observed a weak signal close to the well. For GNRs functionalised with higher DNA concentrations (150 nm to 500 nm) we observed a smeared signal from the wells where the samples were loaded and a weak band that ran like the free SH-DNA-Cy3. As described previously (see Figure 33), the smeared signal comes from the DNA that is attached through the thiol-gold bound to the GNRs and the single band corresponds to the DNA that was immobilised with weaker (presumably electrostatic) bonds to the GNRs surface that desorbed in the gel upon migration. In Figure 34b, the samples were incubated with a large excess of 2-Mercaptoethanol for 10 min and loaded directly in the gel with two SH-DNA-Cy3 references. While the free reference DNA migrated at the same rate than the two reference solutions in

Figure 34a, the migration characteristic of the samples of functionalised GNRs incubated with 2-Mercaptoethanol was different than the migration observed for the functionalised GNRs before incubation with 2-Mercaptoethanol. Indeed, in Figure 34b, no smeared signal could be detected; only a clear band that migrated like the free DNA was seen. Since the DNA in these samples migrated like the reference and no signal could be detected on the GNRs, we concluded that all the immobilised DNA was displaced by the 2-Mercaptoethanol and released into solution.

4.1.3. Standard deviation estimation

Standard deviations were calculated based on measurements carried out on samples after incubation with a large excess of 2-Mercaptoethanol loaded in 3 wells of the same gel (Figure 35). Additionally, a reference solution of 20 nM DNA was also loaded.

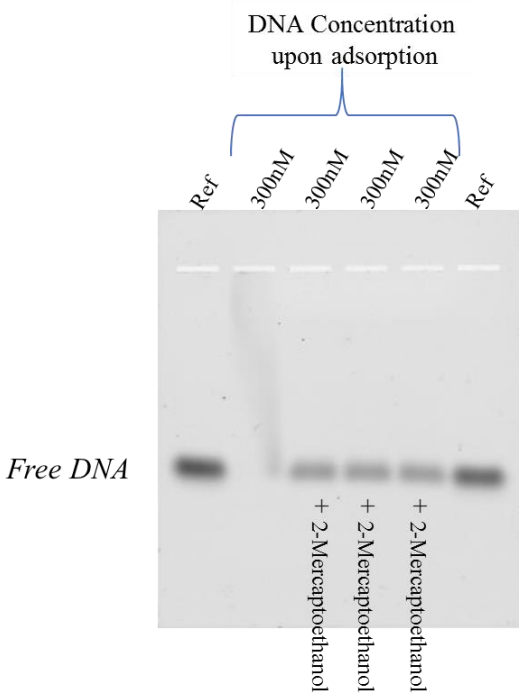

Figure 35: *Agarose gel electrophoresis of the same samples containing GNRs functionalised with SH-DNA-Cy3, rinsed and incubated with 2-Mercaptoethanol. The gel was scanned so the Cy3 emission intensity was detected (the excitation wavelength was 548 nm). Ref corresponds to the lane of the reference that consisted of 20 nM of free SH-DNA40Cy3.*

To calculate the standard deviation, the emission intensity of each was measured using an image-processing program. The results are presented in Table 1. Next to the emission bands, the background emission values were also measured and the results of sample fluorescence were corrected. With all these measurements it was possible to calculate the average emission and standard deviation.

Table 1: emission intensity per pixel (within the specified area) obtained from the gel presented in Figure 3.

Samples emission [a.u.]	782.38	781.41	777.47
Background [a.u.]	289.96	297.08	294.50
Samples correction	492.42	484.33	482.97
Average result	486.57±5.11 (1.05 %)		

The low standard deviation suggests that the variations in the measurements were mostly caused by the background (the background value is collected individually for each sample); the results obtained in this experiment were, however, incorporated into further experiments as part of the calculation of the error bar.

4.1.4. Quantitative determination of thiolated DNA immobilised on GNRs

As the efficiency of DNA desorption from the GNRs surface using a large excess of 2-Mercaptoethanol has been demonstrated and since the standard deviation of the measurement was compatible with quantification, the next step was to focus on the calculation of the DNA surface density on GNRs functionalised with different concentrations of SH-DNA-Cy3. The data were obtained from the measurements presented in Figure 34. It is possible to observe a clear difference between samples before and after 2-Mercaptoethanol treatment. With the oligonucleotides release all of the detected emission intensity comes from the band that had migrated the same distance as the reference. Although the signal that was detected for electrostatically bound DNA in the samples before the incubation with 2-Mercaptoethanol (see Figure 34a) was weak, I considered that this signal should be considered present in the samples after incubation with2-Mercaptoethanol and therefore all the calculations of surface density were corrected accordingly.

Based on the gel electrophoresis from Figure 34 the DNA surface density was calculated (Figure 36). The results are presented as concentrations, because they were compared to the reference expressed in nM.

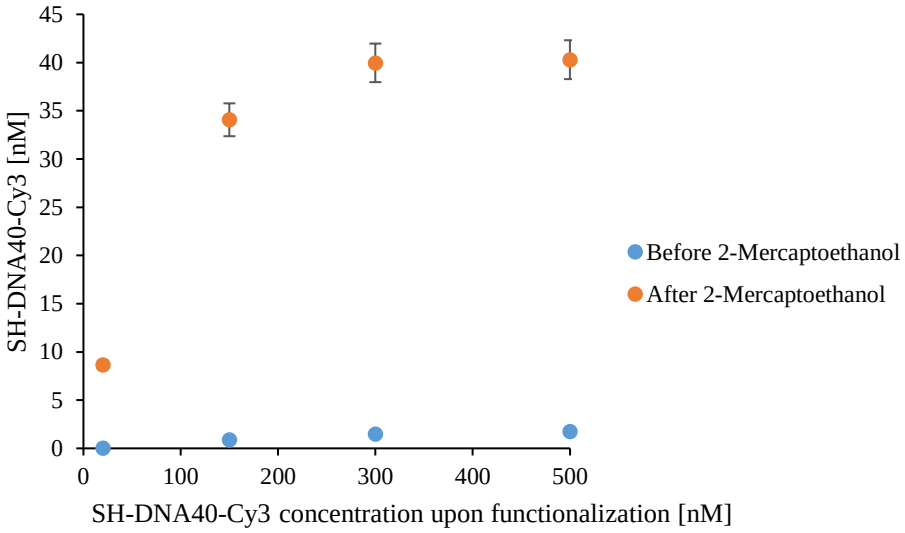

Figure 36: *Concentration of free DNA in samples before (in blue) and after (in orange) the 2-Mercaptoethanol treatment, deduced from the gel electrophoresis presented in Figure 34 as a function of the SH-DNA-Cy3 concentration used to functionalised GNRs.*

In Figure 36, we observed a very small DNA concentration corresponding to the non-specifically bound DNA to the GNRs (in blue), in agreement with the gel electrophoresis in Figure 34. The concentration of free DNA released from the surface of GNRs induced by 2-Mercaptoethanol increased with the concentration of SH-DNA-Cy3 used to functionalise GNRs indicating that the surface density depended strongly on the DNA concentration that was incubated with the GNRs. The concentration of DNA that was bound to GNRs reached a plateau when 300 nM of SH-DNA-Cy3 was incubated with GNRs indicating that the surface density reached a maximum.

In order to quantify the DNA surface density, the concentration of GNRs in each sample had to be identical. The concentration of GNRs that was incubated with SH-DNA-Cy3 during the functionalisation was 0.18 nM. After incubation, each sample was rinsed by 3 cycles of centrifugation and dispersion in the buffer solution, which implied losing some GNRs in the process. Therefore, the concentration of each samples had to be characterised in parallel with gel electrophoresis so the error could be corrected for the surface density quantification.

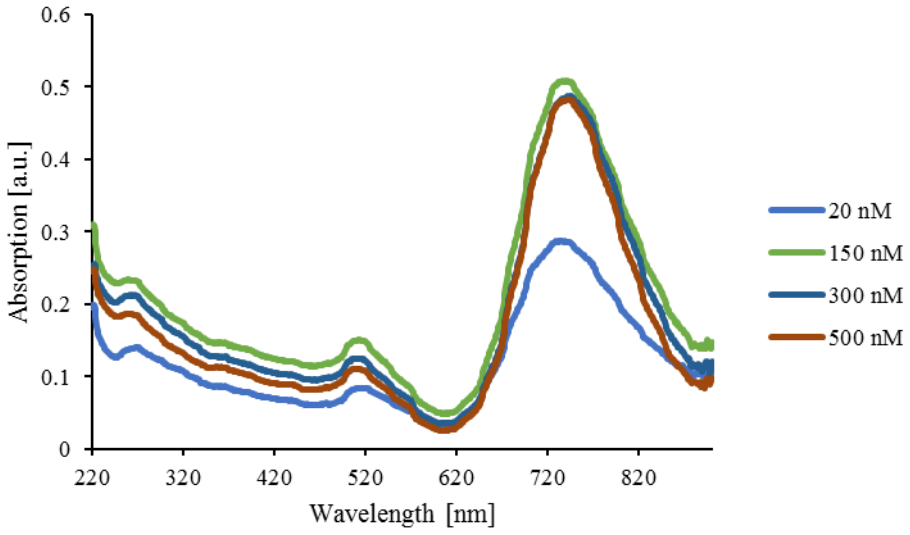

Figure 37: *Absorption spectra of GNRs functionalised with different concentrations of SH-DNA-Cy3, and after 3 cycles or rinsing steps to remove excess DNA from the solution.*

Figure 37 shows an absorption spectrum of the GNRs functionalised with different DNA densities recorded after the 3 rinsing cycles. We noticed a weaker absorption intensity at 750 nm for the samples prepared with 20 nM of SH-DNA-Cy3, than for samples prepared with 150, 300 and 500 nM of SH-DNA-Cy3. The GNRs concentrations calculated from the absorption spectra are given in Table 2.

Table 2: Calculated concentrations from the absorption spectra of GNRs in rinsed samples functionalised with different SH-DNA-Cy3 concentrations. The initial concentration of GNRs was 0.18 nM.

DNA concentration during functionalization (nM)	The final GNRs concentration (nM)
20	0.069
150	0.123
300	0.118
500	0.117

The initial GNRs concentration that was incubated with different concentrations of SH-DNA-Cy3 was 0.18 nM. From Table 2, we conclude that the concentration of GNRs decreased after the 3 rinsing cycles and that the difference was more important when lower concentrations of DNA was used for functionalisation. Therefore, high DNA surface density improves the stability of the hybrid system.

To calculate the surface density, it was therefore important to normalise the amount of DNA that is released from the GNRs surface to the measured GNRs concentration.

The results of these calculations are presented in Figure 6.

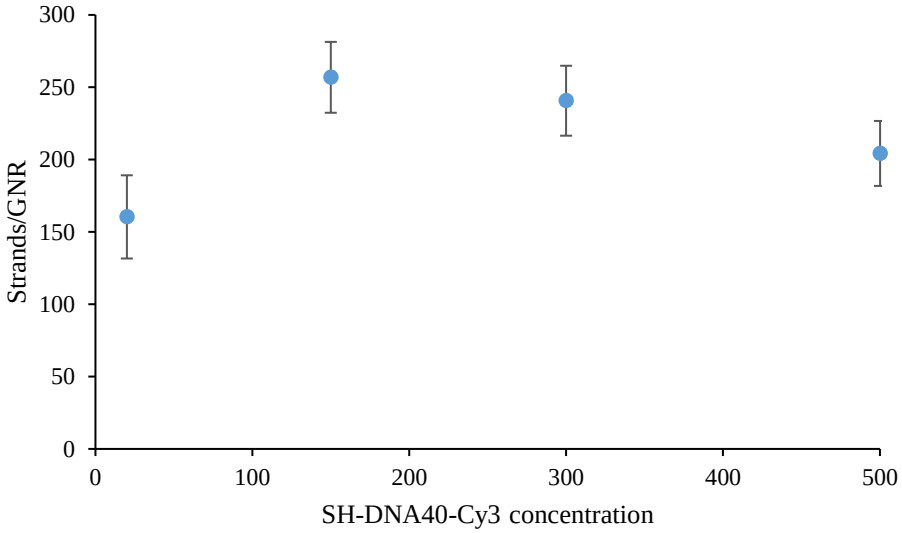

Figure 38: *Number of DNA strands per GNRs calculated from agarose gel electrophoresis and corrected for the non-specific interactions of DNA with the GNRs surfaces and normalised for the GNRs concentration.*

The DNA surface density increased from 150 strands/GNR when 20 nM of DNA was used for functionalisation to a maximum of approximately 250 strands per GNR for higher DNA concentrations. The surface coverage calculation indicated a smaller variation of the strands/GNR than what was deduced directly from gel electrophoresis before the corrections (comparison of Figure 36 and Figure 38). This is due to the fact that with lower DNA concentration (20 nM) used during the functionalisation, the GNRs solution was not as stable as the functionalised GNRs prepared with higher DNA concentrations. For this reason, the concentration in the final sample is lower in the samples prepared with 20 nM than with higher concentrations.

The theoretical maximum surface density of DNA on GNRs of 10 nm of diameter and 35 nm in length was estimated to be 275 DNA/GNRs (see chapter 3). It is interesting to notice that the functionalisation method that was optimised here allowed immobilisation of approximately 250 DNA strands per GNRs, which is very close to the theoretical value. In addition, this experimental maximum strand density was obtained with an excess of DNA of 833 compared to the initial GNRs concentration.

Because nanoparticles with low DNA surface density were partially aggregating during the rinsing steps, I further optimised the surface functionalisation by the addition of thiolated long ethylene glycol polymer.

4.2. SH-PEG addition

4.2.1. Stability influence and biocompatibility

Aggregation of GNRs upon functionalisation is mainly caused by the desorption of CTAB molecules that leads to a decrease of the positive charge on the GNRs surfaces and a tendency towards to neutral charge on their surface (the zeta potential after functionalisation is between -5 and +5)[136].

The measurements of the zeta potential on GNRs functionalised with DNA gave values between –30 and –43 according to the DNA concentration used for functionalisation (see Table 6 chapter 3) while the zeta potential of GNRs in solution was +28. The GNR colloidal solution functionalised with high DNA surface density was stable because particles were negatively charged and therefore repulsed each other electrostatically. Upon centrifugation, GNRs were concentrated at the bottom of the tube where functionalised GNRs with low DNA surface density were more likely to undergo aggregation. In order to prevent aggregation, GNRs needed to be further protected. The mechanism of stability improvement by pegylation is based on mechanical and electrostatic properties. SH-PEG with MW=6000 are long, flexible chains that surround the functionalised nanoparticles[137]. Additionally, PEG is hydrophilic, so water molecules will surround the chain; an additional feature preventing aggregation. Hydrophilicity can also improve the redispersion of GNRs after centrifugation.

An additional feature of PEG is its biocompatibility; among the FDA approved nanomaterials for medical application, most nanoparticles are functionalised with this polymer[138]. PEG increases the retention time of nanomaterials, mainly due to decreased opsonisation[139]. Moreover, phagocytes react faster with charged nanoparticles (fast opsonisation), so “in the shadow” of PEG chains it is possible to hide therapeutic agents (e.g. oligonucleotides) with charge

4.2.2. Functionalisation with SH-PEG and quantification of attached thiolated oligonucleotides

In the last chapter, we anticipated that DNA immobilisation on GNRs was not sufficient to obtain a stable colloidal solution that could undergo all the required steps of centrifugation essential for purification, rinsing and the different final applications envisaged for the samples. Pegylation was therefore chosen to improve sample stability. The protocol introducing pegylation was optimised and the final functionalisation protocol is the following: 1.2 nM of GNRs in 1xPBS, 5 mM CTAB were mixed with SH-DNA40Cy3 (300 nM) and incubated for

4 hrs. The immobilisation of DNA on the GNRs surface could be followed by the change of the solution colour: starting with a pink colour, the solution became colourless. It was observed that once the GNRs were functionalised with DNA, they were adsorbed on the Eppendorf tube walls (see chapter 3). The addition of Tween20 such that the final concentration was 2 % followed by an incubation of 2 hours allowed redispersion of the functionalised GNRS in solution that then recovered its pink colour. (See chapter 3 for more details).

Then, without any further treatment, 10 µL of 4 mM SH-PEG_{6000} was injected in the solution (to a final concentration of 40 µM) and incubated for 30 min after a fast vortex.

It is important to notice that the concentration of PEG was much larger than the concentration of ssDNA used for the functionalisation of GNRs (120-times). The reason is that the PEG polymer was long and the probability of forming a thiol-gold bond was therefore low. The adsorption time was much shorter because the goal was to have few PEG molecules attached to the surface of GNRs so PEG would not replace the immobilised DNA molecules. Subsequently three rounds of centrifugation and redispersion took place: the first two were re-dispersed in aqueous solutions containing 2% of Tween20 and the third in pure 1xPBS. Finally, GNRs-ssDNA were in 0.95xPBS and 0.1 % Tween20.

To characterise the influence of the SH-PEG adsorption on the DNA surface density of DNA immobilized on the GNRs, I characterised the functionalised GNRs with the SH-PEG in the same manner than with no PEG as previously described.

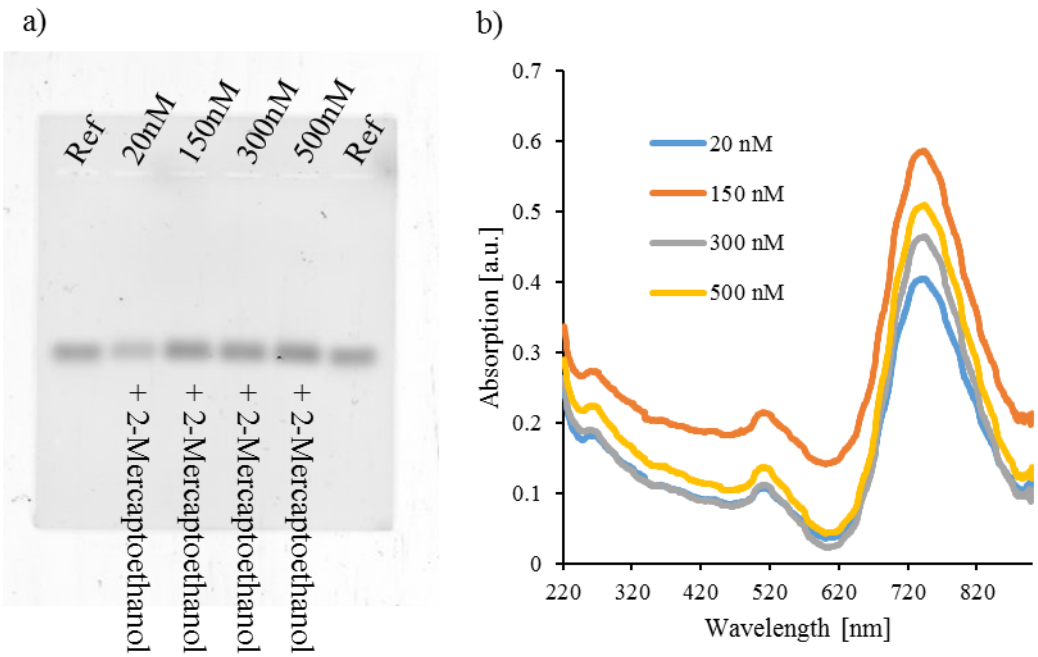

Figure 39: Pegylated functionalised GNRs samples used for the calculation of the number of strands immobilised on GNRs. In a) the agarose gels (excitation 532 nm for collecting the emission intensity of Cy3) of loaded samples after their incubation in 2-Mercaptoethanol and in b) the corresponding extinction spectrum of the same samples but before 2-Mercaptoethanol treatment.

Figure 39a shows agarose gel electrophoresis of functionalised GNRs with different DNA concentrations and with the SH-PEG, rinsed 3 times with centrifugation cycles to remove all the unbound DNA and incubated with 2-Mercaptoethanol to desorb immobilized DNA in solution. As previously described the refs correspond to 20 nM of free SH-DNA-Cy3. In samples prepared with 20, 150, 300 and 500 nM of SH-DNA-Cy3 and after the 2-Mercaptoethanol treatment, we observed that the SH-DNA-Cy3 migrated at the same distance as the free DNA refs. Therefore, the efficiency of the 2-Mercaptoethanol treatment to desorb the immobilised DNA was not affected by the presence of SH-PEG on the surface of the GNRs. Also, the absorption spectrum measurement clearly indicated that the stability of GNRs functionalised with 20 nM SH-DNA is similar to those exposed to higher DNA concentrations. Therefore, we confirmed that the pegylation improves the stability of GNRs functionalised with low DNA surface density.

The calculation of the number of strands per GNRs was performed as described previously.

Figure 40 shows the variation of the number of strands per GNRs as a function of the DNA concentration that was used for GNRs functionalisation.

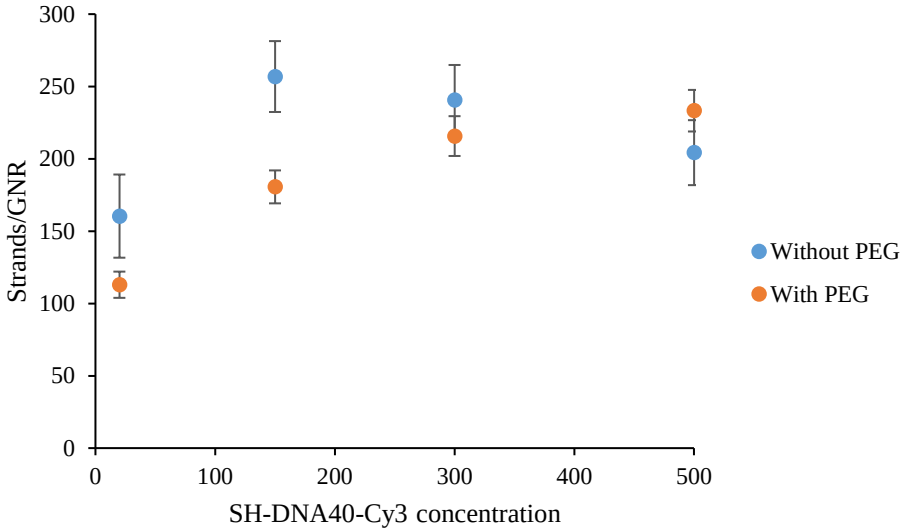

Figure 40: *DNA surface density on GNRs on non-pegylated and pegylated GNRs corrected from the non-specific adsorption and the GNRs concentration.*

First, in the case of pegylated samples it was possible to observe a lower standard deviation. The experiment was more reproducible than with non-pegylated samples. While the maximum strands/GNR ratio reached 250 for a DNA concentration of 150 nM for the non-pegylated samples, the maximum surface density is reached at 300 nM DNA for pegylated samples. The strands/GNRs at 20 nM and 150 nM DNA is lower for pegylated samples than for the non-pegylated samples certainly due to competition between thiolated DNA and thiolated PEG. We confirmed therefore that PEG improves the stability of nanoparticles functionalised with low DNA surface density.

Agarose gel electrophoresis provided detailed data about thiolated oligonucleotides coverage on the GNRs surface. This was extremely important, because it constituted a starting point to analyse the hybridisation efficiency on GNRs surfaces; an essential step for this thesis. Characterisation of the hybridisation efficiency is the subject of the following sections.

4.2.3. Influence on nanomaterial adsorption/desorption properties

The next step was to characterise the accessibility of the immobilised DNA to complementary DNA strands. The formation of duplex DNA on the surface of the GNRs should induce an increase of the average distance of the Cy3 fluorophore for the GNRs surface. Indeed, the SH-ssDNA-Cy3 was labelled at the 5’ end with the thiol that is the anchor point of the DNA

to the GNRs surface and at the 3' end with the Cy3 fluorophore. The ssDNA has a persistence length of 2.2 nm [140] which means that the distance between the fluorophore and the gold surface is much lower than the length of the ssDNA molecules that has 40 bases. The persistence length of double strand DNA is 50 nm,[141] therefore for a double strand of 40 base pairs or 14 nm, it implies that the dsDNA on the surface of the GNRs is linear (in the prescribed conditions of salt concentration and at ambient temperature). At the surface density that we characterised, there was one strand per 10 nm^2 for low DNA density and 4 or 5 nm^2 for high DNA density (the surface of the GNRs is 1100 nm^2 and the maximum number of strands/GNRs is 250). Therefore, the dsDNA on the surface has to be more or less perpendicular to the surface. In conclusion, the average distance between the GNRs surface and the Cy3 fluorophore has to increase upon hybridization.

To check this hypothesis and to characterise the influence of pegylation on the hybridisation efficiency, pegylated and non-pegylated GNRs-SH-DNA40-Cy3 diluted in 0.95xPBS, 0.1 % Tween20 were hybridised using an excess of complementary DNA in solution. The temperature was then increased to 70 °C and incubated for 5 min before a slow cool down of the samples to ambient temperature (overnight).

The effectiveness of dsDNA formation was checked by hybridising 50 nM of the complementary oligonucleotide (DNA35). To follow the fluorescence emission intensity measurements were performed on the samples before and after hybridisation.

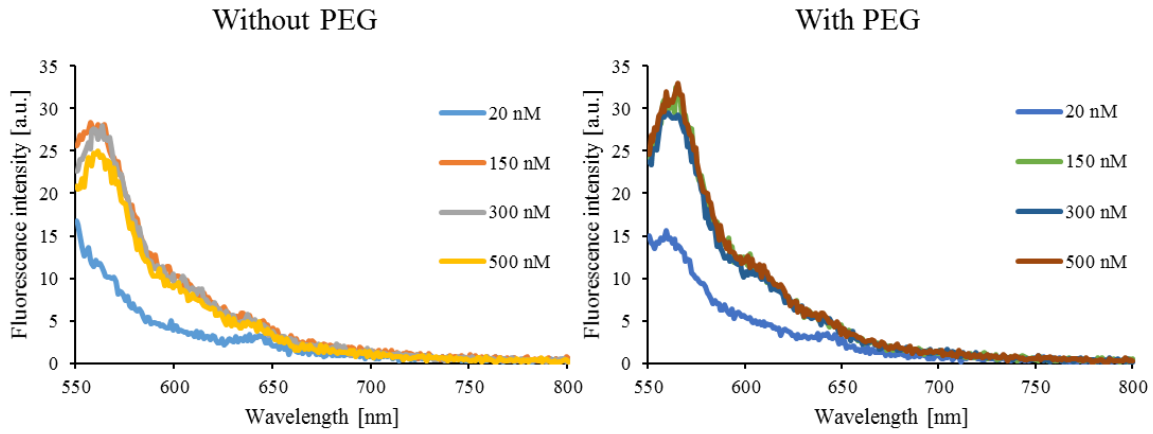

Figure 41: Fluorescence emission intensity of Cy3 of functionalised GNRs without (left) and with (right) and before hybridisation. The excitation wavelength was 530 nm.

The fluorescence emission intensity of GNRs functionalised with 150 nM 300 and 500 nM of DNA before hybridisation was in the range of 25-27 a.u. without SH-PEG and 29-34 a.u.

(with SH-PEG). The emission intensity of GNRs functionalised with 20 nM of SH-DNA40-Cy3 was very low confirming the lower DNA surface density. It is interesting to note that the emission peak of the Cy3 of samples prepared with 20 nm of DNA was higher (15 a.u.) on pegylated samples than with the non-pegylated samples indicating that the average distance of the Cy3 from the surface on the pegylated GNRs was larger than on the non-pegylated samples even if the differences were small. This difference could indicate that the strand arrangement on the GNR surface was different.

The next step was to perform hybridisation with the complementary strand and an overnight incubation in order to form dsDNA; the concentration of complementary DNA35 was in excess compared to the concentration of immobilised DNA on the surface of the GNRs characterised previously (according to the calculations it was twice as concentrated as the attached DNA).

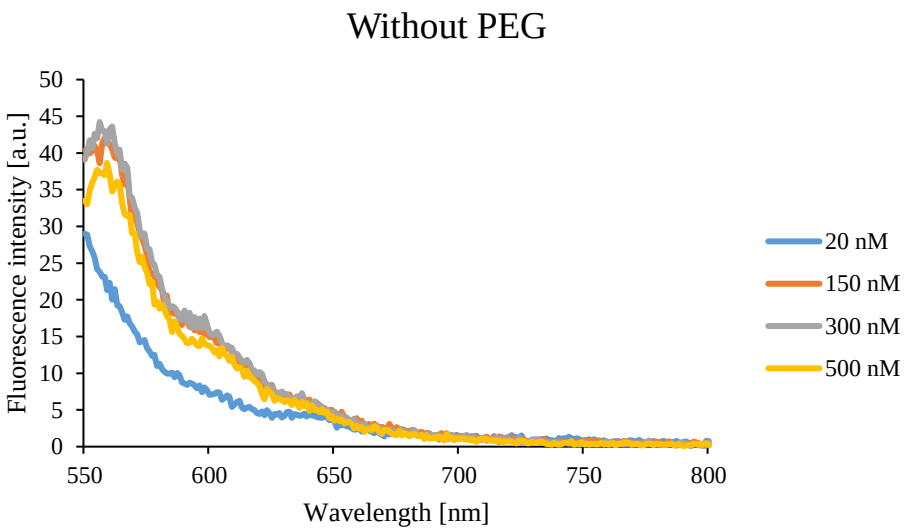

Figure 42: Hybridisation with the complementary DNA strand. Excitation wavelength 530 nm.

The result of this experiment, performed with an excess of DNA35 was in good correlation with the calculated DNA surface density: the emission intensity of Cy3 when 20 nM of thiolated DNA was used for the GNRs functionalisation was low compared to the GNRs functionalised with 150, 300 and 500 nM. The fluorescence emission intensity of all samples after hybridisation was higher than the emission intensity before hybridisation (Figure 41 without PEG). The increase of the emission intensity was up to 38-44 a.u. after hybridisation and 29 to 34 a.u. before hybridisation. This indicated the formation of dsDNA on the GNR surface as an increase of the emission intensity was expected upon hybridisation. As mentioned before, the only problem with samples without SH-PEG was low stability during the

centrifugation steps; the pellet was turning into aggregate although these samples were measured without a rinsing step after hybridisation since the complementary strand was not labelled.

The last part of this experiment was to measure the fluorescence of samples with SH-PEG after hybridization with DNA35 in the same conditions.

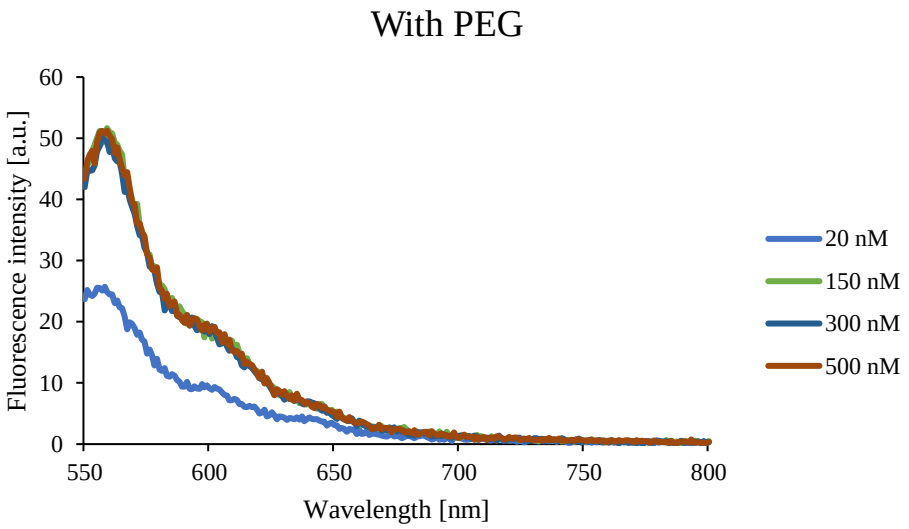

Figure 43: Hybridisation with the complementary DNA on the functionalised GNRs with PEG. Excitation wavelength 530 nm

The samples functionalised with 150-500 nM SH-DNA40-Cy3 had the same emission intensity, in agreement with the DNA surface density quantification that was similar. Additionally, the fluorescence signal was slightly higher than in the case of samples without PEG, so we can conclude that pegylation did not reduce strand accessibility. As described for the GNRs without PEG, the emission intensity before hybridisation was lower than the emission intensity after hybridisation, confirming the change in conformation from a ssDNA to a dsDNA.

The results of this experiment were therefore very encouraging as it was possible to obtain nanomaterial with a mixed-ligand layer (SH-DNA and SH-PEG) on the surface without affecting the fluorescence properties, the DNA surface density nor increasing the nanomaterial stability. Such functionalised GNRs are perfect candidates for further studies focused on the quantification of the number of hybridised strands on the GNRS surface.

4.2.4. Conclusions

At this stage of the project, we have demonstrated that agarose gel electrophoresis is a useful tool for advanced characterisation of nanomaterials. The juxtaposition of results obtained

after the DNA was released from the GNRs surface allowed calculation of the number of strands per nanoparticle. As shown, the electrostatic-based deposition enables attachment of up to 250 SH-DNA to each GNR. Such a result was positive as it allowed control of the DNA surface density from 100 to 200 strands/GNRs keeping the colloidal solution stable.

4.3. Formation of dsDNA on the GNRs surface

The previous chapter was dedicated to optimising the functionalisation of GNRs surfaces with ssDNA and their further modification to obtain stable functionalised GNRs with specific optical properties. It was demonstrated that the addition of SH-PEG_{6000} to the surface of ssDNA functionalised GNRS improved the stability of the colloidal solution in 1x PBS and did not affect the formation of dsDNA on the nanoparticle surfaces. Next, the yield of hybridisation had to be characterised by comparing the number of ssDNA immobilised on the GNRs surface and the number of dsDNA after hybridisation. I developed a protocol that allowed quantification of hybridised strands using gel electrophoresis. In order to get full control over the specificity of the hybridisation I used complementary and non-complementary strands to the ssDNA immobilised on the surface: SH-DNA40-Cy3 was on the GNRs surface and DNA35-Cy5 is the complementary strand while DNA35-Cy5nC is the non-complementary strand. Both complementary and non-complementary strands are labelled at their 5' end with the Cy5 fluorophore. Since the couple of fluorophores Cy3 and Cy5 can efficiently FRET, I used FRET to characterise hybridisation. It is important to recall that Cy3 is labelled on the 3' position of the SH-ssDNA (SH- being at the 5' end), whereas Cy5 is on the 5' end. Therefore, after hybridisation both fluorophores are close to each other and do not limit FRET. In addition, we showed that hybridisation with a non-labelled ssDNA brings the Cy3 fluorophore away from the surface of the GNRs indicating that the dsDNA is standing up toward the solution. As a result, we expected that the emission of the Cy5 would not be quenched as was observed with Cy3 after hybridisation.

4.3.1. Sample preparation for hybridization

All samples were prepared as described previously: 0.18 nM GNRs diluted in 5 mM CTAB and 1x PBS were incubated with 300 nM of SH-DNA40-Cy3 (corresponding to a molar ratio of 1:1666) for 4 hrs. After the Tween20 injection and 30 min incubation, the samples were then incubated with 40 µM SH-PEG_{6000} for 30 min, centrifuged (8 000 rcf, 30 min) and rinsed. The final GNRs concentration of functionalised GNRs was 0.12 nM and the SH-DNA coverage was estimated at 216±14 strands per nanoparticle.

For hybridisation, samples in 1xPBS, were incubated with DNA35-Cy5 or with DNA35-Cy5nC at different concentrations and incubated at 70 °C for 5 min before an overnight slow cool down to ambient temperature (overnight). The samples were then directly characterised without any further rinsing steps.

4.3.2. FRET analysis

Fluorescence measurements of colloidal solution, in order to reveal FRET, were carried out in 1 mL samples, excited at 530 nm. The reason why the excitation wavelength was fixed at 530 nm was due to the influence of CTAB on the absorption spectrum as discussed in chapter 3: placing the excitation wavelength at 530 nm ensured a strongly reduced impact of CTAB at all concentrations. However, the Cy3 absorption spectrum had a plateau (see figure 7 chapter 2, Materials and Methods), from 525 to 535 nm and moving the excitation wavelength within this range did not have an impact on the emission.

The range of the acquisition of the emission intensity was set between 550 and 800 nm.

In the case of agarose gel analysis, the excitation wavelength was fixed to 532 for Cy3 and 648 nm for Cy5 and could not be modified. As the result, the emission intensities at specific wavelengths were collected (570 and 680 nm).

To quantify the number of dsDNA formed on the GNRs surface, the concentration of the complementary strand was varied from 0 nM for control to 20 nM.

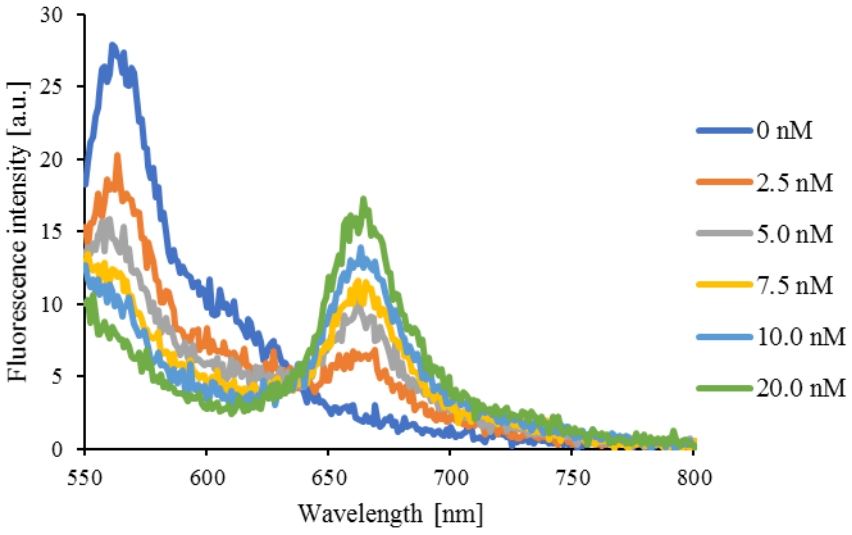

Figure 44: *Fluorescence emission intensity of SH-DNA40Cy3 functionalised GNRs hybridised with different concentrations of DNA35-Cy5 complementary strand. Excitation wavelength 530 nm.*

First, with no complementary strands (0 nM ssDNA) we only observed the emission intensity of Cy3 (Figure 44). As the concentration of the complementary strand labelled with Cy5 increased, we observed a significant decrease of the emission intensity of Cy3. As the concentration of the complementary strand labelled with Cy5 increased, we observed an increase in intensity of the Cy5 emission peak. At 20 nM of the complementary strand, only the Cy5 emission peak could be detected, the emission intensity of Cy3 being undetectable. The correlation between the decrease of the Cy3 emission peak intensity and the increase of the emission peak intensity of Cy5 was indicative of efficient FRET, therefore indicating that hybridisation occurred between the ssDNA immobilised on the GNRs surface and the complementary strand in solution.

For samples incubated with the non-complementary strand, we observed no variation of the Cy3 emission intensity while the emission intensity peak of Cy5 increased with increasing concentrations of the non-complementary strand (Figure 45); indicating that no FRET was detectable.

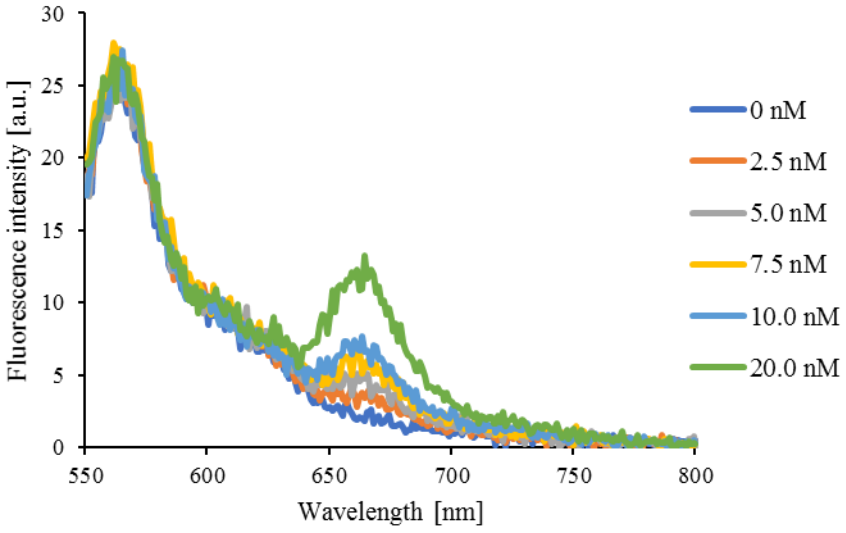

Figure 45: *SH-DNA40Cy3 functionalised GNRs hybridized with DNA35-Cy5nC (non-complementary). Excitation wavelength at 530 nm.*

This experiment indicated two phenomena; Cy3 emission did not vary and Cy5 emission increased following increased concentration of DNA35-Cy5nC.

As a conclusion, FRET is a powerful tool to confirm that hybridisation on the surface of GNRs is efficient. The fact that we do not detect FRET with the non-complementary strand confirmed that no non-specific interactions of the non-complementary strand with the surface of the functionalised GNRS was detected, demonstrating the high performance of the optimised functionalisation method.

Nevertheless, it is important to control the eventual direct excitation of Cy5 at the excitation wavelength of Cy3, at 530 nM. Indeed, as shown in Figure 46, Cy5 was directly excited at 530 nm. The emission intensity of Cy5 excited at the wavelength of Cy3 increased with the concentration of DNA-Cy5 in solution. This effect was problematic, as the emission intensity of Cy5 was not therefore induced only by FRET. The fluorescence emission intensity of the acceptor cannot be directly indicative of FRET and therefore hybridisation.

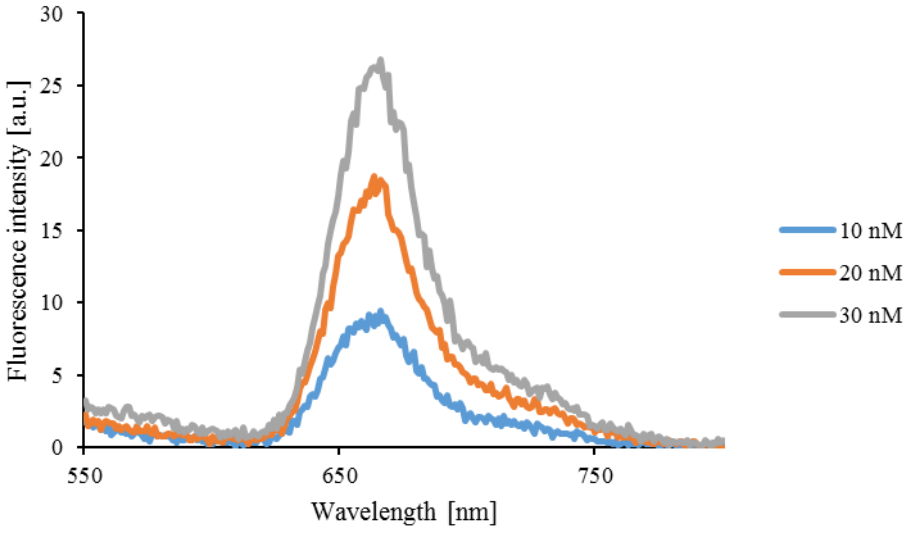

Figure 46: *Fluorescence emission intensity of Cy5 (DNA35-Cy5) caused by an excitation at 530 nm. The all excitation settings were identical to those for Cy3 excitation but with no GNRs in solution.*

We observed in Figure 46 a clear correlation of emission of fluorescence of Cy5 with concentration. Most of my experiments were performed in the range 0-20 nM of Cy5-labelled DNA, therefore in the case of excitation at 530, the peak of Cy5 should be in the range of 15-20 units (through all of the experiments the detector settings did not vary). In comparison to Figure 45, where the non-complementary strand is added to the functionalised GNRs solution at the same concentration range we noticed that the emission intensity of Cy5 is lower than in Figure 46, where the DNA strand is diluted in a pure PBS solution with no GNRs. This is associated with the GNRs scattering.

Nevertheless, it is possible to follow hybridisation on the nanoparticles surface with FRET by following the emission of Cy3, the donor after hybridisation with the complementary strand (Figure 44) as the emission intensity of the Cy3 decreased as the concentration of the complementary strand increased. Nevertheless, following the donor emission cannot be quantitative, because the FRET phenomenon is not yet well characterised in the proximity of plasmonic structures.

4.3.3. FRET acceptor quenching by donor proximity

A different approach would consist of directly exciting the Cy5 at 630 nm and detecting exclusively the intensity of the emission of Cy5 at 660 nm. Figure 47 and Figure 48 show

spectra for samples incubated with increasing concentrations of complementary and non-complementary strands.

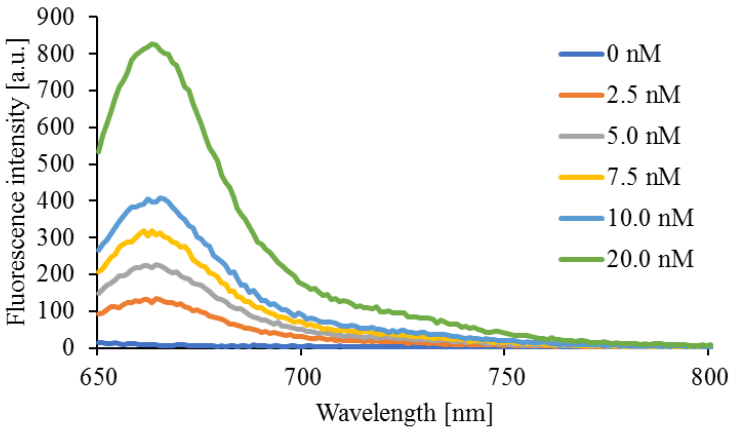

Figure 47: *Fluorescence emission of Cy5 excited at 630 nm, as a function of the DNA35-Cy5nC (non-complementary) concentration. Each sample was incubated with 0.12 nM of GNRs functionalised with SH-DNA40-Cy3 diluted in 1x PBS and 5 mM CTAB following the hybridisation protocol.*

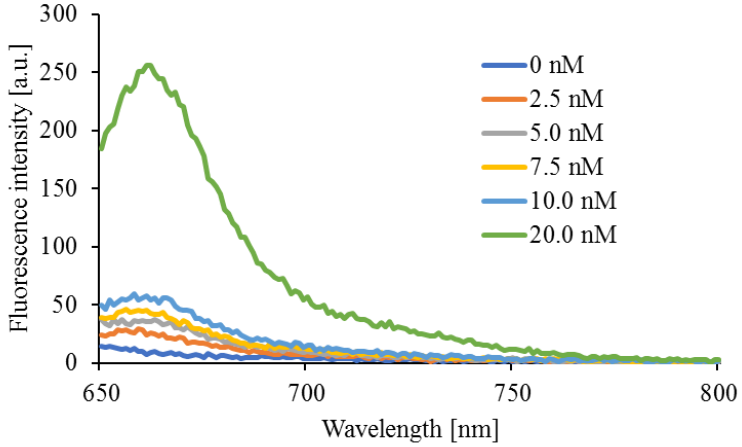

Figure 48: *Fluorescence emission of Cy5 excited at 630 nm, as a function of the DNA35-Cy5C (complementary) concentration. Each sample was incubated with 0.12 nM of GNRs functionalised with SH-DNA40-Cy3 diluted in 1x PBS and 5 mM CTAB following the hybridisation protocol.*

The variation of the intensity of the emission of Cy5 for the non-complementary strand and the complementary strands increased with the concentration of DNA in solution that was incubated with 0.12 nM of GNRs (Figure 47 and Figure 48 respectively).

Figure 49 shows the variation of the maximum of the emission intensity of Cy5 as a function of the DNA concentration in solution (complementary and non-complementary strands) extracted from Figure 47 and Figure 48.

While for the non-complementary strand the variation was clearly linear, for the complementary strand incubated with the functionalised GNRs it appears clearly that the emission intensity of the Cy5 also increased with the concentration but in a non-linear fashion (Figure 48).

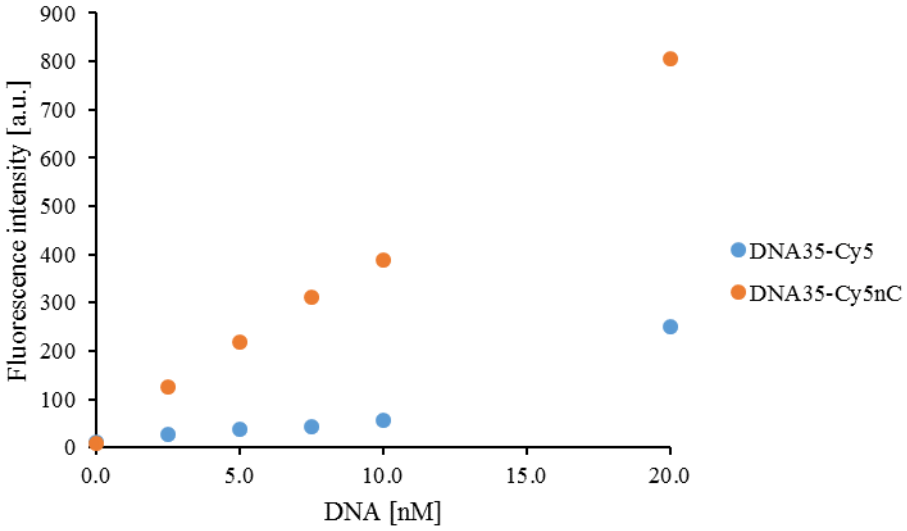

Figure 49: *Variation of the intensity of the emission of Cy5 as a function of the concentration of complementary and non-complementary DNA strand incubated with GNRs at 0.12 nM in 1x PBS and 5 mM CTAB (maximum intensity extracted from Figure 47 and Figure 48 Excitation wavelength 630 nM.*

Indeed, the variation of the peak intensity of the Cy5 increased slowly from 2.5 nM to 10 nM of the complementary strand. At 20 nM of DNA35-Cy5C we noticed a larger increase of the peak intensity (245 a.u.) that was still much lower than the intensity of the peak for non-complementary (836 a.u). Since the FRET experiment confirmed the efficiency of hybridisation as a function of the complementary strand concentration in solution (acceptor emission intensity decreased with increasing concentrations of the complementary strand), the variation of the peak intensity of the emission of Cy5 when Cy5 was excited was certainly affected by the distance of the fluorophore from the surface of the GNRs and also by the proximity of the Cy3 after hybridisation.

This indicates that Cy5 is almost certainly quenched by the plasmonic structure and the proximity of Cy3 in the duplex DNA itself.

The unexpected emission intensity to concentration dependence can only be explained by efficient quenching, when Cy5-containing DNA is in the form of a duplex (immobilised on GNR). Quenching can be partially caused by the oligonucleotide sequence[142], however the measurements performed with SH-DNA40-Cy3 – DNA35-Cy5/DNA50-Cy5 clearly showed that FRET between the fluorophores occurred. The quenching of the acceptor by the donor might be a complementary characteristic indicating hybridization and not only on the nanoparticles surface.

4.3.4. Agarose gel electrophoresis

The advantage of using agarose gel electrophoresis to characterise the efficiency of functionalisation of GNRs was shown in previous sections of the chapter.

We now apply the same approach to characterise hybridisation efficiency. To confirm the feasibility, the samples were first loaded on the gel after a centrifugation step to concentrate them.

Figure 50 shows agarose gel electrophoresis of concentrated samples excited at 648 nM so the detected signal is exclusively due to the emission of Cy5. The Ref lanes correspond to the free complementary strands in solution (no GNRs) at 20 nM. The additional lanes correspond to samples of GNRs at 1.2 nM functionalised with 216 ± 14 strands and incubated with increasing concentrations of the complementary strand (DNA35-Cy5).

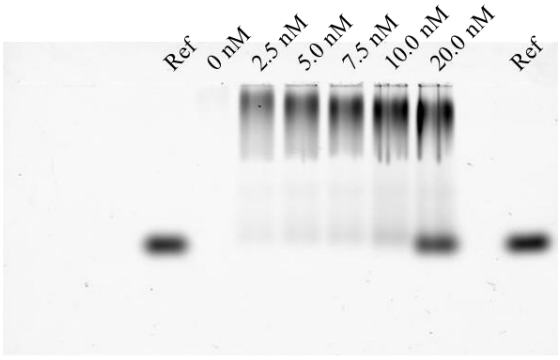

Figure 50: *Agarose gel electrophoresis. The gel is excited for Cy5 (648 nM); functionalised GNRs were incubated with increasing concentrations of the complementary strand. Without any rinsing, each sample was concentrated 25-times and loaded in the gel. Excitation was at 648 nm.*

In samples containing functionalised GNRs, we clearly observed two bands: the first one, closest to the well, corresponded to Cy5 that is bound to GNRs via hybridisation, while the second band corresponded to free DNA-Cy5 that migrated like the ref (free DNA control). The total intensity of the detected free DNA-Cy5 increased with the concentration of the DNA-Cy5 that was introduced to the samples for hybridisation. We therefore confirmed that the efficiency of hybridisation depended strongly on the concentration of the DNA-Cy5 complementary strand. Since the free DNA-Cy5 signal was detected for all concentrations we cannot directly determine the concentration at which the complementary strand is in excess in solution.

4.3.5. Specificity of the hybridization

Figure 51 shows two agarose gels of functionalised GNRs incubated with increasing concentrations of the complementary and the non-complementary stand for hybridisation. Here Cy3 was excited at 530 nm so the detected signal would originate only from DNA bound to the GNRs surface, and not from added DNA-Cy5 in solution.

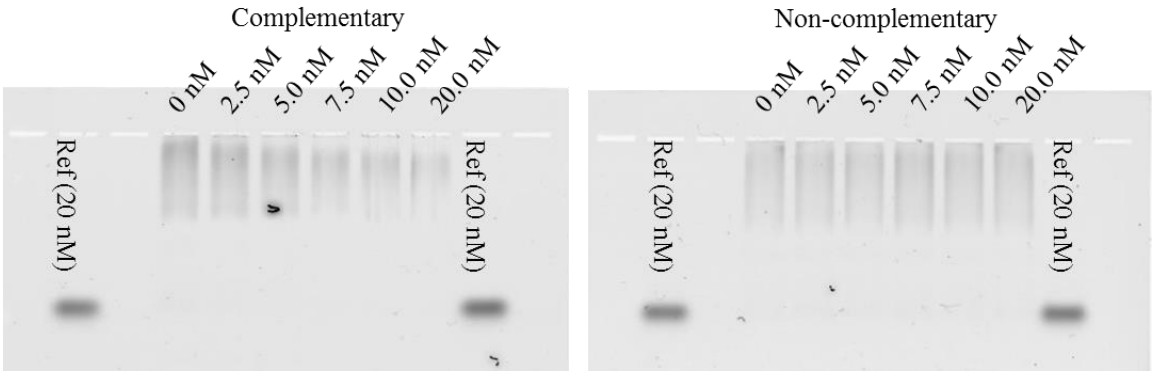

Figure 51 *Fluorescence of Cy3. The same samples as in the case of FRET measurements were used. Excitation took place at 530 nm.*

We clearly observed the signal coming from DNA-Cy3 that was bound to GNRs. The Cy3 emission intensity that was detected on the GNRs when the complementary strand was added to the sample solution decreased with increasing concentration of the complementary strand. In addition, the smeared band detected from the sample with no complementary strand in solution was longer than that seen with increasing concentration of the complementary strand: as the concentration of complementary DNA-Cy5 increased the intensity of the emission intensity of Cy3 decreases and GNRs migration is less smeared. In the case of the non-complementary strands, we observed no difference of the emission intensity of Cy3 as a function of the concentration of non-complementary strand and the migration of all samples is

similar. The results of agarose gel electrophoresis were in agreement with the observations of the fluorescence spectra; the formation of the double strand on the GNRs surface led to a decrease of the emission intensity of the Cy3, while the emission intensity of Cy3 was constant for all conditions. This observation correlated perfectly with measurements of the emission intensity of Cy3 and Cy5 when only Cy3 was excited, that is to say with the FRET experiments showed in Figure 44 and Figure 45.

4.3.6. Quantification of the number of hybridized strands.

The influence of pH on the stability of double strand DNA is known[143,144]. The pKa's of (neutral) guanine and thymine are 9-10[145]. At high pH (>~10), these bases will be deprotonated and exist as negatively charged conjugate bases. As the deprotonated species, part of the G/C and A/T hydrogen bonding will disappear and the DNA will denature[144].

At low pH, DNA phosphodiester groups are protonated, and protonation has been reported to decrease the stability of the double helix[143]. This causes DNA melting. Low pH (pH less than 1) can lead to hydrolysis of the DNA and the phosphodiester bonds will break and therefore DNA become damaged.

In order to find the best pH conditions to denature dsDNA formed on the GNRs without damaging the DNA, the pH of the buffer solution of functionalised GNRs after hybridisation was adjusted in the range between 2.3 and 12. To avoid any DNA damage, the samples were immediately loaded on the gel after the pH was adjusted.

In addition, glycerol is widely used for increasing the viscosity of samples and facilitates samples to be loaded in the gel wells. I have therefore tested two conditions for loading the samples with glycerol.

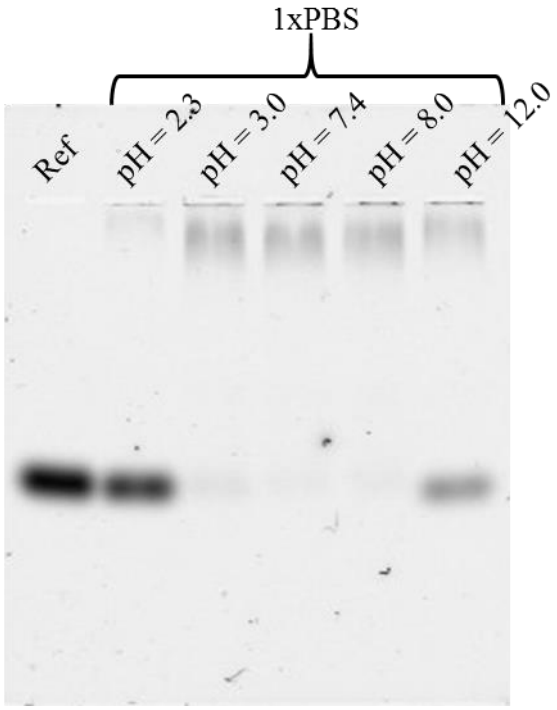

Figure 52 *Experiment with GNRs functionalised with SH-DNA40-Cy3 and hybridised with DNA35-Cy5 and loaded at different pH's. The excitation wavelength was 648 nm to register the Cy5 emission intensity.*

GNRs samples after hybridisation were mixed with solutions at 50% glycerol at different pH. As shown in Figure 22 at pH 2.3 and pH 12, the band corresponding to the free DNA-Cy5 was strong. Simultaneously, the signal detected where the GNRs migrate disappeared totally. At pH 7.4 or 8 we only observed the signal of the complementary labelled strand where the GNRs migrate. Therefore, we confirmed that the dsDNA was denaturing at both high and low pH when the DNA was immobilised on GNRs and that the GNRs colloidal solution was stable during the time of the experiment. Indeed, the GNRs were still migrating in the gel at these pH's.

Since the efficiency of denaturation seemed higher at low pH, I chose to work with 50 % glycerol, pH 2.2, prepared in advance.

The samples were prepared with the already described protocol: GNRs in 1xPBS, 5 mM CTAB were mixed with SH-DNA40-Cy3 (final concentration: 300 nM) and incubated for 4 hrs. Tween20 was then added up to 2 % , stored for 2 hours for GNRs redispersion and SH-PEG_{6000} (up to 40 µM) added. A final three centrifugation and rinsing steps produced a solution containing functionalised GNRs, 0.95xPBS and 0.1 % Tween20. DNA50-Cy5 was then added

to the nanomaterial for hybridisation at 70 °C and left overnight for cooling down to ambient temperature.

In order to clearly observe the migration of the GNRs before (pH 7.4) and after denaturation (pH 2.2) I concentrated up to 25-times before loading the agarose gel. Electrophoresis was for 30 min and performed at 50 V. The gel was scanned so only the GNRs were detected and not the DNA.

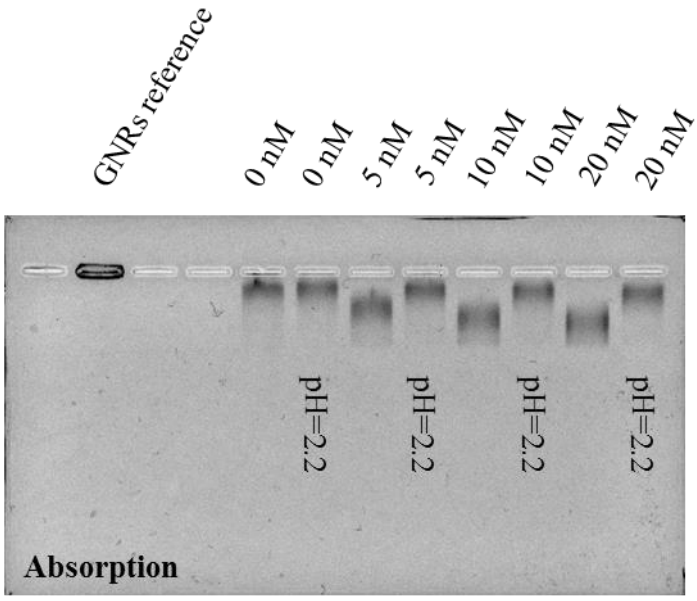

Figure 53 *Agarose gel electrophoresis of functionalised GNRs and hybridised with complementary DNA50- and loaded at pH 7.4 or at pH 2 as indicated in the figure. The gel is scanned so only the absorption of the GNRs is detected.*

The concentration of the complementary strand used for hybridisation on the GNRs samples was 0, 5, 10 and 20 nM. The samples were then diluted in glycerol 50 % at pH 7.4 or at pH 2.2 so the difference in migration of the GNRs could be characterised.

The first lane was non-functionalised GNRs that did not migrate in the gel because of aggregation. The two lanes corresponding to the functionalised GNRs with no complementary strand (0 nM) migrated the same distance independent of the pH. The lanes indicated only with the complementary strand concentration (5, 10 and 20 nM) were loaded at pH 7.4 and migrated longer distances from the wells than the ssDNA-GNRs (line 0 nM) indicating that the dsDNA led to faster migration in the gel. We noticed that the migration distance of the dsDNA-GNRs was further away from the well with increasing concentration of the complementary strand. All the samples that were loaded at pH 2.2 migrated at the same distance as the ssDNA-GNRs (0

nM) confirming that the dsDNA did denature at pH 2.2 for all complementary strand concentrations.

In this experiment, only the absorption of GNRs was shown in order to compare the impact of the presence of ssDNA and dsDNA on the GNRs on the migration distance and to confirm the use of low pH to denature the dsDNA bound to the GNRs.

To quantify the amount of hybridised DNA, the samples of GNRs-dsDNA were directly loaded after hybridisation (with no step of centrifugation to concentrate them) as described in paragraph 4.1.2.

In addition, to calculate the error of the measurements I loaded the same 6 identical solutions composed of free DNA35-Cy5 at 20 nM. (Figure 24).

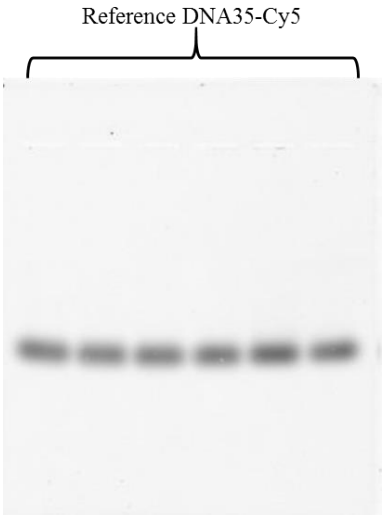

Figure 54 *Gel electrophoresis of 6 identical samples of DNA35Cy5 20 nM that were mixed with glycerol at pH 7.4 just prior to loading in the gel.*

The standard deviation calculated as described earlier is 2.45 nM compared to the 20 nM of the loaded DNA sample. I assume that this error is always present and thus applied it to all calculations.

The measurements of the number of hybridized strands were performed with DNA35-Cy5 (complementary) and DNA35-Cy5nC (non-complementary) as a control. All of the preparation protocol was as described, only the electrophoresis procedure was modified: instead of 30 min I set 40 min (in order to have GNRs at a larger distance from the loading well).

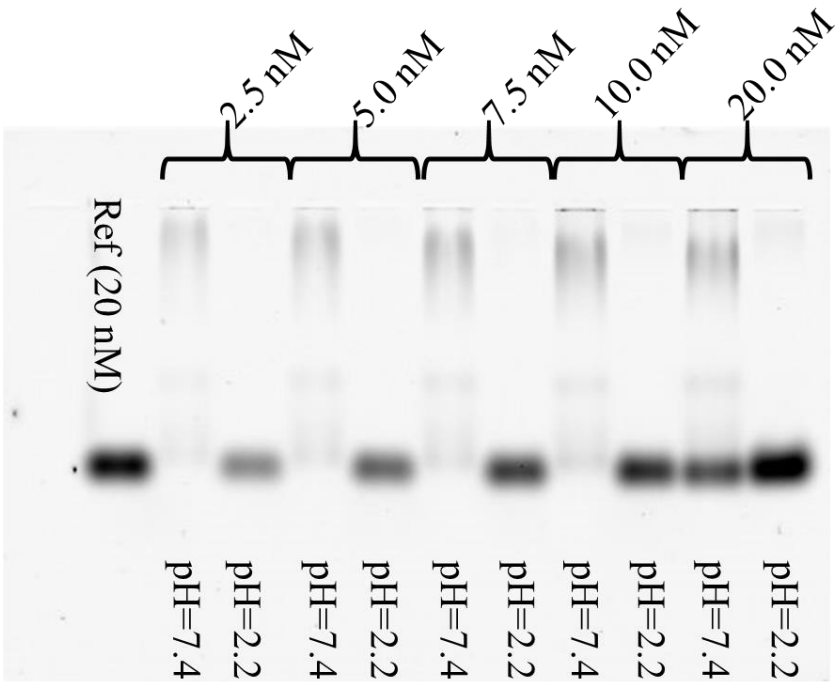

Figure 55: *Fluorescence emission intensity of Cy5 in samples of functionalised GNRs incubated with the complementary DNA35-Cy5 strand for hybridisation. Excitation wavelength fixed at 648 nm.*

Figure 55 shows gel electrophoresis of samples after hybridisation with the complementary strand at different concentrations and loaded in glycerol either at pH 7.4 or at pH 2.2. The gel was scanned to detect exclusively the DNA35-Cy5 complementary strand. The samples were not rinsed after hybridisation and were loaded on the gel with no centrifugation step to concentrate the functionalised dsDNA. From left to write is free DNA35-Cy5 loaded at 20 nM, the functionalised GNRs hybridised with 2.5, 5, 7.5, 10 and 20 nM alternatively loaded at pH 7.4 and pH 2.2. On all lanes corresponding to the samples loaded at pH 7.4 we observed 3 main bands: first a smeared band corresponding the hybridised DNA on the GNRs surface, then a weakly defined band certainly corresponding to spherical nanoparticles that remained in the stock solution of GNRs that can be also functionalised and a lowest weak band corresponding to the free DNA35-Cy5 that did not hybridise. As indicated earlier, gel electrophoresis was run for longer times for a better separation and quantification. We assume that this is the reason why we saw an additional band corresponding to smaller gold nanoparticles.

For samples loaded at pH 2.2, the signal detected where the nanoparticles migrate disappeared compared to the same samples loaded at pH 7.4, and a clear strong band of the free DNA35-Cy5 appeared. We confirmed, as in Figure 52, that the hybridised DNA was released from the surface of the GNRs and migrated therefore like the reference free DNA. The emission intensity on the band of the free DNA in samples loaded at pH 2.2 increased with increasing concentrations of DNA35-Cy5 complementary strand incubated with GNRs for hybridisation.

To appreciate the effect of the complementary DNA in solution on the efficiency of hybridisation the quantification analysis of the gel was performed as described for the quantification of the thiolated DNA on GNRs (Figure 56).

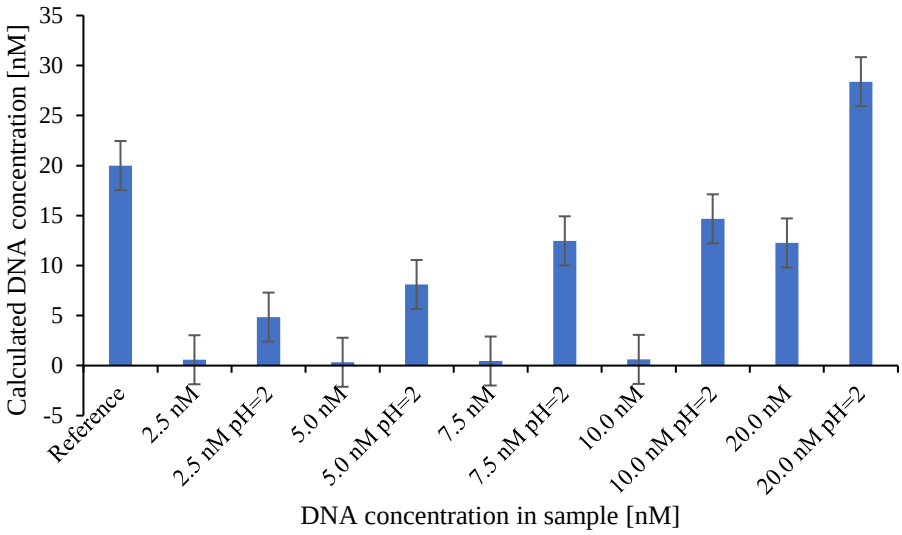

***Figure 56**: Quantitative analysis of the Cy5 fluorescence emission intensity extracted from the gel presented Figure 55.*

First, the calculation of the free complementary strand concentration in the functionalised GNRs solution after hybridisation loaded at pH 7.4 was below the standard deviation that I calculated from Figure 54, which was 2.45 nM for all DNA35-Cy5 concentrations that were used for the hybridisation lower than 10 nM. When 20 nM of complementary strand DNA was incubated with the functionalised GNRs for hybridisation, the remaining free DNA35-Cy5 increased to 12 nM. Therefore, in the range of 2.5 to 10.0 nM most of the complementary strands were hybridised. When 20 nM of the complementary strand was incubated with the functionalised GNRs, it appears that a large part of free DNA remained in solution (12 nM) indicating that the complementary strand was in excess or that the maximum

number of hybridised strands on the surface of GNRs was reached at 10 nM of the complementary strand.

When the same samples were loaded at pH 2.2, the dsDNA formed on the GNRs were denatured and ran as free DNA in the agarose gel. The concentration of the released complementary DNA strand increased from 5 nM to 12 nM with increasing concentration of the complementary strand used for hybridisation. When 20 nM of the complementary strand was incubated with the functionalised GNRs, it appeared that the concentration of total free complementary strand (DNA in excess and DNA that was released at pH 2.2) was higher than the reference free DNA that was also loaded at 20 nM.

In order to control for the non-specific interaction of the complementary strand with the GNRs surface at high concentrations, the functionalised GNRs samples were incubated with the non-complementary DNA (DNA35-Cy5nC) for the hybridisation experiment and were loaded at pH 7.4 and 2.2 in the agarose gel electrophoresis.

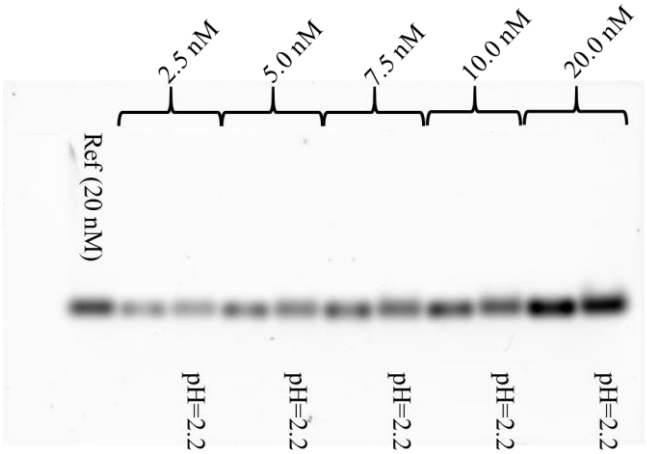

Figure 57 *Fluorescence emission intensity of Cy5 in samples of functionalised GNRs incubated with the non-complementary DNA35-Cy5nC strand for hybridisation. Excitation wavelength fixed at 648 nm.*

Gel electrophoresis where the non-complementary strand was detected reveals that no DNA was adsorbed on the GNRs, all the DNA35-Cy5nC migrated like the reference free DNA at pH 7.4 and at pH 2.2. We conclude that there was negligible non-specific interaction of ssDNA with the functionalised GNRs (Figure 57). The analysis of samples incubated with the non-complementary DNA strand were performed as previously to extract the concentration of free DNA (Figure 58).

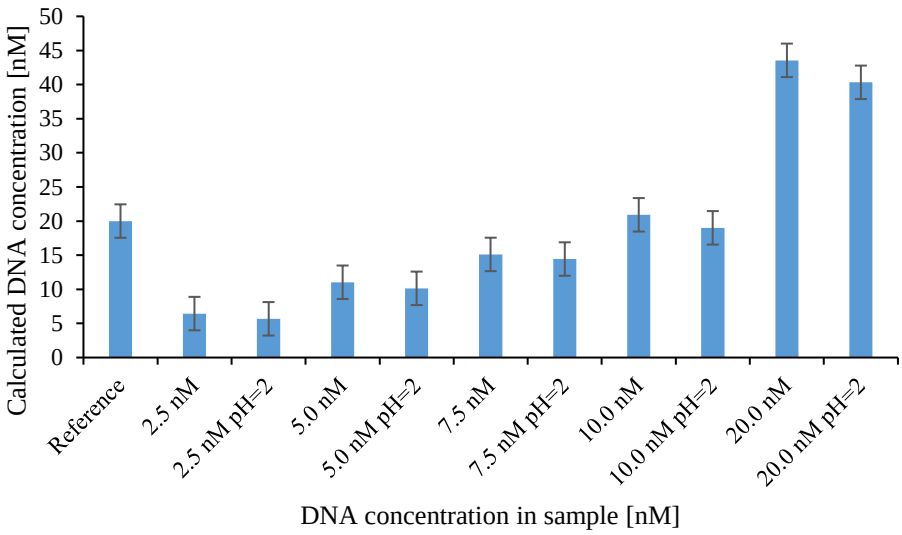

Figure 58: *Quantitative analysis of the Cy5 fluorescence emission intensity extracted from the gel presented Figure 57.*

The quantitative analysis of the gel electrophoresis presented in Figure 57 confirmed that the concentration of the detected DNA35-Cy5nC was identical when the samples were loaded at pH 7.4 and pH 2.2, indicating that there was no non-specific interaction on the GNRs surface. The differences between the concentrations calculated at both pH were below 12 %. However, the concentration that was obtained for the GNRs samples incubated with 20 nM of the non-complementary strand was significantly higher than the reference free DNA loaded at the same concentration. Despite the fact that this observation was reproducible, we did not find any explanation for this behaviour.

The last step of the analysis was to quantify the number of complementary ssDNA hybridised on the GNRs surface. For this purpose, the values of fluorescence from samples loaded in the gel at pH 2.2 were corrected from the emission intensity of the free DNA characterised on samples that was loaded at pH 7.4 and compared with the reference free DNA loaded at 20 nM Figure 59.

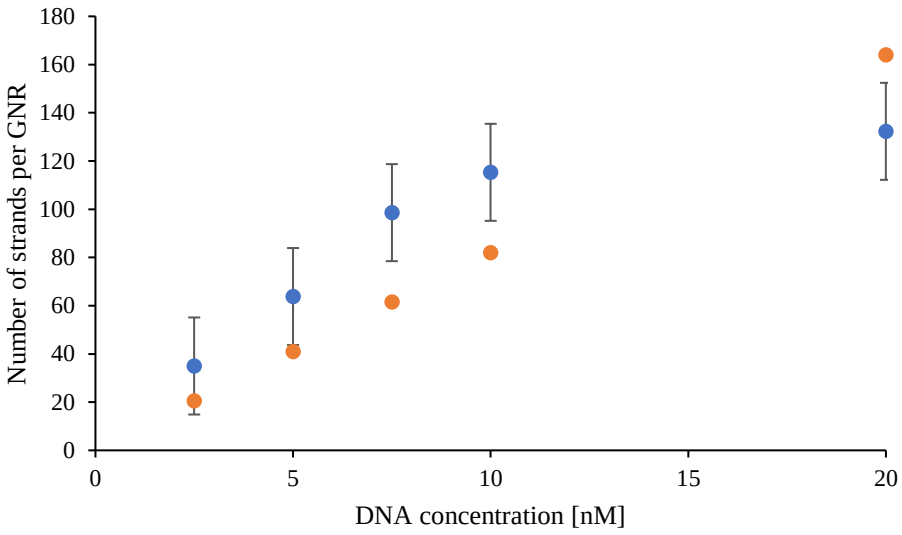

Figure 59: *Calculation of the number of complementary strands per GNR (in blue). The orange dots correspond to the theoretical surface density if all complementary DNA strand that was used for the hybridisation hybridised with the functionalised GNRs.*

From the calculated dsDNA surface density, we confirm that hybridisation reached a maximum when 10 nM of the complementary strand was hybridised with the functionalised GNRs. The dsDNA / GNRs was then 115 ± 20 while the surface density of ssDNA immobilised on the GNRs was 216 ± 14 ssDNA / GNRs (see paragraph 4.2.2).

The following table presents the results of the calculation of the dsDNA surface density.

Table 3 Number of dsDNA per GNR

DNA concentration used for the hybridisation (nM)	Experimental number of dsDNA/GNR	Theoretical dsDNA/GNR
2.5	35±20	21
5.0	64±20	41
7.5	99±20	62
10.0	115±20	82
20.0	132±20	164

For 2.5 nM of the complementary DNA35-Cy5 incubated with functionalised GNRs and loaded at neutral pH, no free DNA was detected. Therefore, we concluded that most of the complementary strands hybridised with the DNA that was immobilised on the GNRs surface. Indeed, the measurements made in the agarose gel indicated that 35±20 complementary strands

were released from the GNR surface at low pH, in agreement with the theoretical number for 100% of hybridisation (21 strands/GNR). For 5.0 nM, the situation was similar; most of the complementary strands were hybridised on the GNRs, however, the calculations indicated a gap between the measurements and the theoretical surface density of dsDNA (64±20 dsDNA/GNRs in the experimental calculation and 41 strands/GNR in the theoretical calculation). For the GNRs sample that was incubated with 7.5 nM of the DNA35-Cy5, a stronger fluorescence signal was detected from the released complementary DNA after hybridisation; this was probably the point where the efficiency of hybridisation was limited by the steric hindrance or the difficulty to hybridise more DNA. However, the number of dsDNA hybridised on the GNRs was higher (99±20 to 62 strands/GNR) than with samples incubated with lower complementary strand concentrations. A similar situation occurred with GNRs samples incubated with 10.0 nM of complementary strands; the free DNA signal calculated from the samples loaded at neutral pH was low so most of the oligonucleotides were hybridised on the GNRs (confirmed by the calculations (115±20 strands/GNR compared with the maximum theoretical dsDNA/GNRs of 82 strands/GNRs)

The experimental values based on the agarose gel analysis were always higher than the theoretical maximum dsDNA surface density. The only explanation, based on my experimental experience is that the loaded samples were diffusing with time in the wells of the gel. Since the reference of free DNA was always loaded first, this means that the reference sample had more time to diffuse than the other samples when all samples are loaded on the 12 well agarose gel.

The last issue was with samples incubated with 20 nM of DNA35-Cy5. Already from the gel analysis it was clear that there was an excess of complementary strands that did not hybridise. This situation was confirmed by the calculations where, for the first time the theoretical value was higher than the measured dsDNA surface density. This clearly shows that the analysis based on the agarose gel calculations has to be improved. In my opinion, the solution could be to use smaller gels with 6 wells; this should reduce the loading time and therefore limit the diffusion of the samples once loaded on the gel wells. An alternative would be to load the reference twice, at the beginning and at the end of the loading process. In addition, FRET experiments demonstrated that the Cy5 emission is quenched when the Cy5 is close to the Cy3 fluorophore after hybridization. Therefore, to improve the quantification method, it would be interesting to functionalise GNRs with a thiolated DNA with no label.

Nevertheless, the characterisation of hybridisation on GNRs with complementary DNA in the range between 2.5 and 10 nM was efficient and proved that we can control the surface density of the thiolated DNA and the amount of hybridised DNA.

4.3.7. Summary

The aim of this thesis was to determine the amount of dsDNA immobilised on GNR surfaces and in spite of the limitations discussed above was mostly successful. A key element in the success of the approach was the use of agarose gel electrophoresis and the fact that an acidic environment (pH 2.2) denatures dsDNA at room temperature within seconds.

FRET proved to be useful in calculating the dsDNA density on surfaces, because it is a fast and very precise technique. Formation of duplex DNA causes a decrease in donor emission intensity. However, this approach is associated with two drawbacks; first the equilibrium of dsDNA formation is unknown; second the dynamic changes of the donor emission are limited as the drop of the emission intensity is difficult to measure when small amounts of DNA are hybridised on the surface of GNRs. Nevertheless, the donor emission intensity drop permits one to follow hybridisation between the starting point where no DNA is hybridised and the final point where a large amount of DNA is hybridised. Therefore, quenching of the acceptor fluorescence emission intensity can also be used to estimate the amount of DNA attached to nanoparticles via hybridisation; this promising approach deserves more detailed investigation.

5. Changes of nanohybrid optical properties under temperature variations

5.1. Experimental approach

5.1.1. Determination of the temperature around nanoparticles using hairpin DNA

Interactions between gold nanoparticles and electromagnetic waves in the range of UV-Vis-NIR are dependent on the nanostructure size and shape[146]. In the case of GNRs, aspect ratio modifications allow selection of the wavelength at which the light-nanostructure interaction would be increased. The uniqueness of such rods is their ability to efficiently absorb light at 750-800 nm with relatively small dimensions (diameter 10 nm, length 35-40 nm); this highly reduces scattering in comparison with other particles absorbing in the same range e.g. nanoshells (diameter 150 nm). The absorbed energy is then transformed into heat and increases the nanostructure's temperature; as mentioned before, it can be used for oligonucleotide release.

The need to create a temperature map around GNRs is a basis of this thesis, because it is crucial to know those laser beam parameters to induce a controlled increase in temperature (power/area). The issue of thermometry in micro and nanoscale has been widely discussed, both in terms of techniques and materials[147,148,149]. In this thesis the evaluation of GNRs thermal properties was planned in two parallel ways: experimental and theoretical.

The general assumption for the experiments was to obtain data from fluorescence emission; the difference in emission dependent on the surface-fluorophore distance has been investigated[150,151]. For this purpose, a hairpin DNA (hDNA-Cy5) was proposed; these oligonucleotides have the ability for self-hybridisation and to form a loop structure. In my experiments the 5' end was thiolated (to attach to the gold surface) and the 3' end with Cy5 labelled; when hDNA was in a closed state the fluorophore was in close proximity to the metal surface (Figure 60).

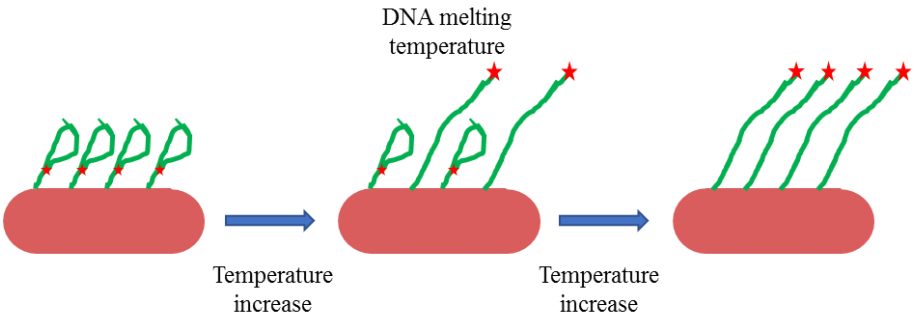

Figure 60: *Scheme of hairpin-based temperature measurements. hDNA (green line) is attached to GNRs and initially self-hybridised, caused low emission from the fluorophore (red star).*

Several experiments were performed, but numerous problems appeared: first, the functionalisation method was different (SH-DNA was incubated with GNRs in 5 mM CTAB overnight and subsequently salt aging up to 100 mM NaCl was performed) and was found to be inefficient. The problem of this method was that each rinsing step decreased the fluorescence signal. This suggested that oligonucleotides were not immobilised on the nanoparticles via the thiol-gold bound. For this reason throughout the thesis, I focused on the mechanism of thiolated oligonucleotides attachment to gold surface. Additionally, in the selected sequence, five base pairs hybridised to form a loop. The melting temperature of the closed form was 38 °C thus suitable for heating-cooling experiments. However, it turned out that it was not possible to demonstrate self-hybridisation by acrylamide gel done at 4 °C or with fluorescence emission. In addition, choosing cyanine-derivatives as the fluorophore (Cy5) was a problem as their emission depends strongly on the environmental temperature. All these problems led to results that were not reliable. On the other hand, it allowed modification of the initial plan and the idea of using Cy5 directly as thermometer was proposed.

5.1.2. Cyanine-derivative fluorophores as molecular thermometers

Many of the organic dyes, often used in biological experiments have emissions highly dependent on the local medium viscosity (e.g. caused by change of temperature). In the case of cyanine derivatives this is sufficient to consider such molecules as molecular thermometers[152]. The mechanism derives from the structure of the fluorophores that can be delineated into three domains: 1) electron donor, 2) electron acceptor, 3) electron-rich conjugated spacer (alternating single and double bonds). When these units are in a planar, or near-planar configuration the excitation causes charge transfer from the donor to the acceptor unit and the emission of a photon takes place. However, the electrostatic forces twist the groups and in such cases excitation requires lower energy, but causes red-shifted, or non-fluorescent emission. As the

twisting ability is strongly related to the local viscosity, this appears to be the source of temperature-dependent emission.

The other issue concerned finding conditions allowing effective temperature measurement around the GNRs under illumination. For this purpose, it is obvious that the fluorophores need to be kept at a constant distance from the metal surface; this is effected by the formation of full double stranded DNA on the GNRs surface. However, the increase of temperature can denature the dsDNA to ssDNA if the melting temperature of the dsDNA is low compared to the light induced increased of the GNRs temperature.

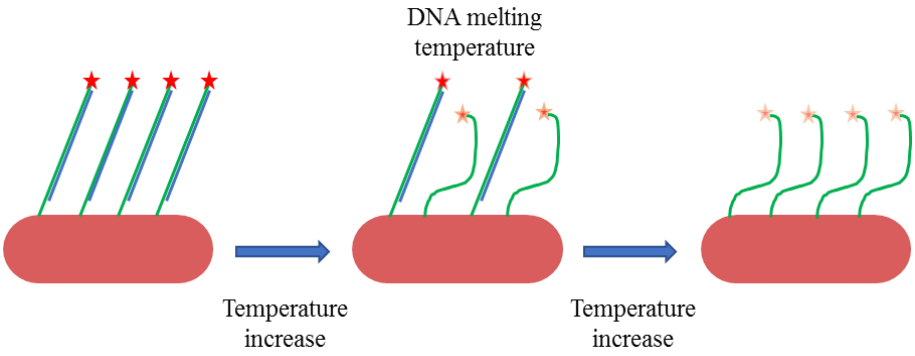

Figure 61: Scheme *The thiolated DNA (green line) is hybridized with a non-labelled oligonucleotide (blue line). At the initial point all SH-DNA were assumed to be in form of duplex.*

With increasing temperature, the fluorescence emission intensity decreases (the red star in Figure 61), but also dsDNA denaturation may occur. A short analysis of such a model illustrated the downsides of such an approach; in the previous chapter (chapter 4) it was shown that not all the immobilised thiolated DNA on the GNRs surface could form double stranded DNA (I obtained below 50 % of dsDNA).

The last proposal involved placing temperature-sensitive fluorophores on the complementary strands. This should allow, under certain conditions, almost 100 % immobilisation onto GNRs since I demonstrated that at certain concentrations all the complementary DNA forms a duplex with the immobilised DNA.

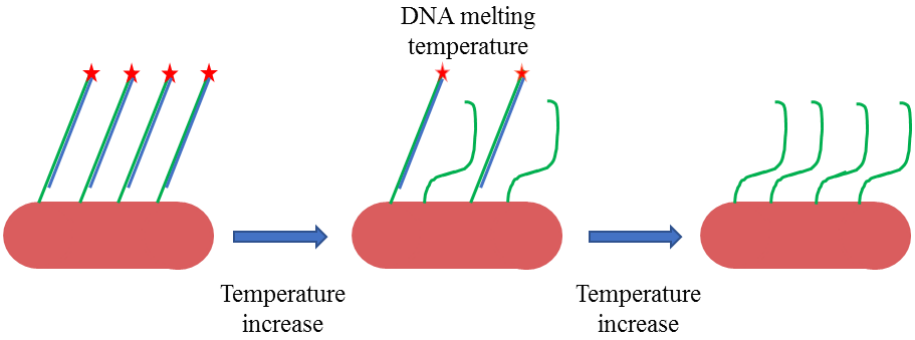

Figure 62: *Scheme of the final model of the experiment: the complementary strands (blue line) are labelled with fluorophore (red star).*

With Cy5 labelled to the complementary strand it is possible to keep them at a constant distance from the metal surface. This requires specific concentrations of functionalised GNRs and complementary DNA. As described in chapter 4 this was indeed possible. In this case the temperature range should also be below the melting temperature to avoid DNA denaturation and the release of the complementary strand (containing fluorophore) so as not to impact on the measured fluorescence emission intensity. Nevertheless, such experiments allowed precise temperature measurements.

5.1.3. Cyanine-based temperature measurements

The temperature was measured with a Universal Thermocouple Connector (UTC-USB) made by Omega. The volume of the solutions was 2 mL and heating was carried out by a system connected to the spectrofluorometer. The spectrum between 650 and 800 nm was registered three times for each sample. As described in the previous chapter, the first step was to check if the complementary DNA created a duplex on the GNR surface. For this purpose, the agarose gel presented in Figure 63 was performed.

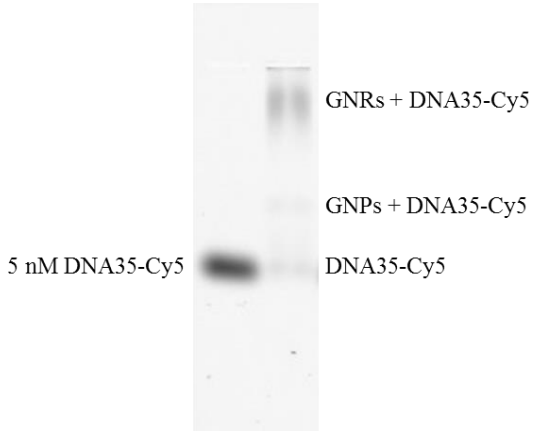

Figure 63: *Agarose gel electrophoresis of samples used for temperature experiments. The lane on the left is the reference containing 5 nM of DNA35-Cy5 in 0.95xPBS and 0.1xPBS. The lane on the right is GNRs functionalized with SH-DNA40 and hybridised with 5 nM DNA35-Cy5 in 0.95xPBS and 0.1xPBS.*

The samples were prepared using the same Cy5-labelled stock solution, so that the amount of DNA was equal in the reference and in the GNRs-containing solution. The reference DNA gave one band corresponding to the migration of free ssDNA, as expected (Figure 63). For samples with GNRs, we detected three bands. The first one was close to the well and was associated with the complementary DNA that hybridised with the immobilised DNA on the GNRs. The second one was a band corresponding to the functionalised spherical nanoparticles that were present in the stock GNRs solution. The third band corresponded to the free complementary strand that did not hybridise. As these results were obtained for samples that were not rinsed after hybridisation it was highly promising, because a comparison of free DNA emission intensity with the reference shows that most of the complementary strands were immobilised on nanoparticles. This gave the opportunity to measure the temperature around nanostructures by varying the temperature of the solution between 25 and 60 °C with steps of 5 degrees. Making three spectra at each temperature allowed estimation of the standard deviation. The first approach was to select one wavelength at which the fluorescence emission intensity would be measured and, based on this, compare the differences (Figure 64). However, such an approach has two obstacles: first, the deviation of the emission peak position can be quite large, second, in the case of e.g. microscopic measurements the fluorescence emission is recorded over a range of wavelengths. Therefore, I decided to select the range between 670 and 680 nm and calculate the average fluorescence emission intensity and the standard deviation (Figure 65).

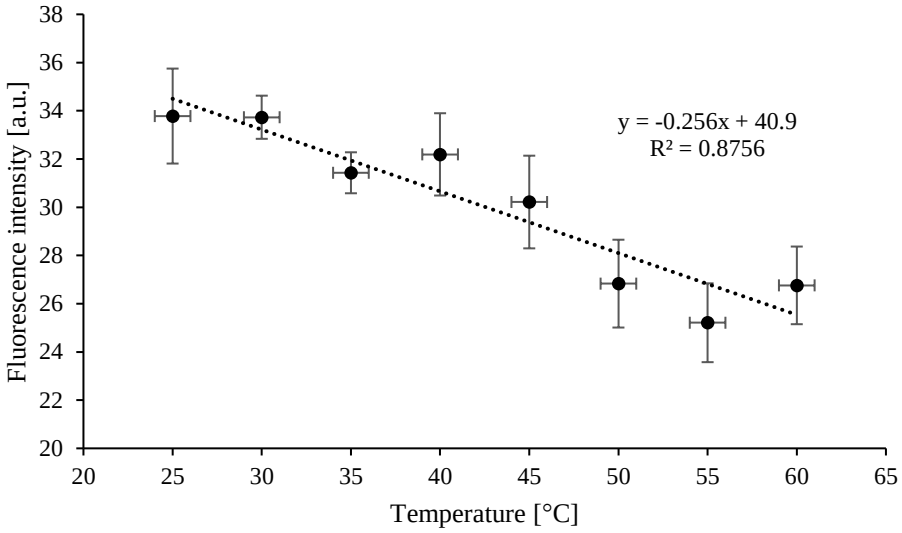

***Figure 64**: Example of one-wavelength based fluorescence analysis of sample containing GNRs functionalised and hybridised with 5 nM DNA35-Cy5. The fluorescence was registered at 670 nm.*

In the case of single wavelength analysis the crucial factors are fluorophore emission and its ratio to scattering. As scattering can vary with samples (e.g. it is induced by the hybridisation process), the essential part of the experimental work involved obtaining high fluorescence output. Unfortunately, in the prepared samples the emission intensity was not very high and the results were not useful for temperature determination. Attention should be also be paid to the large standard deviation, indicating how the emission intensity fluctuated between three measurements on the same sample.

However, using the same data it was possible to obtain much more promising results; as mentioned before, the average values of 670-680 nm range were calculated (Figure 65). With this approach, the fluorescence emission intensity fluctuations did not play a crucial role.

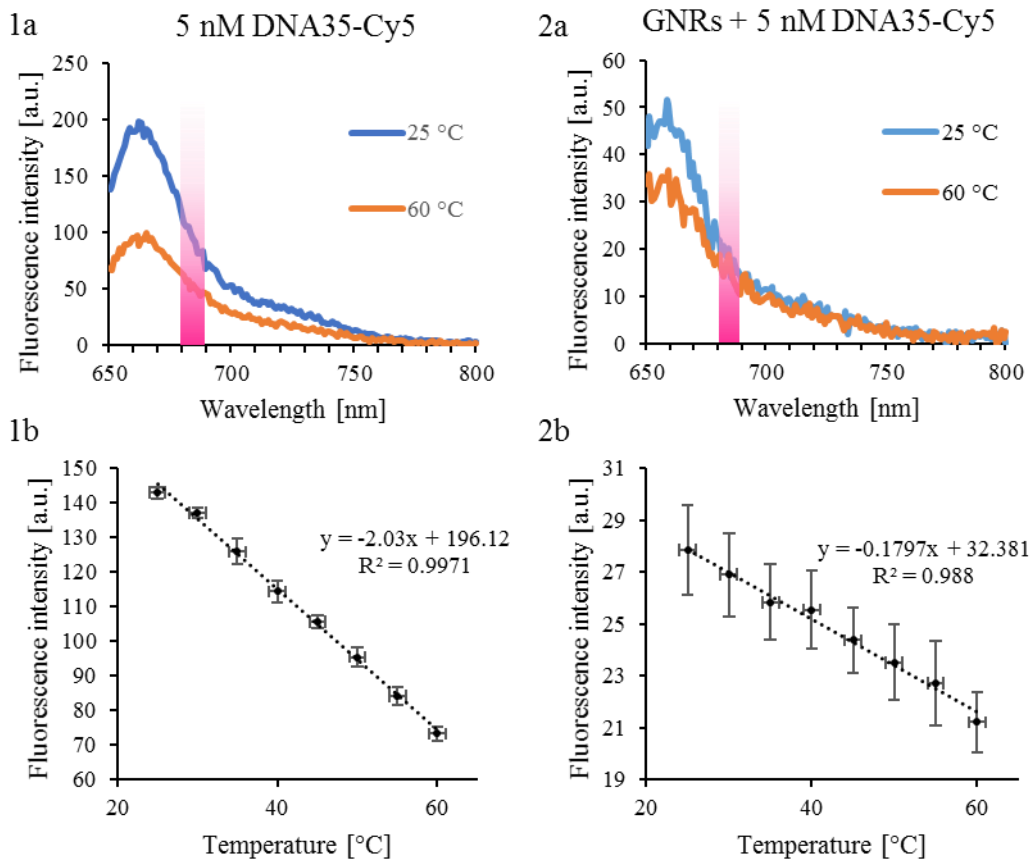

Figure 65: *1a) difference between the emission spectrum of Cy5 at 25 and at 60 ºC. In pink is the wavelength range in which I did the analysis. The excitation wavelength was 630 nm; 1b) Analysis of the fluorescence emission intensity as a function of the temperature changes of samples described in 1a. The measurement range was selected between 670 and 680 nm; 2a) difference between the emission spectrum of Cy5 on the GNRs surface after hybridisation at 25 and at 60 ºC. The excitation wavelength was 630 nm; 2b) Analysis of the fluorescence emission intensity as a function of the temperature changes of samples described in 2a. Measurement range was selected between 670 and 680 nm.*

The reference sample (without GNRs) indicated a fast linear decrease of the fluorescence emission intensity as a function of the increase of temperature (Figure 65 1a and 1b).

As indicated in Figure 5, the emission intensity drop can be seen using a single wavelength, but with less accurate sensitivity than when the measurements are averaged in the range between 670-680 nm. In the case of 10 nm wide range analysis the situation is strongly improved, as the dependence linearity is more accurate. It is important to notice again that gel electrophoresis indicated that most of the complementary strands were immobilised onto the GNRs surface. This was useful information for microscopy-based experiments.

A disadvantage was the presence of non-attached DNA in solution (their impact on results should be low, because of intensity comparison with emission from GNRs), standard

deviation values (often more than 5 %) and change of emission by degree (per 1 °C it is lower that 1 % ,the explanation could be scattering, not change with temperature).

Nevertheless, this approach is highly promising for distance-controlled temperature measurements and further investigation e.g. in a microscopic approach should be performed. It could be especially useful for checking the impact of laser illumination on objects containing GNRs; following fluorescence can, in an easy way, indicate the thermal impact of irradiation (if the other factors do not influence fluorescence[153]).

5.2. Theoretical approach

5.2.1. Physical background of calculations

The first issue is the way photons interact with gold nanoparticles. This is quite complicated, as it involves different physical phenomena; a model with ultra-short laser pulse at the wavelength corresponding to Surface Plasmon Resonance (SPR)[154] was used for analysis. Some, electrons instantaneously gain energy due to photon absorption. This leads to an out-of-equilibrium electron distribution as other electrons have lower energy. The internal thermal equilibrium is next restored by electron-electron collisions. The dynamics of this process depends on the input power: the higher the power, the faster the equilibration. In parallel electron-phonon coupling takes place with a characteristic time of a few picoseconds. The real physical process is an energy exchange between the vibration modes of the ionic lattice and the heated electrons. The NP temperature then increases. At this point all of the processes are taking place inside the nanoparticle structure ; the relevance for this thesis lies in the next step: interaction with the environment. For this, heat is released through the interface by phonon-phonon interaction, decreasing the temperature of the nanostructure while increasing the temperature of the surrounding medium. The duration of this process depends on the shape and size of the NP, but above all on the interface thermal resistance and on the thermal conductivity of the host medium. This indicates that gold nanoparticles are possible heat sources. Therefore, the next step was to calculate the effectiveness of this process.

The instantaneous power density (dependent on time) absorbed by a nanoparticle can be described by the formula:

$$P_{abs}(t) = \frac{I_{inc}(t)\sigma_{abs}}{V_{NP}}$$

P_{abs} = power density absorbed by the nanoparticle

I_{inc} = intensity of light

σ_{abs} = absorption cross-section of the nanoparticle

V_{NP} = nanoparticle volume.

This formula clearly shows that nanoparticle absorption cross-section and incident intensity are essential for power absorption. The absorption cross-section describes the probability of the absorption process (strongly dependent on nanoparticle material properties) under the light illumination at a specified wavelength. The following formula describes the situation for spheres (radius R < 25 nm), but it indicates more globally the main factors determining σ_{abs}:

$$\sigma_{abs} = \frac{18\pi V_{NP}}{\lambda} \frac{n_m^3 \varepsilon_2}{\left[\varepsilon_1 2\sqrt{n_m}\right]^2 + \varepsilon_2^2}$$

λ = incident wavelength (in vacuum)

n_m = host medium refractive index

ε_1 = real component of the metal dielectric function

ε_2 = imaginary component of the metal dielectric function.

This shows that absorption cross section is dependent on the incident wavelength, nanoparticle volume and both metal and host medium electromagnetic properties. Importantly, σ_{abs} varies by changing the host medium, e.g. by covering gold nanoparticles by a layer of silica.

In the case of GNRs the Discrete Dipole Approximation (DDA) or the Boundary Element Method (BEM) can be applied to evaluate σ_{abs}. The absorption cross-section at the longitudinal SPR of a nanorod can be much higher than that of the SPR of a nanosphere of the same volume (dependent on the nanorod aspect ratio). In the case of nanorods prepared for this thesis, calculations were based on the dimensions evaluated from TEM image analysis; radius 5.65 nm, length 40.00 nm. For such GNRs the absorption cross-section at LSPR was calculated to be 9000 nm^2, obtained through BEM (boundary element method) computation. Knowing this value, it was possible to calculate thermal energy transfer. Assuming (at this step) that nanoparticles are illuminated with a continuous wave laser it is possible to determine the rise of temperature in the structure[154]:

$$\Delta T_{NP}^{cw} = \frac{P_0}{4\pi\kappa_m R}\left(1 + \frac{l_K}{R}\right)$$

P_0 = power absorbed by nanoparticle

κ_m = host medium thermal conductivity

R = nanoparticle radius (or effective radius in case of a NR)

l_K = Kapitza length (in the case of the presence of an interface thermal resistance).

However, knowing the temperature of GNRs under illumination does not provide any idea about the thermal influence on the surrounding medium (the essential part of this thesis). To calculate the increase in the medium temperature around the nanostructure the following formula is used:

$$\Delta T_m^{cw}(r) = T_m^{cw}(r) - T_0 = \frac{P_0}{4\pi\kappa_m r}$$

r = distance from the nanoparticle centre.

In the case of GNRs, their spatial orientation relative to the field polarisation has to be considered since such nanoparticles are not isotropic, the absorption associated with the LSPR depends on this parameter. In the case of a random orientation of an ensemble of GNRs (in solution for instance), this implies that the calculated temperature increase is 1/3 of the value calculated for a longitudinal polarization when shining at the LSPR.

5.2.2. The energy transfer from nanoparticles to the host medium

The formula presented in the previous section contains the Kapitza length, a factor used when interface thermal resistance is present. This paragraph will focus on a short description of GNRs-medium thermal interactions and describe the meaning of the Kapitza length. The increase of GNR temperature causes heating of the surrounding medium, however, this process is dependent on several factors. The first boundary condition states that the heat flux released by the nanoparticle equals that absorbed by its environment:

$$\kappa_{Au} \left.\frac{\partial T_m}{\partial r}\right|_{R^-} = \kappa_m \left.\frac{\partial T_m}{\partial r}\right|_{R^+}.$$

Then, we have to consider the contact type at the interface; if it is a perfect one, the temperature continuity while crossing the boundary is ensured. These two conditions allow calculation of the evolution of temperature (with time) of both the nanoparticle and the host medium. The situation becomes more complicated in the case of a non-perfect contact. In this case, another parameter has to be introduced, namely, the thermal interface conductance, g (W m^{-2} K^{-1}). The physical background of this comes from two different phenomena: first, the thermal resistance can be caused by the nature of the contact (every type of interaction, or surface structure which does not allow medium molecules to surround the object tightly, e.g. porosity, or hydrophobicity); this is contact thermal resistance. The second factor is the difference in thermal impedance between the two media (it occurs also in case of perfect contact); this is known as the Kapitza thermal resistance. These phenomena both lead to a global interface thermal resistance, $1/g$, and are responsible for a temperature jump ΔT at the interface

separating the nanoparticle and the host medium. This implies that the heat flux exiting the nanoparticle (and then entering the host medium) is linked with ΔT through:

$$\kappa_{Au} \left.\frac{\partial T_m}{\partial r}\right|_{R^-} = \kappa_m \left.\frac{\partial T_m}{\partial r}\right|_{R^+} = -g\Delta T.$$

Therefore, for evaluating the temperature difference, the following formula can be used:

$$\Delta T = -l_K \left.\frac{\partial T_m}{\partial r}\right|_{R^+},$$

where l_K (Kapitza length) is equal to κ_m/g. At this point it is important to apply this theoretical situation to the samples I was able to prepare. The GNRs were covered by a layer of CTAB, or PEG/DNA ligands, therefore the situation was of non-perfect contact. For the first case, a reference in the literature[155], indicated an interface conductance of 130 MW m^2 K^{-1} for a stable CTAB bi-layer. The issue of surfactant coverage stability was solved by a set of experiments measuring the effective thermal interface conductance indicating 3-fold increase in free CTAB concentration range 1-10 mM. The subsequent measurements and calculations indicated differences in g values with surfactant amount variations, e.g., 1 mM - 450±100 MW m^2 K^{-1}, 5 mM - 250±50 MW m^2 K^{-1}, 50 mM - 130±20 MW m^2 K^{-1}.

5.2.3. Simulations

The simulation of the temperature around GNRs (water as surrounding medium) was performed using the *Comsol Multiphysics* software. The data used in calculation are:

Absorption cross section = 9000 nm^2

Laser power (785 nm continuous wave) = 0 – 1000 mW

Beam diameter = 10 µm

Interface thermal conductance = 130 MW m^2 K^{-1}

GNR length = 40.0 nm

GNR diameter = 11.3 nm

Gold thermal conductivity = 314 W m^{-1} K^{-1}

Water thermal conductivity = 0. 591 W m^{-1} K^{-1}.

The result of simulation for a continuous wave laser with illumination power equal to 100 mW is displayed in Figure 8. It is important to note that the temperature calculated here cannot account for the global temperature of the solution, as only one nanorod is considered. However, the temperature of the nanorod itself and its direct vicinity is close to the real case, provided the nanorod is parallel to the polarization direction of the incoming light wave as discussed above. At first order, accounting for the warming of the overall solution due to the presence of many other heat nanosources would only add a thermal background to the gradients.

The initial temperature of the host medium was set to 25 °C, which was also the temperature set as a condition at the boundaries of our virtual sample in the simulation.

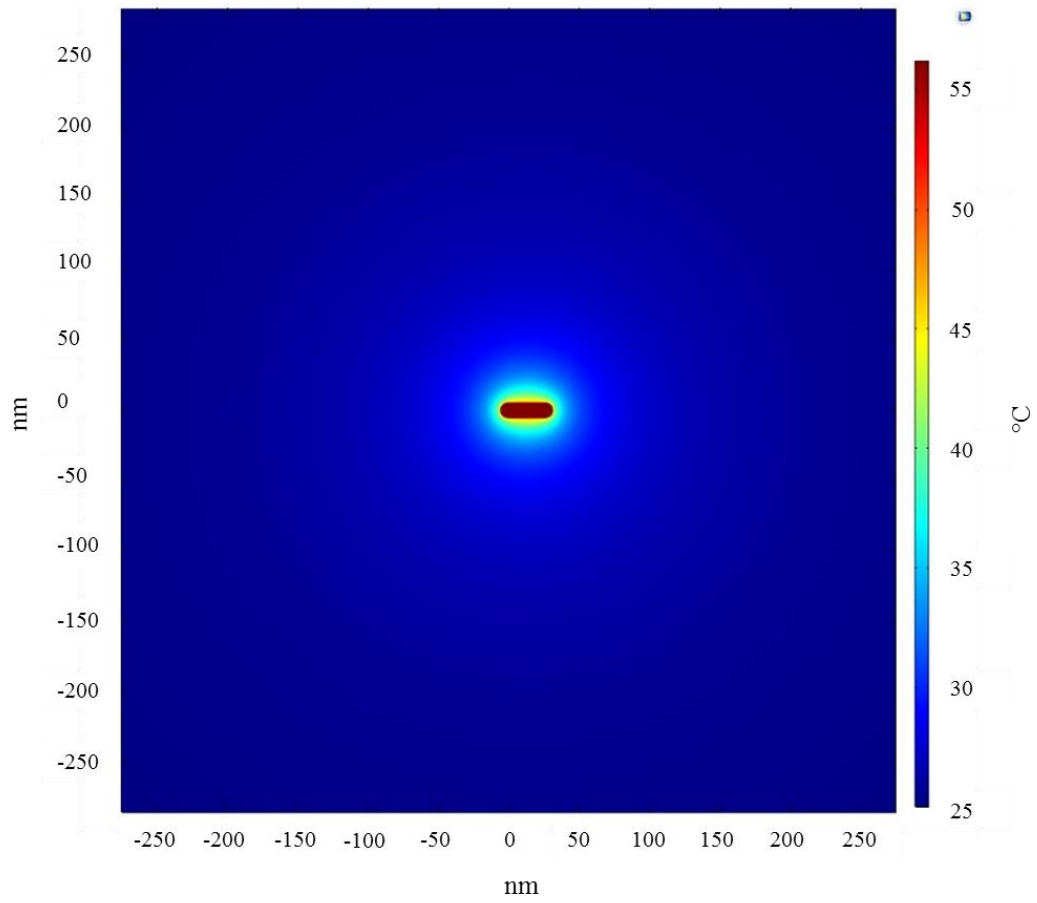

Figure 66: *The temperature gradient around a GNR (in water) when illuminated by a continuous laser beam with power 100 mW, 785 nm wavelength (LSPR of the GNR) and polarized parallel to the nanorod long axis. The colour scale indicates temperature modifications (from 25 ºC – blue, up to 57 ºC – dark red). The nanoparticle was placed in the middle of a square with 500 nm long side.*

It can be observed that the heat topography profile is similar for every applied power; the ellipsoid-like shape with the nanorod in the middle. To be more precise, Fig. 9 shows the variation of the host medium temperature as a function of the distance to the GNR in the direction along with the nanorod.

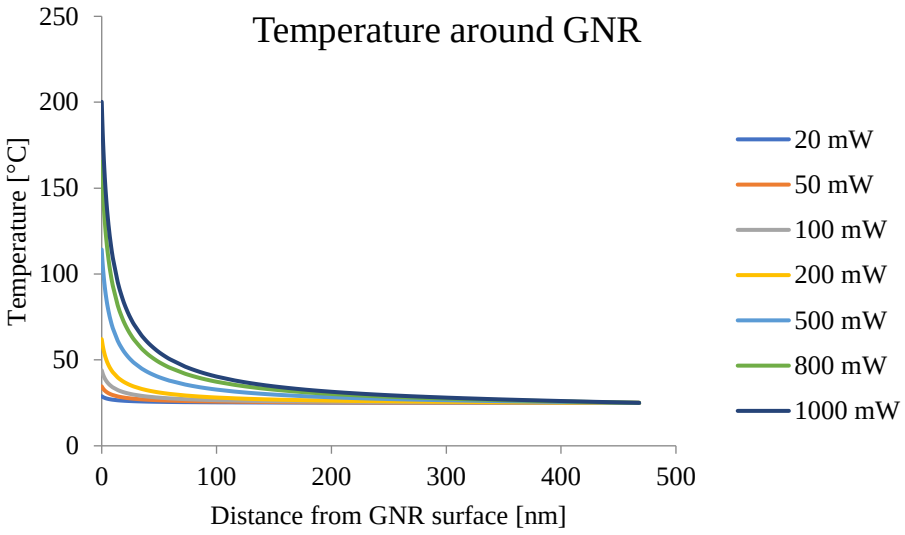

Figure 67: *The temperature distribution around GNR (the line along which data was collected starts at the tip of the nanostructure). It is possible to observe the strong dependence of surface temperature to illumination power.*

The temperature evolves, at 1000 mW, from 200 °C to 25 °C. However, this representation does not indicate precisely in what kind of thermal environment the oligonucleotides are. For this purpose, Figure 10 shows a graph covering the range 2-15 nm (distance from surface).

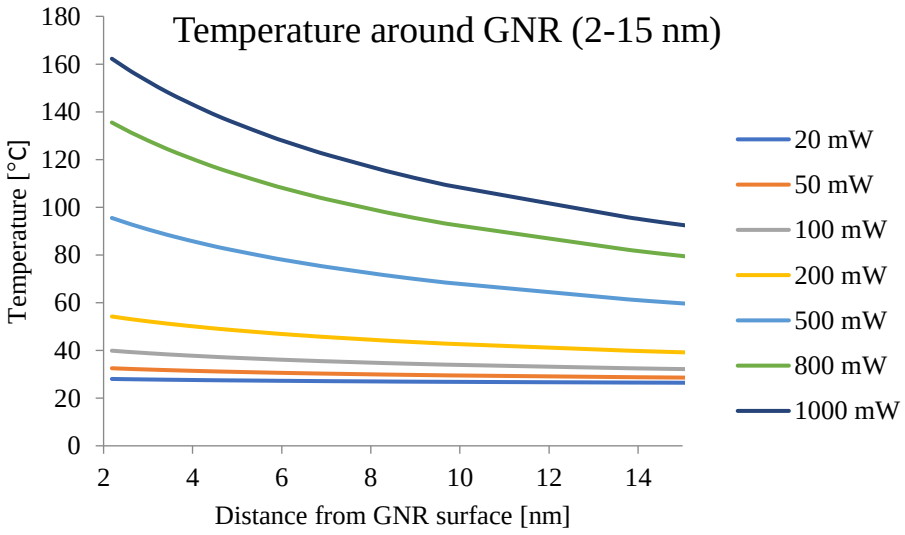

Figure 68: *The temperature distribution at range the dsDNA is present around GNR.*

Comparison of both graphs indicates the preferred conditions for temperature measurements based on fluorescence changes and turns out to be for a power between 100 and 200 mW (with beam diameter 10 µm). The first argument is the temperature on the surface; in both cases it is lower than 80 °C and at this temperature the thiol-gold bond dissociation starts

to be fast (within minutes ligands can be removed from the surface). Additionally, the change of temperature in the zone 10-15 nm (at which the fluorophore labelled to DNA will be present) is large enough to be clearly detected. Importantly, such an environment should not cause dsDNA denaturation, so that the distance Cy5-GNR would be constant.

6. Summary

6.1. The performed work

6.1.1. Nanomaterial synthesis

Despite having a very extensive literature, studies on oligonucleotide functionalisation by GNRs is still not an easy task. To date, the main focus in research in the field of thiol-based DNA-gold attachment, has been on combatting nanoparticle aggregation and has not concerned itself with DNA-CTAB interactions. On the whole, studies on surfactant-oligonucleotides were carried out independently of approaches developed in surface chemistry functionalisation.

The work done during this thesis covered the process of metal surface functionalisation and the nature of electrostatic interactions between DNA, CTAB and GNRs. The first results demonstrated the property of surfactants to surround oligonucleotides at certain concentrations. This has already been reported in the literature where it was shown that CTAB is able to tighten the double strand oligonucleotide structure (decrease the diameter). Moreover, other studies revealed that duplex strands could decorate micelles. Additionally, it was shown that CTAB-assisted hybridisation is more efficient. Together these studies clearly indicated that the properties of dsDNA could be modified in the presence of surfactant. However, there are no reports in the literature that show that in the presence of CTAB, pre-mixed non-complementary ssDNA can give FRET signals in a way similar to complementary strands. This phenomenon occurring in aqueous solutions of CTAB sheds important information on the first stage of functionalisation: namely the presentation of oligonucleotides to GNRs. The addition of thiolated DNA to a surfactant-containing solution has an important impact on the efficiency of the reaction. It transpires that groups of oligonucleotides can be maintained in relatively close proximity, even in the absence of direct interactions between strands (non-complementarity). This experiment clearly illustrated the difficulty behind the attachment of SH-DNA to GNRs in aqueous solutions of CTAB; strands are probably unable to approach the metal surface, simply because they are surrounded by a layer of surfactant. Additionally, because nanoparticles are covered by a bi-layer of the same amphiphilic compound, there are no means by which these structures can interact; both surfaces being composed of CTAB).

This therefore became the starting point of the thesis; layers formed by CTAB covered both GNRs and oligonucleotides consequently hampered functionalisation (due essentially to electrostatic repulsion between the hydrophilic parts of the CTAB).

Based on this, several approaches were considered to aid functionalisation. In addition to methods involving long incubation times of GNRs in CTAB with SH-DNA, attempts were made to modify the environment in specific ways. High salt concentrations were used and the pH was lowered in an attempt to elucidate the mechanisms involved in the effects of these processes. The stability of both CTAB bilayers on the GNRs surface as well as that of nanostructures themselves (when their surface charge was changed from positive to negative due to DNA strand adsorption) was followed. Because we succeeded in finally functionalising GNRs we did not go into the CTAB binding to oligonucleotides in any great depth. My idea was to catalogue the behaviour of DNA present at different CTAB concentration solutions over a widely used range ionic strength of phosphate buffer saline. Results showed that the range of oligonucleotide concentration within the CTAB layer was disturbed, and that judging by FRET measurements the DNA strands seemed to be separated. This demonstration of oligonucleotide separation by loss of FRET was crucial, because it demonstrated that the DNA was not trapped inside the surfactant layer. Another factor was to see the effects on the stability of GNRs with respect to aggregation as this was decisive for selecting an environment to facilitate efficient oligonucleotide immobilisation on metal surfaces. This was done by keeping CTAB concentrations much higher than the critical micellar concentration (CMC). Having pre-determined conditions that optimised GNRs stability, yet perturbed the CTAB bi-layer and ensured that non-complementary ssSH-DNA strands remained separated it became possible to focus on functionalisation itself.

The incubation of ssDNA (both thiolated and non-thiolated) with GNRs caused the solution to change colour from light pink to colourless. This process was clearly dependent on the oligonucleotide concentration; samples with the lowest concentration did not change. The question now concerned the nature of the observed solution bleaching. Analysis of changes in the absorption spectrum as a function of DNA concentration clearly confirmed that aggregation did not take place, there was no displacement of the plasmon absorption maximum. This strongly suggested that the GDRs were being deposited on the walls of the reaction vessels. As this behaviour was a function of DNA concentration, the theory was that the DNA strands were attaching to the metallic surfaces and by changing the surface charge resulted in removal from solution. It also explained the loss of the optical properties of the solution i.e. the change of

colour. Importantly, this behaviour was observed for both thiolated and non-thiolated DNA suggesting that the interaction was electrostatic. Close proximity between oligonucleotides and nanoparticles could cause thiol-gold bond formation in the case of SH- labelled strands, however in order to confirm this, the GNRs had to be detached from the walls of the Eppendorf tubes.

Deposition onto the walls of reaction vessels can be reversed by the addition of surfactants with opposite charge, e.g. CTAB (positive) or SDS (negative). However, SDS forms precipitates in the presence of PBS (due to the presence of K^+ ions), therefore I decided to try a non-charged surfactant: Tween20. This is supposed to intercalate (by hydrophobic-hydrophilic interactions) between CTAB groups, causing nanostructure release back into solution. This approach turned out to be effective, so subsequent experiments were conducted in the presence of Tween20. Additionally, this surfactant is more biologically compatible than CTAB, so using it was a step toward a biologically applicable drug carrier.

As soon as a method of nanostructure redispersion was elaborated, the next step was to check if electrostatic-based oligonucleotide immobilisation on GNRs surface could lead to thiol-gold bond formation. A number of procedures to test the success of immobilisation were attempted: measurement of fluorescence emission from colloidal solutions, zeta potential, migration distance during electrophoresis and fluorescence emitted from separating gels. The most efficient technique turned out to be separation by electrophoresis in agarose gels and detection by fluorescence emission because it was clearly possible to show samples with thiolated oligonucleotides, whereas zeta potential and emission from colloidal solutions were not unequivocal e.g. negative zeta potentials was measured for all samples exposed to ssDNA (including non-thiolated samples). As a result, electrostatic-based immobilisation on GNRs was an effective way to form thiol-gold bonds (as shown by agarose gel electrophoresis). The next step was to optimise functionalisation and to calculate the number of immobilised oligonucleotide strands. A number of quantitative techniques were considered, such as radioactivity measurements using ^{32}P (for ^{32}P end labelled oligonucleotide chains), or fluorescence. In this thesis ,since DNA double-labelled with thiol and dye was already used, then fluorophore emission was the easiest to apply. The problem was that the distance between the emitter and the GNRs was small enough to be influence by the plasmon, therefore measured values may be partially quenched/enhanced. Therefore, a means of eliminating plasmonic structure proximity had to be developed. Exposing nanohybrid samples to 2-Mercaptoethanol allowed thiolated DNA to be removed from gold surfaces. Subsequently, gel electrophoresis of

such samples enabled a relatively easy means to calculate concentrations based on fluorescence, due to the lack of plasmon influence (GNRs, SH-DNA have different migration rate). This also gave an idea of the equilibrium present in the system (GNRs/SH-DNA during immobilisation) and the maximum number of attached strands; reaching up to 275 strands per nanoparticle. In comparison to methods proposed before it clearly was not superior, but did have the advantages of having readily available material (PBS), allowing the reaction to be followed (deposition on reaction vessel walls) and granting access to the reaction time; one day processing provided GNRs functionalised by more than 200 strands without CTAB (no phase transfer needed).

With a reliable thiolated DNA functionalisation method, the next step was to hybridise the DNA and to find a way of calculating the number of strands immobilised during the process. The initial idea was to measure colloidal solution fluorescence in order to observe FRET phenomena (complementary strands had to be labelled with FRET-able pairs of fluorophores). Such an approach was supposed to indicate the concentration at which complementary DNA is in excess (the decrease of donor emission should reach a plateau). An interesting observation was found with FRET itself; it turned out that the acceptor, when paired with donor within dsDNA on a GNR surface, is quenched when directly excited. This suggested that donor-acceptor energy transfer could be two-way under some circumstances; this should be investigated in more detail in order to elucidate the mechanism. Tests of the FRET method conformed its usefulness in the field, but the problem was the unknown equilibrium between hybridised and free strands; this information could not be obtained by such fluorescence measurements (it could however be done by measuring the fluorophore lifetime). A solution was provided by agarose gel electrophoresis; in this technique provided that the temperature of the running buffer did not increase, it was possible to keep dsDNA intact. Thus, hybridised DNA migrated with the GNRs, whereas free DNA migration (and fluorescence emission) was not influenced by nanostructures. This method turned out to be even more effective when low pH glycerol solutions were used for nanostructure deposition onto the bottom of wells in the agarose gels; such an environment caused full dehybridisation (all of the complementary strands were free in solution). With this phenomenon it become possible to compare fluorescence in neighbouring wells, at the same migration distance, and thus compare the total number of complementary strands (sample in low pH) with non-hybridised one (samples in neutral pH). The technique also allowed direct measurement of samples with excess of complementary oligonucleotides and an idea of the ss-dsDNA equilibrium occurring in system.

The result was the preparation of DNA-functionalised GNRs, without CTAB and with pegylation. Additionally, control of the surface chemistry was increased, and it was possible to estimate the average number of thiolated and hybridized DNA per nanoparticle. This opens up the exciting possibility of following biological research, because such a level of nanohybrid verification is rare among nanomaterials and the issue of the detailed structure composition is usually unsolved.

6.1.2. Biological studies

Biological studies were not actually performed to any great extent but the project proved useful data for the use of nanoparticles in future research. First, the nanoparticles were pegylated; after desorption from reaction vessel walls, they were exposed to SH-PEG. That the reaction had taken place was confirmed by the subsequent behaviour of the nanostructures; their resistance against aggregation during centrifugation clearly increased. Therefore, it was possible to additionally protect nanoparticles and, probably, to decrease opsonization in the presence of biological material.

An interesting research topic in the near future that would not require modifications in nanomaterial synthesis would be to check uptake with respect to the ssDNA/dsDNA surface ratio. The literature shows that ssDNA functionalised nanoparticles are internalised more or less efficiently according to the nanohybrid surface properties. The idea of the project was to provide as many oligonucleotides as possible to the cell, consequently the uptake properties of nanoparticles with different ssDNA/dsDNA ratio should be examined. It could perhaps be that there is a threshold in the number of dsDNA needed for the internalisation process beyond which there is actually a drop in the number of GNRs entering cell.

At this point the biological studies can be separated into two lines: the first covering the release of complementary strands, the second dealing with uptake in the presence of biological substances, e.g. serum components. The demonstration of efficient release under NIR illumination is one of the most important goals of the whole thesis but is unfortunately missing. With the uptake, probably by an endocytosis mechanism, the nanomaterial accumulates into lysosomes which are organelles designed to destroy any object hazardous for the cell. The defensive reaction involves a pH decrease inside lysosomes coupled with the presence of enzymes able to fragment biological material. The result of this should be degradation of DNA/RNA, since if the pH reaches close to two, denaturation will occur. A published solution to this problem consisted of introducing a proton sponge able to absorb H^+ ions, as a result the

lysosome would rupture. A different proposition, connected with this thesis would be laser heating; GNRs will be accumulated in the lysosome, so relatively low power may locally increase the temperature to a level that destroys the lysosome and releases material into the cytoplasm. Therefore, the main points of these experiments would be to provide an indication of uptake ability and to look for alternative methods (without the proton sponge) of escaping from the lysosome.

Examination of GNRs optical activity inside cells should be correlated with experiments covering uptake of nanohybrids in the presence of serum whose components will be able to opsonize structures modifying surface properties. Opsonization is probably an essential part of the phagocytosis process and may affect internalisation by cells. In order to reduce non-specific protein-GNRs interactions, SH-PEG has to be considered. The only work in this thesis associated with pegylation was to use it successfully as an agent against aggregation. Nevertheless, there are no data to give an idea of the number of PEG strands per single GNR required to reduce opsonization. In order to control this, a set of experiments has to be performed without cell. Migration in agarose gel under electrophoresis should shed a light on modifications of the surface properties compared to GNRs not exposed to serum. With these experiments a synthesis protocol may be devised in order to optimise the surface composition. A set of tests with different pegylation levels should indicate the most promising material which could then be further modified (preferably only with respect to thiolated oligonucleotides) in order to introduce targeting.

6.2. Future research

6.2.1. GNRs targeting

A logical continuation of this project should be focused on active targeting; as discussed before, in my opinion, from a functionalisation point of view the most promising would be to use aptamers. Because they are oligonucleotides it would be possible to attach them to GNRs surfaces using the same protocol as ss/dsDNA. Additionally, in the case of aptamers, as for ssDNA, basic targeting can be controlled without cells; the mechanism of recognition is base complex formation, therefore such experiments may be done in the presence of serum. Based on the experience from previous experiments (e.g. the number of PEG molecules needed for opsonization reduction) the replacement of oligonucleotides by aptamers for gene transporting will be a small nanostructure modification. Therefore, initial experiments concerning aptamer activity can be e.g. hybridisation (with fluorophore-labelled target) in the presence of serum;

this would be a test of accessibility. It is known that opsonisation decreases the "activity" of molecules, but the issue is whether it forms double strands at all. In further investigation it may be necessary to widen to check the equilibrium status and the reaction rate at 37 °C.

If hybridisation between aptamer and targets occurs in serum it may be possible to check its effectiveness in a system containing cells. The attachment to the surface can be followed by confocal/total internal reflection microscopy, uptake effectiveness by FACS. Combining these two techniques gives the possibility of ensuring that nanomaterial is able to be internalised even in media containing opsonizing molecules. The next step would be to release oligonucleotides using a NIR laser.

However, target therapy should be approached by following the expression of the carried genes. For this purpose reporting gene technology for example based on the introduction of sequences causing GFP synthesis in cells would be very promising. Such an approach allows the time between DNA/RNA release and the appearance of protein fluorescence to be monitored. The detailed information covering nanomaterial composition, and the average number of genes per GNR would open up the possibility of a better understanding of biological mechanisms occurring in cells.

6.2.2. Temperature measurements

An important part of project was simulating the thermal properties of GNRs illuminated by NIR laser. Unfortunately, the work outline had to be modified, in order to better understand the functionalisation process and the time devoted to understanding the temperature gradient around nanoparticles was strongly reduced. However, as for the biological part of this thesis, an approach can be proposed which can be applied in this field.

First, we considered the possibilities of using ssDNA/dsDNA as a thermometer or temperature-indicative fluorophore carrier. The main advantage in using oligonucleotides is the ability to control their distance from metal surfaces. The initial idea was to use molecular beacons, double-labelled (thiol and fluorophore) nucleotides, in order to observe the dissociation of "closed" states. The opening of structures could be correlated with temperature according to the melting temperature of the closed formation. However such an approach was difficult for a number of reasons: the 5-10 hybridised base pairs close to a nanoparticle surface have unknown stability, the melting temperature of this duplex being unknown (when attached to GNR), the result will always be an indication covering a zone around the GNRs (the hybridization zone for 5 bp = 1.66 nm), some organic fluorophores emission intensity may vary

due to changes in the local environment viscosity (caused e.g. by the temperature of the medium). The issue of organic dyes is very important, because the approach used in experiments covering temperature measurements should be applied later in biological experiments (covering toxicity and uptake). Because of this the fluorophore cannot be toxic, this reduces the number of possibilities for wide use by biologists. It also raises another problem; most fluorophores have a molecular rotor structure, so their emission can be affected by changes in local viscosity. Therefore the properties of a molecular beacon attached to gold surfaces and the need for non-toxic fluorophores makes hairpin DNA a far from perfect candidate for temperature measurements. However, from this point, it was clear that as an "active" measurement tool, fluorophores could be used; such an approach increases the number of possibilities, because ssDNA and dsDNA can be labelled with fluorophores. The ssDNA was eliminated from consideration, because such strands do not provide control of distance due to their flexibility. On the other hand, dsDNA which is rigid over distances covering tens of base pairs provide a sort of molecular ruler, where fluorophores can be precisely placed in different zones around GNRs. There were two options for dye labelling: on the thiolated strand, or on the complementary strand. The first one was eliminated, because hybridisation to the surface was not 100% efficient so there was always a mix of labelled ssDNA and dsDNA. Therefore, the second option was selected, because such an approach is the only one allowing effective distance control. The limitation of this method is strict temperature range so as not to induce duplex dissociation, but measurements of thermal efficiency could be made in the range of 25-55 °C.

The experimental part of the project ended with a check on the temperature dependence of the Cy5 emission; the heat source was external and the temperature of the colloidal solution controlled by a thermocouple. Such an approach should determine if the predicted dependence occurred in situations where dyes are immobilised in close proximity to the GNR surface; indeed, results proved this theory. However, problems were associated with relatively low starting emissions of fluorophore (temperature increase causes fluorescence drop), but nevertheless a linear spectral dependence was shown.

Simulations were focused on using a continuous wave laser due to the fact of possessing real data concerning power and beam diameter. The set of calculations indicated that the power needed for efficient heating (more than 30 °C) of a single GNR requires 200 mW power with a laser beam diameter equal to 10 μm. Such a result can be a starting point for engineering experiments covering NIR laser heating of nanostructures; the important issue is the technical

background of this. Laser beams of such diameter can be clearly observed under the microscope, therefore the most promising would be to use the thin layer of colloidal solutions under TIRF microscope. The light pathway in liquids should not be too long, because of beam energy losses (scattering). An interesting situation would be to immobilise GNRs onto e.g. silica, but this comes with technological and simulation issues (very close proximity of silica, nanoparticles would be at the interface of two media with different thermal properties). On the other hand, the orientation differences of GNRs in colloidal solution means that longitudinal absorption of GNRs varies from 0 to 100 %. In summary, this experiment may appear to be easy to conduct, but it comes with problems in analysis associated with variable nanoparticle orientation.

Finally, an interesting issue is what can be done in the near future based on the results from this thesis. First, the theoretical approach outlined those laser properties needed to carry out a temperature increase process crucial for biological experiments. Additionally, we showed that Cy5 can act as a thermometer when linked to GNRs, so a variety of experiments can be done; most preferably under the optical microscope. This also allows monitoring of the temperature inside cells, albeit with some uncertainty (the salt concentration in cytoplasm can vary during experiment and impact molecular rotors emission).

7. Bibliography

[1] C. W. Pouton, K. W. Wagstaff, D. M. Roth, G. W. Moseley, D. A. Jans, "Targeted delivery to the nucleus", Adv. Drug Deliv. Rev., 59, 698-171 (2007)

[2] C. E. Dunbar, K. A. High, J. K. Joung, D. B. Kohn, K. Ozawa, M. Sadelain, "Gene therapy comes of age", Science 359, 175 (2018)

[3] C. S. Manno, G. F. Pierce, V. R. Arruda, B. Glader, M. Ragni, J. J. E. Rasko, M. C. Ozelo, K. Hoots, P. Blatt, B. Konkle, M. Dake, R. Kaye, M. Razavi, A. Zajko, J. Zehnder, P. Rustagi, H. Nakai, A. Chew, D. Leonard, J. F. Wright, R. R. Lessard, J. M. Sommer, M. Tigges, D. Sabatino, A. Luk, H. Jiang, F. Mingozzi, L. Couto, H. C. Ertl, K. A. High, M. A. Kay, "Successful transduction of liver in hemophilia by AAV-Factor IX and limitations imposed by the host immune response" Nat. Med. 12, 342–347 (2006).

[4] G. P. Niemeyer, R. W. Herzog, J. Mount, V. R. Arruda, D. M. Tillson, J. Hathcock, F. W. van Ginkel, K. A. High, C. D. Lothrop Jr, "Long-term correction of inhibitor-prone hemophilia B dogs treated with liver-directed AAV2-mediated factor IX gene therapy", Blood 113, 797–806 (2009).

[5] L. A. George, S. K. Sullivan, A. Giermasz, J. E.J. Rasko, B. J. Samelson-Jones, J. Ducore, A. Cuker, L. M. Sullivan, S. Majumdar, J. Teitel, C. E. McGuinn, M. V. Ragni, A. Y. Luk, D. Hui, J. F. Wright, Y. Chen, Y. Liu, K. Wachtel, A. Winters, S. Tiefenbacher, V. R. Arruda, J. C.M. van der Loo, O. Zelenaia, D. Takefman, M. E. Carr, L. B. Couto, X. M. Anguela, K. A. High, "Hemophilia B gene therapy with a high-specific-activity factor IX Variant" N. Engl. J. Med., 377, 2215–2227 (2017)

[6] A. M. Maguire , K. A. High, A. Auricchio, J. F. Wright, E. A. Pierce, F. Testa, F. Mingozzi, J. L. Bennicelli, G. Ying, S. Rossi, A. Fulton, K. A. Marshall, S. Banfi, D. C. Chung, J. I. W. Morgan, B. Hauck, O. Zelenaia, X. Zhu, J. Bennett, "Age-dependent effects of RPE65 gene therapy for Leber's congenital amaurosis: A phase 1 doseescalation trial" Lancet 374, 1597–1605 (2009)

[7] W.-L. Hwu, S. Muramatsu, S.-H. Tseng, K.-Y. Tzen, N.-C. Lee, Y.-H. Chien, R. O. Snyder, B. J. Byrne, C.-H. Tai, R.-M. Wu, "Gene therapy for aromatic L-amino acid decarboxylase deficiency" Sci. Transl. Med. 4, 134ra61 (2012)

[8] K. Talbot, E. F. Tizzano, "The clinical landscape for SMA in a new therapeutic era", Gene Ther. 24, 529–533 (2017)

[9] S. H. Orkin, P. Reilly, "Paying for future success in gene therapy" Science 352, 1059–1061 (2016)

[10]https://european-biotechnology.com/up-to-date/latest-news/news/uniqure-withdraws-eur1m-drug-glybera-from-market.html [11/09/2018]

[11] D. Bobo, K. J. Robinson, J. Islam, K. J. Thurecht, S. R. Corrie, "Nanoparticle-based medicines: a rewiev of FDA-approved materials and clinical trials to date", Pharm. Res., 33, 2373-2387 (2016)

[12] R. Brayner, "The toxicological impact of nanoparticles", NanoToday, 3, 48-55 (2008)

[13] L. Sun, Y. Li, X. Liu, M. Jin, L. Zhang, Z. Du, C. Guo, P. Huang, Z. Sun, "Cytotoxicity and mitochondrial damage caused by silica nanoparticles", Toxicol In Vitro., 25, 1619-1629 (2011)

[14] A. E. Nel, L. Madler, D. Velegol, T. Xia, E. M. V. Hoek, P. Somasundaran, F. Klaessig, V. Castranova, M. Thompson, "Understanding biophysicochemical interactions at the nano–bio interface", Nat. Mater., 8, 543-547 (2009)

[15] C. W. Pouton, K. M. Wagstaff, D. M. Roth, G. W. Moseley, D. A. Jans, "Targeted delivery to the nucleus", Advanced Drug Delivery Reviews, 59, 698-717 (2007)

[16] K. J. Ewer, T. Lambe, C. S. Rollier, A. J. Spencer, A. V. S. Hill, L. Dorrell, "Viral vectors as vaccine platforms: from immunogenicity to impact", Current Opinion in Immunology, 41, 47-54 (2016)

[17] P. D. Robbins, S. C. Ghivizzani, "Viral vectors for gene therapy", Pharmacol. Ther., 80, 35-47 (1998)

[18] C. E. Thomas, A. Ehrhardt, M. A. Kay, "Progress and problems with the use of viral vectors for gene therapy", Nat. Rev., 4, 346-358 (2003)

[19] D. J. Glover, H. J. Lipps, D. A. Jans, "Towards safe, non-viral therapeutic gene expression in humans", Nat. Rev. Genet., 6, 299-310 (2005)

[20] H. Yin, R. L. Kanasty, A. A. Eltoukhy, A. J. Vegas, J. R. Dorkin, D. G. Anderson, "Non-viral vectors for gene-based therapy", Nature Reviews Genetics volume 15, pages 541–555 (2014)

[21] I. Roy, S. Mitra, A. Maitra, S. Mozumdar, „Calcium phosphate nanoparticles as novel non-viral vectors for targeted gene delivery", International Journal of Pharmaceutics, 250, 25-33 (2003)

[22] S. Mansouri, P. Lavigne, K. Corsi, M. Benderdour, E. Beaumont, J. C. Fernandes, "Chitosan-DNA nanoparticles as non-viral vectors in gene therapy: strategies to improve transfection efficacy", European Journal of Pharmaceutics and Biopharmaceutics, 57, 1–8 (2004)

[23] D. J. Bharali, I. Klejbor, E. K. Stachowiak, P. Dutta, I. Roy, N. Kaur, E. J. Bergey, P. N. Prasad, M. K. Stachowiak, „Organically modified silica nanoparticles: A nonviral vector for in

vivo gene delivery and expression in the brain", Proc. Natl. Acad. Sci. USA, 102, 11539–11544 (2005)

[24] Y. Ding, Z. Jiang, K. Saha, C. S. Kim, S. T. Kim, R. F. Landis, V. M. Rotello, " Gold nanoparticles for nucleic acid delivery", Molecular Therapy, 22, 1075-1083 (2014)

[25] J. Zhang, Z.-Y. Lu, Z.-Y. Sun, "A possible route to fabricate patchy nanoparticlesviaself-assembly of a multiblock copolymer chain in one step" Soft Matter, 7, 9944-9950 (2011)

[26] J. Chen, Z. Guo, H. Tian, X. Chen, "Production and clinical development of nanoparticles for gene delivery", Mol Ther Methods Clin Dev., 3, 16023 (2016)

[27] L. Shi, L. A. Sordillo, A. Rodriguez-Contreras, R. Alfano, "Transmission in near-infrared optical windows for deep brain imaging", J Biophotonics., 9, 38–43 (2016)

[28] C. R. Martin, "Membrane-based synthesis of nanomaterials", Chem. Mater., 8,1739–1746 (1996)

[29] Y.-Y. Yu, S.-S. Chang, C.-L. Lee, C. R. Chris Wang, "Gold nanorods: electrochemical synthesis and optical properties", J. Phys. Chem. B, 101, 6661-6664 (1997)

[30] N. R. Jana, L. Gearheart, C. J. Murphy, "Seed-mediated growth approach for shape controlled synthesis of spheroidal and rod-like gold nanoparticles using a surfactant template", Adv. Mater., 13, 1389-1393 (2001)

[31] N. R. Jana, L. Gearheart, C. J. Murphy, "Wet chemical synthesis of high aspect ratio cylindrical gold nanorods", J. Phys. Chem. B, 105, 4065-4067 (2001)

[32] B. Nikoobakht, M. A. El-Sayed, "Preparation and growth mechanism of gold nanorods (NRs) using seed-mediated growth method", Chem. Mater., 15, 1957-1962 (2003)

[33] X. Kou, S. Zhang, C-K Tsung, Z. Yang, M. H. Yeung, G. D. Stucky, L. Sun, J. Wang, C. Yan, "One-step synthesis of large-aspect-ratio single-crystalline gold nanorods by using CTPAB and CTBAB surfactants", Chem. Eur. J., 2929-2936 (2007)

[34] P. Wang, M. Liu, G. Gao, S. Zhang, H. Shi, Z. Li, L. Zhanga Y. Fang, "From gold nanorods to nanodumbbells: a different way to tailor surface plasmon resonances by a chemical route", J. Mater. Chem., 22, 24006-24011 (2012)

[35] M. Iqbal, G. Tae, "Unstable reshaping of gold nanorods prepared by a wet chemical method in the presence of silver nitrate", J. Nanosci. Nanotechnol., 6, 3355-3359 (2006)

[36] D. A. Zweifel, A. Wei, "Sulfide-arrested growth of gold nanorods", Chem. Mater., 17, 4256–4261 (2005)

[37] A. Liberman, N. Mendez, W. C. Trogler, A. C. Kummel, "Synthesis and surface functionalization of silica nanoparticles for nanomedicine", Surf Sci Rep., 69, 132-158 (2014)

[38] B. Isomaa, J. Reuter, B. M. Djupsund, "The subacute and chronic toxicity of Cetyltrimethylammonium Bromide (CTAB), a cationic surfaetant, in the rat", Arch. Toxicol. 35, 91-96 (1976)

[39] J. Wan, J.-H. Wang, T. Liu, Z. Xie, X.-F. Yu, W. Li, "Surface chemistry but not aspect ratio mediates the biological toxicity of gold nanorods in vitro and in vivo", Sci Rep., 5, 11398 (2015)

[40] J. Li, B. Zhu, Z. Zhu, Y. Zhang, X. Yao, S. Tu, R. Liu, S. Jia, C. J. Yang, "Simple and rapid functionalization of gold nanorods with oligonucleotides using an mPEG-SH/Tween 20-assisted approach", Langmuir, 31,7869–7876 (2015)

[41] B. Liua, J. Liu, "Methods for preparing DNA-functionalized gold nanoparticles, a key reagent of bioanalytical chemistry", Anal. Methods, 9, 2633-2643 (2017)

[42] G. Wei, J. Yu, J. Wang, P. Gu, D. J. Birch, Y. Chen, "Hairpin DNA-functionalized gold nanorods for mRNA detection in homogenous solution", J Biomed Opt. 21, 97001 (2016)

[43] M.-C. Daniel, D. Astruc, "Gold nanoparticles: assembly, supramolecular chemistry, quantum-size-related properties, and applications toward biology, catalysis, and nanotechnology", Chem. Rev., 104, 293−346 (2004)

[44] A. Elbakry, A. Zaky, R. Liebl, R. Rachel, A. Goepferich, M. Breunig, "Layer-by-layer assembled gold nanoparticles for siRNA delivery", Nano Lett., 9, 2059-2064 (2009)

[45] J. Li, A. V. Krasavin, L. Webster, P. Segovia, A. V. Zayats, D. Richards, "Spectral variation of fluorescence lifetime near single metal nanoparticles", Sci Rep., 6, 21349 (2016)

[46] H. Sahoo, "Förster resonance energy transfer – a spectroscopic nanoruler: principle and applications", J. Photochem. Photobiol. C, 12, 20-30 (2011)

[47] R. Chhabra, J. Sharma, H. Wang, S. Zou, S. Lin, H. Yan, S. Lindsay, Y. Liu, "Distance-dependent interactions between gold nanoparticles and fluorescent molecules with DNA as tunable spacers", Nanotechnology, 20, 485201 (2009)

[48] D. Darvill, A. Centeno, F. Xie, "Plasmonic fluorescence enhancement by metal nanostructures: shaping the future of bionanotechnology" Phys. Chem. Chem. Phys., 15, 15709-15726 (2013)

[49] C. Tserkezis, N. Stefanou, M. Wubs, N. A. Mortensen, "Molecular fluorescence enhancement in plasmonic environments: exploring the role of nonlocal effects" Nanoscale, 8, 17532-17541 (2016)

[50] T. A. Larson, P. P. Joshi, K. Sokolov, "Preventing protein adsorption and macrophage uptake of gold nanoparticles via a hydrophobic shield", ACS Nano., 6, 9182–9190 (2012)

[51] C. D. Walkey, J. B. Olsen, H. Guo, A. Emili, W. C. W. Chan, "Nanoparticle size and surface chemistry determine serum protein adsorption and macrophage uptake", J. Am. Chem. Soc., 134, 2139–2147 (2012)

[52] E. Blanco, H. Shen, M. Ferrari, "Principles of nanoparticle design for overcoming biological barriers to drug delivery" Nat Biotechnol., 33, 941–951 (2015)

[53] A. E. Nel, L. Mädler, D. Velegol, T. Xia, E. M. V. Hoek, P. Somasundaran, F. Klaessig, V. Castranova, M. Thompson, "Understanding biophysicochemical interactions at the nano–bio interface" Nature Materials, 8, 543–557 (2009)

[54] G. von Maltzahn, J.-H. Park, A. Agrawal, N. K. Bandaru, S. K. Das, M. J. Sailor, S. N. Bhatia, "Computationally guided photothermal tumor therapy using long-circulating gold nanorod antennas", Cancer Res., 69, 3892–3900 (2009)

[55] E. C. Dreaden, L. A. Austin, M. A. Mackey, M. A. El-Sayed, "Size matters: gold nanoparticles in targeted cancer drug delivery", Ther Deliv., 3, 457–478 (2012)

[56] M. H. Jazayeri, H. Amani, A. A. Pourfatollah, H. Pazoki-Toroudi, B. Sedighimoghaddam, "Various methods of gold nanoparticles (GNPs) conjugation to antibodies", Sensing and bio-sensing research, 9, 17-22 (2016)

[57] X. Wang, Z. Mei, Y. Wang, L. Tang, "Comparison of four methods for the biofunctionalization of gold nanorods by the introduction of sulfhydryl groups to antibodies", Beilstein J. Nanotechnol., 8, 372–380 (2017)

[58] M. Borrajo, V. Puntes, (2018) "Janus antibody protein corona onto gold nanoparticles". Poster session presented at the Gold 2018, Paris, France

[59] M. E. Gallina, Y. Zhou, C. J. Johnson, D. Harris-Birtill, M. Singh, H. Zhao, D. Ma, T. Cass, D. S. Elson, "Aptamer-conjugated, fluorescent gold nanorods as potential cancer theradiagnostic agents", Mater. Sci. Eng. C., 59, 324-332 (2016)

[60] A. C. Wong, D. W. Wright, "Size-dependent cellular uptake of DNA functionalized gold nanoparticles" Small, 12, 5592-5600 (2016)

[61]T. B. Huff, M. N. Hansen, Y. Zhao, J. X. Cheng, A. Wei, "Controlling the cellular uptake of gold nanorods", Langmuir, 23, 1596-1599 (2007)

[62] A. M. Alkilany, P. K. Nagaria, C. R. Hexel, T. J. Shaw, C. J. Murphy, M. D. Wyatt, "Cellular uptake and cytotoxicity of gold nanorods: molecular origin of cytotoxicity and surface effects", Small, 5, 701–708 (2009)

[63] H. Yang, Z. Chen, L. Zhang, W. Y. Yung, K. C. Leung, H. Y. Chan, C. H. Choi, "Mechanism for the cellular uptake of targeted gold nanorods of defined aspect ratios", Small, 12, 5178-5189 (2016)

[64] L. R. Hirsch, R. J. Stafford, J. A. Bankson, S. R. Sershen, B. Rivera, R. E. Price, J. D. Hazle, N. J. Halas, J. L. West, "Nanoshell-mediated near-infrared thermal therapy of tumors under magnetic resonance guidance", Proc Natl Acad Sci U S A, 100, 13549–13554 (2003)

[65] D. P. O'Neal, L. R. Hirsch, N. J. Halas, J. D. Payne, J. L. West, "Photo-thermal tumor ablation in mice using near infrared-absorbing nanoparticles", Cancer Letters, 209, 171-176 (2004)

[66] Y. Sun, N. C. Harris, C.-H. Kiang, "Phase transition and optical properties of DNA-gold nanoparticle assemblies", Plasmonics., 2, 193–199 (2007)

[67] J. Xu, S. L. Craig, "Thermodynamics of DNA hybridization on gold nanoparticles", J. Am. Chem. Soc., 127, 13227-13231 (2005)

[68] B. Lang, "Hybridization thermodynamics of DNA bound to gold nanoparticles", J. Chem. Thermodyn., 42, 1435-1440 (2010)

[69] K. Akamatsu, M. Kimura, Y. Shibata, S. Nakano, D. Miyoshi, H. Nawafune, N. Sugimoto, „A DNA duplex with extremely enhanced thermal stability based on controlled immobilization on gold nanoparticles", Nano Lett., 6, 491–495 (2006)

[70] A. K. R. Lytton-Jean, C. A. Mirkin, "A thermodynamic investigation into the binding properties of DNA functionalized gold nanoparticle probes and molecular fluorophore probes", j. Am. Chem. Soc., 127, 12754-12755 (2005)

[71] D. G. Cahill, K. Goodson, A. Majumdar, "Thermometry and thermal transport in micro/nanoscale solid-state devices and structures" J. Heat Transfer 124, 223–241 (2002).

[72] N. Kawamoto, M. S. Wang, X. Wei, D. M. Tang, Y. Murakami, D. Shindo, M. Mitome, D. Golberg, "Local temperature measurements on nanoscale materials using a movable nanothermocouple assembled in a transmission electron microscope", Nanotechnology, 22, 485707 (2011)

[73] C. D. S. Brites, P. P. Lima, N. J. O. Silva, A. Millan, V. S. Amaral, F. Palacio, L. D. Carlos, "Thermometry at the nanoscale", Nanoscale 4, 4799–4829 (2012).

[74] C. Colliex, "Taking temperature at the nanoscale", Science, 347, 611-612 (2015)

[75] P. C. Ray, H. Yu, P. P. Fu, "Toxicity and environmental risks of nanomaterials: challenges and future needs", J Environ Sci Health C Environ Carcinog Ecotoxicol Rev., 27, 1–35 (2009)

[76] E. Yasun, C. Li, I. Barut, D. Janvier, L. Qiu, C. Cui, W. Tan, "BSA modification to reduce CTAB induced nonspecificity and cytotoxicity of aptamer-conjugated gold nanorods", Nanoscale., 7, 10240–10248 (2015)

[77] S. Wang, W. Lu, O. Tovmachenko, U. S. Rai, H. Yu, P. C. Ray, "Challenge in understanding size and shape dependent toxicity of gold nanomaterials in human skin keratinocytes", Chem Phys Lett., 463, 145–149 (2008)

[78] S. Ghosh, S. P. Moulik, "Interfacial and micellization behaviors of binary and ternary mixtures of amphiphiles (Tween-20, Brij-35, and Sodium Dodecyl Sulfate) in aqueous medium", J. Colloid Interface Sci. 208, 357–366 (1998)

[79] T. Sidim, G. Acar, "Alcohols effect on critic micelle concentration of Polysorbate 20 and Cetyl Trimethyl Ammonium Bromine mixed solutions", J Surfactants Deterg., 16, 601–607 (2013)

[80] B. Tah, P. Pal, M. Mahato, G. B. Talapatra, "Aggregation behavior of SDS/CTAB catanionic surfactant mixture in aqueous solution and at the air/water interface", J Phys Chem B., 115, 8493-8499 (2011)

[81] L. Wang, X. Jiang, Y. Ji, R. Bai, Y. Zhao, X. Wu, C. Chen, "Surface chemistry of gold nanorods: origin of cell membrane damage and cytotoxicity", Nanoscale., 21, 8384-8391 (2013)

[82] K. Park, L. F. Drummy, R. C. Wadams, H. Koerner, D. Nepal, L. Fabris, R. A. Vaia, "Growth Mechanism of gold nanorods" Chem. Mater., 25, 555–563 (2013)

[83] L. J. Cristina, G. Ruano, R. Salvarezza, J. Ferron, "Thermal stability of self-assembled monolayers of n-Hexanethiol on Au(111)-(1 x 1) and Au(001)-(1 x 1)", J. Phys. Chem. C, 121, 27894-27904 (2017)

[84] C. Chen, W. Wang, J. Ge, X. S. Zhao, "Kinetics and thermodynamics of DNA hybridization on gold nanoparticles", Nucleic Acids Res. 37, 3756–3765 (2009)

[85] Z. J. Hu, S. Hou, Y. L. Ji, T. Wen, W. Q. Liu, H. Zhang, X. W. Shi, J. Yan, X. C. Wu, "Fast characterization of gold nanorods ensemble by correlating its structure with optical extinction spectral features", AIP Advances 4, 117137-117149 (2014)

[86] J. Zhu, "Shape dependent full width at half maximum of the absorption band in gold nanorods", Physics Letters A 339, 466–471 (2005)

[87] T. Handel, M. Wuithschick, F. Kettemann, A. Birnbaum, K. Rademann, J. Polte, "In situ determination of colloidal gold concentrations with UV-Vis spectroscopy: limitations and perspectives", Anal. Chem. 86, 11115-11124 (2014)

[88] C. J. Orendorff, C. J. Murphy, "Quantitation of metal content in the silver-assisted growth of gold nanorods", J. Phys. Chem. B 110, 3990-3994 (2006)

[89] C. Hamon, T. Bizien, F. Artzner, P. Even-Hernandez, V. Marchi, "Replacement of CTAB with peptidic ligands at the surface of gold nanorods and their self-assembling properties", Journal of Colloid and Interface Science 424, 90–97 (2014)

[90] B. Mujumdar, A. Ernst, S.R. Mujumdar, C.J. Lewis, A.S. Waggoner, "Cyanine dye labeling reagents: Sulfoindocyanine succinimidyl esters", Bioconjugate Chemistry. 4 (2): 105–111 (1993)

[91] B. Mujumdar, A. Ernst, S.R. Mujumdar, C.J. Lewis, A.S. Waggoner, "Cyanine dye labeling reagents: Sulfoindocyanine succinimidyl esters", Bioconjugate Chemistry. 4 (2): 105–111 (1993)

[92] K. A. Kang, J. Wang, J. B. Jasinski, S. Achilefu, "Fluorescence manipulation by gold nanoparticles: from complete quenching to extensive enhancement" J Nanobiotechnology 9:16, (2011)

[93] J. Szöllosi, S. Damjanovich, P. Nagy, G. Vereb, L. Mátyus, "Principles of resonance energy transfer" Curr Protoc Cytom. chapter 1: unit 1.12 (2006)

[94] J. R. Lakowicz (2006) "Energy Transfer", In J. R. Lakowicz "Principles of Fluorescence Spectroscopy" (p. 446), 3rd Edition, Springer, New York, United States of America

[95] H. C. Ishikawa-Ankerhold, R. Ankerhold, G. P. Drummen, "Advanced fluorescence microscopy techniques--FRAP, FLIP, FLAP, FRET and FLIM" Molecules, 17, 4047-4132 (2012)

[96] V. V. Didenko, "DNA probes using Fluorescence Resonance Energy Transfer (FRET): Designs and applications", Biotechniques 31, 1106–1121 (2001)

[97] H. E. Grecco, P. J. Verveer, "FRET in Cell Biology: Still shining in the age of super-resolution?", ChemPhysChem 12, 484-490 (2011)

[98] T. Ha, I. Rasnik, W. Cheng, H. P. Babcock, G. H. Gauss, T. M. Lohman, S. Chu, "Initiation and re-initiation of FNA unwinding by the Escherichia coli Rep helicase", Nature 419, 638-641 (2002)

[99] K. Park, L. F. Drummy, R. C. Wadams, H. Koerner, D. Nepal, L. Fabris, R. A. Vaia, "Growth Mechanism of gold nanorods" Chem. Mater., 25, 555–563 (2013)

[100] Y. Hong, Y.-M. Huh, D. S. Yoon, J. Yang, "Nanobiosensors Based on Localized Surface Plasmon Resonance for Biomarker Detection," Journal of Nanomaterials, 2012, 759830 (2012)

[101] B. Nikoobakht, M. A. El-Sayed, "Preparation and growth mechanism of gold nanorods (NRs) using seed-mediated growth method" Chem. Mater., 15, 1957-1962 (2003)

[102] B. N. Khlebtsov, V. A. Khanadeev, J. Ye, G. B. Sukhorukov, N. G. Khlebtsov, "Overgrowth of gold nanorods by using a binary surfactant mixture" Langmuir 30, 1696–1703 (2014)

[103] S. Gomez-Grana, F. Hubert, F. Testard, A. Guerrero-Martinez, I. Grillo, L. M. Liz-Marzan, O. Spalla, "Surfactant (bi)layers on gold nanorods" Langmuir 28, 1453–1459 (2012)

[104] C. Yu, L. Varghese, J. Irudayaraj, "Surface modification of cetyltrimethylammonium bromide-capped gold nanorods to make molecular probes" Langmuir, 23, 9114–9119 (2007)

[105] C. L. John, S. L. Strating, K. A. Shephard, J. X. Zhao, "Reproducibly synthesize gold nanorods and maintain their stability" RSC Adv.,3, 10909-10918 (2013)

[106] A. Techen, C. Hille, C. Dosche, M. U. Kumke, "Fluorescence study of drug–carrier interactions in CTAB/PBS buffer model systems" J. Colloid Interface Sci., 377, 251–261 (2012)

[107] M. J. Qazi, R. W. Liefferink, S. J. Schlegel, E. H. G. Backus, D. Bonn, N. Shahidzadeh, "Influence of surfactants on sodium chloride crystallization in confinement" Langmuir, 33, 4260−4268 (2017)

[108] R. M. Pashley, B. W. Ninham, "Double-layer forces in ionic micellar solutions" The Journal of Physical Chemistry, 91, 2902-2904 (1987)

[109] Y. Wang, L. Tang, "Chemisorption assembly of Au nanorods on mercaptosilanized glass substrate for label-free nanoplasmon biochip", Anal. Chim. Acta, 796, 122-129 (2013)

[110] B. Tah, P. Pal, M. Mahato, G. B. Talapatra, "Aggregation behavior of SDS/CTAB catanionic surfactant mixture in aqueous solution and at the air/water interface" J. Phys. Chem. B, 115, 8493-8499 (2011)

[111] P. M. R. Paulo, P. Zijlstra, M. Orrit, E. Garcia-Fernandez, T. C. S. Pace, A. S. Viana, S. M. B. Costa, "Tip-specific functionalization of gold nanorods for plasmonic biosensing: effect of linker chain length" Langmuir, 33, 6503–6510 (2017)

[112] S. B. Lioi, X. Wang, R. Islam, E. J. Danoff, . S. English, "Catanionic surfactant vesicles for electrostatic molecular sequestration and separation" Phys. Chem. Chem. Phys., 11, 9315-9325 (2009)

[113] D. Santhiya, S. Maiti, "An Investigation on Interaction between 14mer DNA Oligonucleotide and CTAB by Fluorescence and Fluorescence Resonance Energy Transfer Studies", J. Phys. Chem. B 114, 7602–7608 (2010)

[114] T. Oh, T. Takahashi, S. Kim, M. J. Heller, "CTAB enhancement of FRET in DNA structures", J. Biophotonics 9, 49–54 (2016)

[115] K. M. Koo, A. A. I. Sina, L. G. Carrascosa, M. J. A. Shiddiky, M. Trau, "DNA–bare gold affinity interactions: mechanism and applications in biosensing" Anal. Methods, 7, 7042-7054 (2015)

[116] C. Yu, L. Varghese, J. Irudayaraj, "Surface modification of cetyltrimethylammonium bromide-capped gold nanorods to make molecular probes" Langmuir, 23, 9114-9119 (2007)

[117] B. Thierry, J. Ng, T. Kriega, H. J. Griesser, "A robust procedure for the functionalization of gold nanorods and noble metal nanoparticles" Chem. Commun., 0, 1724-1726 (2009)

[118] S. R. Bagloua, T. T. Moghadama, B. Ranjbara, „Biofunctionalization of gold nanorods: a comparative study on conjugation methods for fabrication of nanobiosensors" J. Biomacromol. 2, 191-199 (2016)

[119] C.-C. Chen, Y.-P. Lin, C.-W. Wang, H.-C. Tzeng, C.-H. Wu, Y.-C. Chen, C.-P. Chen, L.-C. Chen, Y.-C. Wu, "DNA-gold nanorod conjugates for remote control of localized gene expression by near infrared irradiation" J. Am. Chem. Soc. 128, 3709-3715 (2006)

[120] H. J.Paraba, C. J. Joo-Hyung, L. Hyun, G. Park, "A gold nanorod-based optical DNA biosensor for the diagnosis of pathogens", Biosens. Bioelectron. 26, 667-673 (2010)

[121] D. Shi, C. Song, Q. Jiang, Z.-G. Wang, B. Ding, "A facile and efficient method to modify gold nanorods with thiolated DNA at a low pH value" Chem. Commun. 49, 2533-2535 (2013)

[122] Q. Jiang, Y. Shi, Q. Zhang, N. Li, P. Zhan, L. Song, L. Dai, J. Tian, Y. Du, Z. Cheng, B. Ding, "A self-assembled DNA origami-gold nanorod complex for cancer theranostics" Small, 11, 5134-5141 (2015)

[123] P. Zhan, P. K. Dutta, P. Wang, G. Song, M. Dai, S.-X. Zhao, Z.-G. Wang, P. Yin, W. Zhang, B. Ding, Y. Ke, "Reconfigurable three-dimensional gold nanorod plasmonic nanostructures organized on DNA origami tripod" ACS Nano, 11, 1172−1179 (2017)

[124] Q. Jiang, Q. Liu, Y. Shi, Z.-G. Wang, P. Zhan, J. Liu, C. Liu, H. Wang, X. Shi, L. Zhang, J. Sun, B. Ding, M. Liu, "Stimulus-responsive plasmonic chiral signals of gold nanorods organized on DNA origami" Nano Lett., 17, 7125-7130 (2017)

[125] A. Elbakry, A. Zaky, R. Liebl, R. Rachel, A. Goepferich, M. Breunig, "Layer-by-layer assembled gold nanoparticles for siRNA delivery" Nano Lett., 9, 2059–2064 (2009)

[126] Z. Maa, L. Tian, T. Wang, "Optical DNA detection based on gold nanorods aggregation" Analytica Chimica Acta 673, 179-184 (2010)

[127] T. E. Pylaev, V. A. Khanadeev, B. N. Khlebtsov, L. A. Dykman, V. A. Bogatyrev, N. G. Khlebtsov, "Colorimetric and dynamic light scattering detection of DNA sequences by using positively charged gold nanospheres: a comparative study with gold nanorods" Nanotechnology 22, 28550-285512 (2011)

[128] L. M. Demers, C. A. Mirkin, R. C. Mucic, R. A. Reynolds, R. L. Letsinger, R. Elghanian, G. Viswanadham, "A Fluorescence-based method for determining the surface coverage and hybridization efficiency of thiol-capped oligonucleotides bound to gold thin films and nanoparticles" Anal. Chem., 72, 5535–5541 (2000)

[129] S. Vijayakumar, “In vitro stability studies on gold nanoparticles with different stabilizing agents” Int. J. Curr. Sci., 11, 84-93 (2014)

[130] H. J. Parab, C. Jung, J. H. Lee, H. Gyu, H. G. Park, “A gold nanorod-based optical DNA biosensor for the diagnosis of pathogens” Biosens. Bioelectron. 26, 667-673 (2010)

[131] [https://patents.google.com/patent/CN104759620A/en] 28/08/2018

[132] R. A. Sperling, W. J. Parak, “Surface modification, functionalization and bioconjugation of colloidal inorganic nanoparticles” Phil. Trans. R. Soc. A, 368, 1333–1383 (2010)

[133] J. Chen, Y. Jin, N. Fahruddin, J. X. Zhao, “Development of gold nanoparticle-enhanced fluorescent nanocomposites” Langmuir, 29, 1584–1591 (2013)

[134] A. Kudelski, “Chemisorption of 2-Mercaptoethanol on silver, copper, and gold: direct raman evidence of acid-induced changes in adsorption/desorption equilibria” Langmuir, 19, 3805–3813 (2003)

[135] F. Li, H. Zhang, B. Dever, X.-F. Li, X. C. Le, “Thermal stability of DNA functionalized gold nanoparticles” Bioconjug Chem., 24, 1790–1797 (2013)

[136] I. Ostolska, M. Wiśniewska, „Application of the zeta potential measurements to explanation of colloidal Cr2O3 stability mechanism in the presence of the ionic polyamino acids” Colloid Polym Sci., 292, 2453–2464 (2014)

[137] C. Cruje, D. B. Chithrani, “Polyethylene Glycol Density and Length Affects Nanoparticle Uptake by Cancer Cells” J Nanomed Res, 1, 1, (2014)

[138] D. Bobo, K. J. Robinson, J. Islam, K. J. Thurecht, S. R. Corrie, “Nanoparticle-based medicines: a review of FDA-approved materials and clinical trials to date” Pharm Res 33, 2373–2387 (2016)

[139] J. V. Jokerst, T. Lobovkina, R. N. Zare, S. S. Gambhir, “Nanoparticle PEGylation for imaging and therapy” Nanomedicine, 6, 715–728 (2011)

[140] G. S. Manning, “The persistence length of DNA is reached from the persistence length of its null isomer through an internal electrostatic stretching force” Biophys J., 91, 3607–3616 (2006)

[141] Q. Chi, G. Wang, J. Jiang, “The persistence length and length per base of single-stranded DNA obtained from fluorescence correlation spectroscopy measurements using mean field theory” Physica A Stat. Mech. Appl., 392, 1072-1079 (2013)

[142] M. E. Sanborn, B. K. Connolly, K. Gurunathan, M. Levitus, “Fluorescence properties and photophysics of the Sulfoindocyanine Cy3 linked covalently to DNA” J. Phys. Chem. B, 111, 11064-11074 (2007)

[143] V. A. Sorokin, G. O. Gladchenko, V. A. Valeev, "DNA protonation at low ionic strength of solution" Makromol. Chem., 187, 1053-1063 (1986)

[144] X. Wang, H. Jeong Lim, A. Son, "Characterization of denaturation and renaturation of DNA for DNA hybridization" Environ Health Toxicol., 29, 2014007 (2014)

[145] V. Verdolino, R. Cammi, B. H. Munk, H. B. Schlegel, "Calculation of pKa values of nucleobases and the guanine oxidation products guanidinohydantoin and spiroiminodihydantoin using density functional theory and a polarizable continuum model" J. Phys. Chem. B, 112, 16860–16873 (2008)

[146] B. Palpant (2017) "Photothermal properties of plasmonic nanoparticles". In C. Louis, O. Pluchery "Gold Nanoparticles for Physics, Chemistry and Biology" (pp. 87-130), World Scientific Publishing Europe Ltd, London, United Kingdom

[147] C. D. S. Brites, P. P. Lima, N. J. O. Silva, A. Millan, V. S. Amaral, F. Palacio, L. D. Carlos, "Thermometry at the nanoscale", Nanoscale, 4, 4799–4829 (2012)

[148] O. M. Wilson, X. Hu, D. G. Cahill, P. V. Braun, "Colloidal metal particles as probes of nanoscale thermal transport in fluids", Phys. Rev. B 66, 224301 (2002)

[149] X. Wang, O. S. Wolfbeis, R. J. Meier, "Luminescent probes and sensors for temperature", Chem. Soc. Rev., 42, 7834―7869 (2013)

[150] M. Swierczewska, S. Lee, X. Chen, „The design and application of fluorophore–gold nanoparticle activatable probes", Phys Chem Chem Phys., 13, 9929–9941 (2011)

[151] G. Schneider, G. Decher, N. Nerambourg, R. Praho, M. H. V. Werts, M. Blanchard-Desce, "Distance-Dependent Fluorescence Quenching on Gold Nanoparticles Ensheathed with Layer-by-Layer Assembled Polyelectrolytes", Nano Lett., 6, 530–536 (2006)

[152] M. A. Haidekker, E. A. Theodorakis, "Environment-sensitive behavior of fluorescent molecular rotors", Journal of Biological Engineering, 4:11, (2010)

[153] G. Baffou, H. Rigneault, D. Marguet, L. Jullien, "A critique of methods for temperature imaging in single cells", Nature Methods, 11, 899-901 (2014)

[154] B. Palpant (2017) "Photothermal properties of plasmonic nanoparticles". In C. Louis, O. Pluchery "Gold Nanoparticles for Physics, Chemistry and Biology" (pp. 87-130), World Scientific Publishing Europe Ltd, London, United Kingdom

[155] A. J. Schmidt, J. D. Alper, M. Chiesa, G. Chen, S. K. Das, K. Hamad-Schifferli, "Probing the gold nanorod-ligand-solvent interface by plasmonic absorption and thermal decay", J. Phys. Chem. Lett. 112, 13320–13323 (2008)

université PARIS-SACLAY
ÉCOLE DOCTORALE
Structure et dynamique des systèmes vivants (SDSV)

Titre : Transfert thermique photo-induit par des nanoparticules d'or appliqué à la thérapie génique

Mots clés : nanoparticules d'or, plasmonique, photothermique, ADN, CTAB

Résumé : La thérapie génique est probablement l'approche la plus ambitieuse de l'histoire de l'humanité pour éliminer des maladies, souvent complètement résistantes à d'autres traitements. Cependant, c'est une approche qui doit encore être développée afin de réduire les coûts et d'obtenir un meilleur contrôle du processus de délivrance des médicaments. À cette fin, le projet visait à tester la capacité des nanobâtonnets d'or à être des « transporteurs » efficaces. Pour cela, il était nécessaire de mettre au point un protocole de fonctionnalisation adapté, avec une densité d'oligonucléotides contrôlée. De plus, les changements à la surface des nanomatériaux ont été caractérisés de manière précise et reproductible. À la suite, des travaux portant sur des questions allant de la synthèse de nanobâtonnets fonctionnalisés aux tests biologiques ont été effectués.

Title : Light induced thermal energy conversion of gold nanorods applied to gene therapy

Keywords : gold nanoparticles, plasmonics, photothermal, DNA, CTAB

Abstract: Gene therapy is probably the most ambitious approach in human history that aims to eliminate diseases, often those completely resistant to other treatments. However, it is an approach that requires further development in order to reduce costs and obtain better control over the process of drug delivery. For this purpose, the project has focused on testing the ability of gold nanorods as efficient carriers. To achieve this, it was necessary to create functionalisation protocols suitable for the task of producing nanoparticles with high oligonucleotide coverage density. Additionally, characterisation of changes on nanomaterial surfaces in a precise and reproducible way was required. As a result, the work in this project covers issues from nanorods synthesis to the production of nanomaterials ready for biological tests.

Université Paris-Saclay
Espace Technologique / Immeuble Discovery
Route de l'Orme aux Merisiers RD 128 / 91190 Saint-Aubin, France